

HARVARD UNIVERSITY
Graduate School of Arts and Sciences



DISSERTATION ACCEPTANCE CERTIFICATE

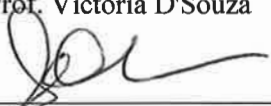
The undersigned, appointed by the
Department of Molecular and Cellular Biology
have examined a dissertation entitled
"Biochemical Studies of TRP Channel Activation and Modulation"
presented by Monique Brewster,
candidate for the degree of Doctor of Philosophy and hereby
certify that it is worthy of acceptance.

Signature _____


Typed name: Prof. Catherine Dulac

Signature _____


Typed name: Prof. Victoria D'Souza

Signature _____


Typed name: Prof. Stephen Blacklow

Date: August 30, 2016

Biochemical studies of TRP channel activation and modulation

A dissertation presented by

Monique Brewster

to

The Department of Molecular and Cellular Biology

in partial fulfillment of the requirements

for the degree of

Doctor of Philosophy

in the subject of

Biochemistry

Harvard University

Cambridge, Massachusetts

August 2016

© 2016 Monique Brewster

All rights reserved.

Biochemical studies of TRP channel activation and modulation

Abstract

TRP channels are the cellular sensors behind many elements of somatosensation, including temperature sensing and the perception of pain. In fact, two channels, TRPV1 and TRPA1, expressed in pain-sensing nociceptor neurons, are direct molecular receptors for a number of painful thermal and chemical stimuli. Activation of those channels triggers action potentials in nociceptor neurons that signal pain to the central nervous system. Given the roles of TRPA1 and TRPV1 at the forefront of nociception, they are promising targets for reducing pain and inflammation through pharmacological intervention. Advancing our knowledge of the molecular mechanisms behind TRPV1 and TRPA1 channel activation and function is essential for the rational design of medically- and agriculturally-relevant channel modulators.

With the entrance of TRP channels into the structural era, we are in the unique position to use structural information to direct, inform, and complement biochemical experiments. Together this knowledge helps us probe the molecular mechanical workings of TRP channels during activation.

Here I present efforts to understand two modes of TRP channel activation: the vanilloid molecule-based activation of TRPV1 and the modulation of TRPA1

temperature sensitivity. Through mutagenesis and fluorescence-based characterization of TRPV1 channel function in insect cells, we identified a minimal set of residues responsible for species-specific differences in vanilloid sensitivity and engineered this sensitivity into a normally insensitive TRPV1 homolog. By systematic truncation and electrophysiological analysis of a highly temperature sensitive isoform of TRPA1, we identified a helix necessary for promoting temperature sensitivity and propose a structural role for the newly-recognized element. These insights on TRPV1 and TRPA1 function provide some of the missing molecular details of TRP channel activation by vanilloid compounds and temperature.

Chapter 1

Introduction

1.1 Somatosensation and Pain

The ability to sense and respond to the environment, either on a macroscopic or microscopic level, is key to homeostasis and survival. As a result, organisms from bacteria to humans have specialized ways of perceiving and responding to environmental variables. Animals have complex systems that contribute to the five basic senses: sight, hearing, smell, taste, and somatosensation. Somatosensation is an umbrella category that encompasses all of the ways the body perceives its interaction with the environment, including the perception of mechanical, thermal, and chemical stimuli. Touch, the most commonly recognized example of somatosensation, describes the perception of mechanical stimuli like pressure. The five basic senses share a similar general mechanism. The stimulus, be it light, or sound, or a chemical, activates a molecular receptor present in a sensory neuron. This leads to depolarization of the neuron and relaying of the message as an action potential to the central nervous system. The molecular receptors in olfaction, taste, and somatosensation are often membrane proteins, such as G-protein coupled receptors or ion channels (Lindemann).

Nociception, the detection of noxious or potentially harmful conditions, is an especially important subset of somatosensation. To protect itself, the body must be able to quickly respond to tissue damage, extremes in temperature, or the presence of hazardous chemicals. This function is performed by nociceptors, specialized primary sensory neurons of the peripheral nervous system that respond specifically to noxious stimuli rather than innocuous ones. The dendrites of these nociceptors innervate the entire body, including the skin and internal organs, providing a network that warns of immediate or potential damage. When hazardous conditions are sensed at

nociceptor dendrites, the neurons depolarize and action potentials travel to the central nervous system to trigger protective reflexes or behaviors as well as the conscious awareness of pain (Figure 1.1).

Nociceptor neurons are distinct from their counterparts involved in sensing innocuous stimuli. Nociceptor neurons are not required to respond to a single type of stimulus; they can respond to various thermal and chemical stimuli that are associated with irritation, inflammation, and/or pain (Julius; Tominaga & Caterina). Ion channels play an essential role in the initial recognition of painful stimuli; in fact, ion channels are often the direct molecular receptors for those stimuli. Nociceptors often express combinations of ion channels with sensitivity to diverse stimuli resulting in the multimodality of those neurons (Basbaum et al.). In addition, some of the pain-associated ion channels are themselves polymodal. Together, this system allows the integration of multiple stimuli into a single response: pain. This dissertation focuses on two such channels, TRPV1 and TRPA1, which are the first step in sensing pain caused by a variety of thermal and chemical-based stimuli. Given the role of ion channels as the first step in sensing pain prompted by a variety of stimuli (Julius; Tominaga & Caterina), they are attractive targets for pharmaceutical intervention. More detailed understanding of the molecular mechanisms behind channel function is essential for the rational design of channel modulators.

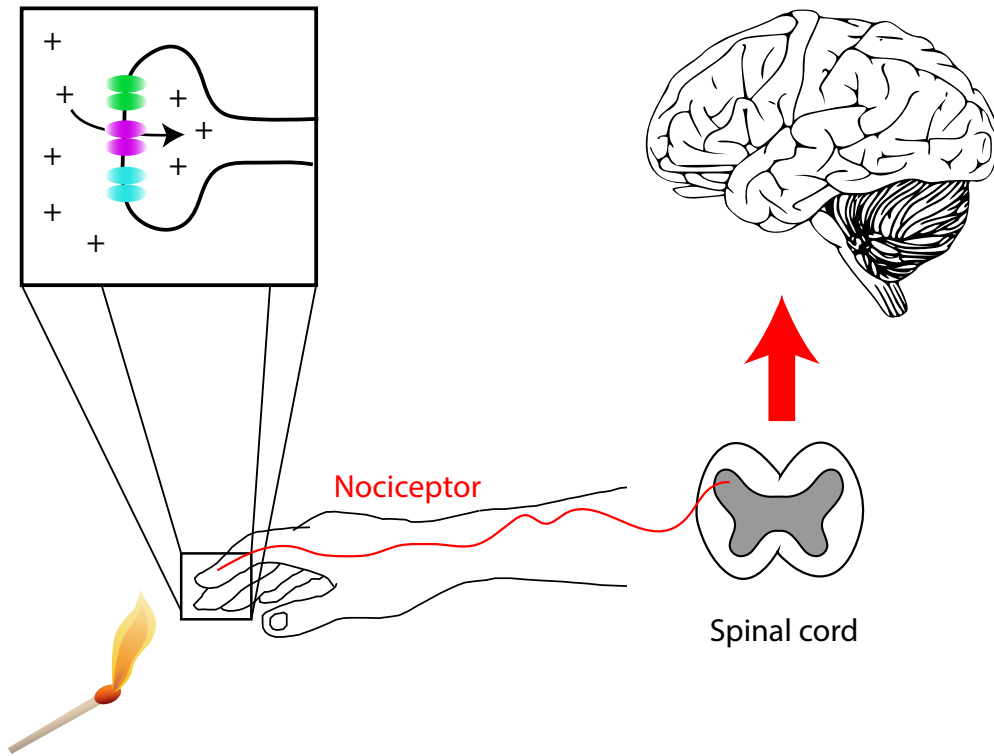


Figure 1.1 Nociceptors sense noxious stimuli and trigger signals perceived as pain. Nociceptor neurons are responsible for sensing harmful conditions and relaying that message to the central nervous system to trigger protective responses and the awareness of pain. Ion channels are the molecular receptors of painful stimuli in nociceptors. When triggered, the channels open triggering action potentials that propagate down the nociceptors to the spinal cord.

1.1 TRP Channels as Molecular Receptors

1.2.1 The TRP superfamily

The first TRP channel was identified based on a *Drosophila* screen. Mutation of the *trp* (transient receptor potential) locus causes transient voltage responses of photoreceptors to continuous light, rather than the typical sustained response seen in photoreceptors from wildtype flies. In 1989, Montell and Rubin discovered that the locus encoded a transmembrane protein, and aptly named the protein TRP based on the phenotype of the mutant (Montell & Rubin). Since then, the number of known TRP-like channels in organisms from yeast to humans has grown to populate a superfamily of cation channels. These channels are often involved in cellular sensory transduction and respond to different factors like osmolarity, temperature, and mechanical stimuli, and also to various chemical stimuli (Clapham; Venkatachalam & Montell; Wu et al.). All TRPs are tetrameric and most are relatively non-selective cation channels with six-segment transmembrane domains similar to that of potassium or sodium voltage-gated ion channels. There are seven TRP channel subtypes: TRPV, TRPA, TRPM, TRPML, TRPC, TRPP, and TRPN; the divisions primarily reflect differences in the N- and C-terminal cytoplasmic domains (Hellmich & Gaudet). These cytoplasmic domains contain allosteric regulation domains including small-molecule and protein interaction domains (Clapham; Hellmich & Gaudet). As a result, the different channel subtypes are activated and modulated by unique patterns of stimuli.

1.2.2 TRPV1 Function, Modulation, and Structure

As its name implies, TRPV1, transient receptor potential vanilloid 1, was the first mammalian member identified in the “vanilloid” subfamily of TRP channels. Its name reflects TRPV1’s ability to be modulated by compounds that contain a vanillyl moiety, a hydroxyl and methoxy-substituted six-carbon aromatic ring (Figure 1.2). TRPV1 was cloned and heterologously characterized in 1997 by Caterina et al. who identified it as the molecular receptor for capsaicin, a vanilloid compound responsible for the spiciness of chili peppers (Caterina et al.). The channel is also activated by temperatures above 45 °C, a range corresponding to noxious heat (Caterina et al.). The activation of a single channel by both capsaicin and heat provides a molecular reason for why spicy food results in a hot or burning sensation. Resiniferatoxin is another vanilloid small-molecule activator of TRPV1 that is found in resin sponge, cactus-like plants of the *Euphorbia* genus (Figure 1.2).

TRPV1 is also activated by a number of factors associated with tissue damage and inflammation. For example, the channel is activated by external acidification (Caterina et al.), a process that occurs in injury or inflammation. The divalent peptide double-knot toxin (DkTx) is a component of tarantula venom that induces severe pain and inflammation through activation of TRPV1 (Siemens et al.).

In addition, TRPV1 sensitivity is modulated by multiple factors. One modulator of TRPV1 phosphatidylinositol-4,5-bisphosphate, PIP₂, has been reported as both a sensitizer and desensitizer of the channel. Some studies point to PIP₂ binding to sensitize the channel while other suggest PIP₂ hydrolysis and release is what increases TRPV1’s sensitivity. (Chuang et al.; Liu et al.; Lukacs et al.; Rohacs et al.; Stein et al.).

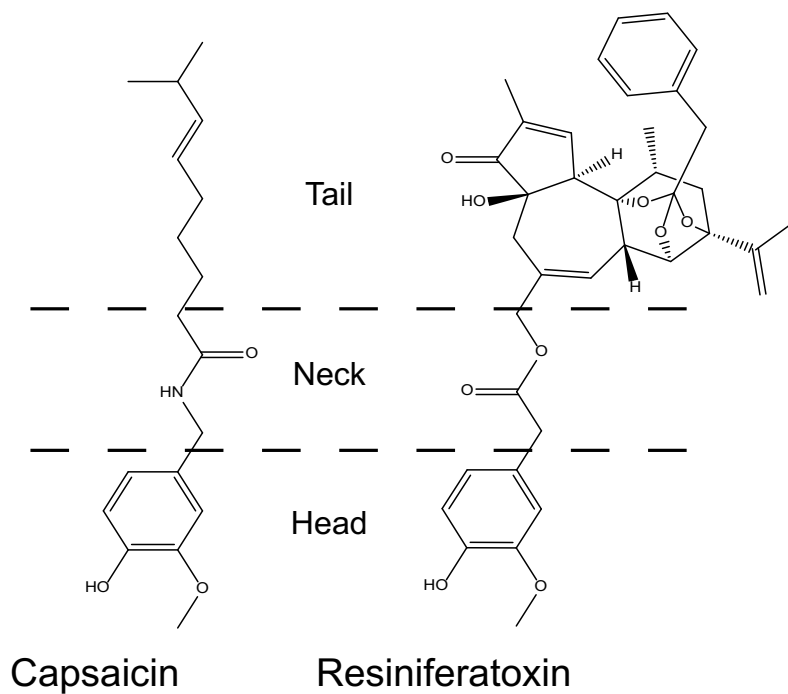


Figure 1.2 TRPV1 agonists capsaicin and resiniferatoxin have similar structures. Capsaicin and resiniferatoxin have an identical vanilloid moiety “head.” The necks of both molecules are polar, but contain different groups. Tail region of resiniferatoxin is much larger than that of capsaicin.

PIP₂ is a signaling molecule downstream of inflammation mediator pathways including the bradykinin pathway, providing a potential link that explains TRPV1-dependent exacerbation of inflammation-related pain (Chuang et al.). ATP acts intracellularly to sensitize TRPV1 and prevent channel desensitization (Kwak et al.; Lishko et al.), while the calcium-binding protein calmodulin does the opposite (Lishko et al.). The tunable nature of TRPV1 allows the integration of multiple signals to modulate pain threshold.

The connection of TRPV1 to pain and inflammation has further been confirmed through studies of TRPV1 null mice. These mice lack vanilloid-induced pain responses and have reduced inflammation-dependent thermal hypersensitivity compared to wildtype mice (Caterina et al.; Davis et al.). As a major gateway to pain signaling, TRPV1 is an enticing target for pharmaceutical intervention focused on reducing pain and inflammation (Julius; Premkumar & Abooj). Both channel antagonists and agonists have the potential for analgesic effects. Molecules that inhibit TRPV1 would incapacitate a major receptor for painful thermal and chemical stimuli. Since TRPV1 shows strong deactivation after repeated or continuous stimulation (Koplas et al.) agonists also have therapeutic value. For example, over the counter capsaicin-containing creams are available for the treatment of arthritis and muscle pain (Zhang & Li Wan Po).

Interest in the molecular mechanisms behind TRPV1 activation have prompted a wealth of biochemical, electrophysiological, and structural studies of the channel. Over a hundred engineered mutations in TRPV1 have been reported that alter channel function (Winter et al.). This includes mutations, truncations, and deletions that alter virtually every known characteristic of the TRPV1 channel. For example, pH sensitivity,

capsaicin sensitivity, double-knot toxin activation, and regulation by PIP₂ have all been targeted with biochemistry and mutagenesis (Winter et al.).

Until relatively recently, only low resolution information was available for the TRPV1 channel (Moiseenkova-Bell et al.). With advances in cryoEM detectors, new higher resolution structures were solved giving us a first look at the atomic detail of the TRPV1 channel in 2013 (Cao et al.; Liao et al.) (Figure 1.3). As expected from sequence analysis, the structures of TRPV1 show that it is a six-transmembrane segment ion channel with intracellular N- and C-termini. At the N-terminus is a stack of six ankyrin repeats, which are the binding sites for calmodulin and PIP₂, regulators of channel sensitivity (Lishko et al.; Rohacs et al.). The ankyrin repeats lead into a linker that contributes to a small β -sheet with a portion of the channel C-terminus. Then, the linker leads into the transmembrane domain, specifically the S1-S4 bundle of helices on the periphery of the channel. A short S4-S5 helix connects the bundles to the remaining transmembrane helices, S5 and S6 that line the pore. A reentrant loop between S5 and S6 forms the turret and pore helix (Figure 1.3 A). Domain-swapping places S1-S4 of one subunit in contact with the S5 and S6 of an adjacent subunit (Figure 1.3 B). This transmembrane domain topology is similar to that of the distantly-related voltage-gated ion channels (Catterall & Swanson; Kuang et al.). Select sidechains on the S5 and S6 helices project into the pore forming the upper and lower channel gates (Cao et al.; Gao et al.; Liao et al.). Modulators of channel function must act allosterically to target these gates and regulate channel opening and closing.

One unexpected feature of the TRPV1 structure is the presence of an additional helix just after S6. Originally the TRP domain was identified as conserved sequence

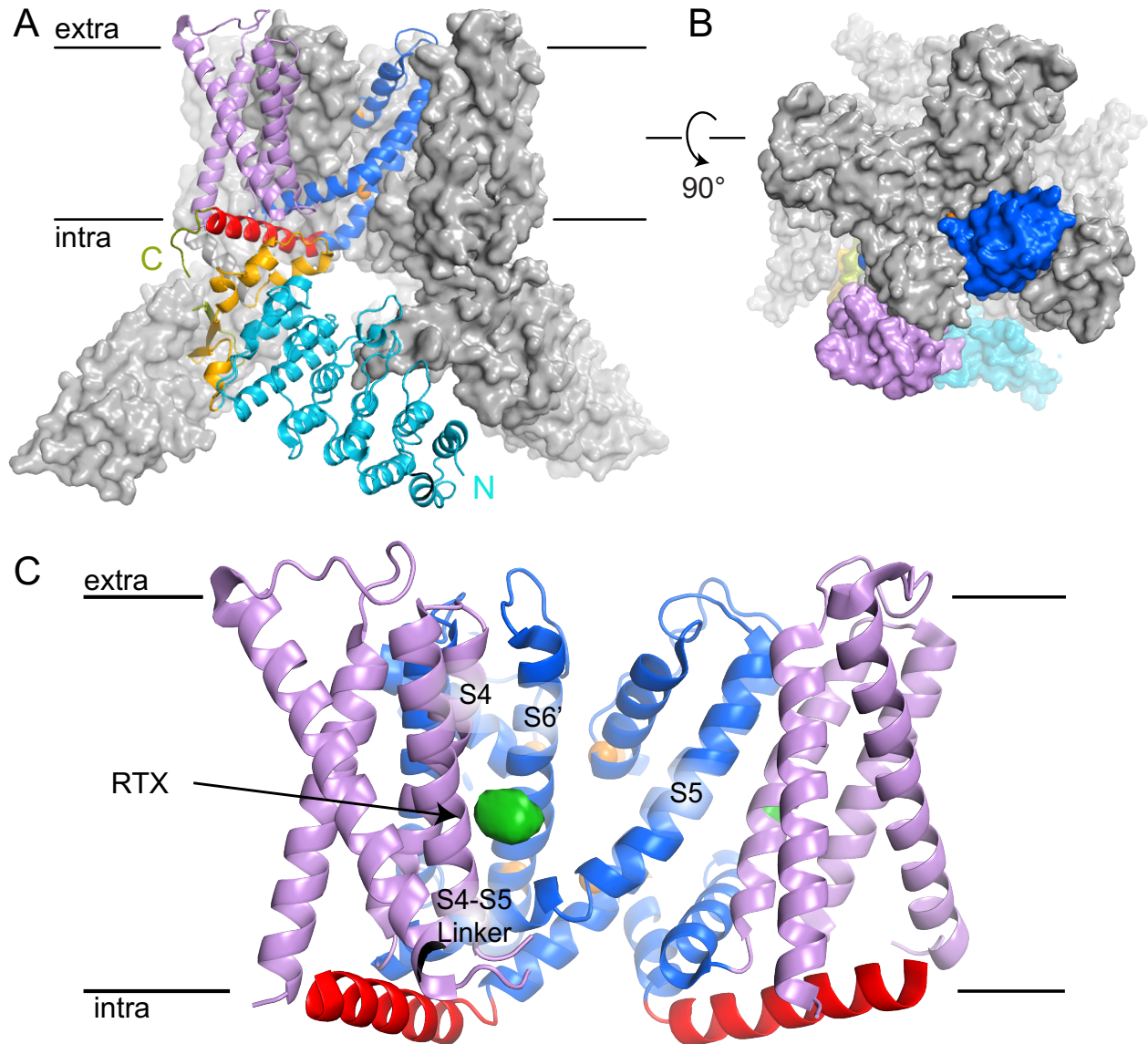


Figure 1.3 High resolution cryoEM structure of TRPV1 and its vanilloid agonists. (A) TRPV1 (PDB ID: 3j5r) is depicted as a gray surface with one subunit represented as a cartoon according to the following color scheme from N- to C-terminus: ankyrin repeats, turquoise; linker, gold; preS1, gray; S1-S4, lavender; S5-S6, blue; TRP-box helix, red; C-terminus, forest green. Gate residues, which form the constrictions in the pore, are indicated as orange spheres. The extracellular and intracellular sides of the membrane are indicated. (B) A surface representation of the channel is shown seen from the extracellular face downwards. One colored subunit illustrates the domain-swapping of the S1-S4 and S5-S6 helices (C) Resiniferatoxin (RTX) is seen binding in the S4-S5 pocket formed by S4, the S4-S5 linker, and the S6 helix from an adjacent subunit.

motif in TRPV, TRPM, and TRPC channels (Venkatachalam & Montell; Wu et al.). The structure of TRPV1 revealed that the TRP box is a helix that runs from S6 parallel to the membrane underneath the S1-S4 bundle and interacting with the linker (Figure 1.3; See also Figure 1.6). The helix's placement, bridging the cytoplasmic and transmembrane domains, points to a role as a nexus of communication that can integrate signals from the cytoplasmic domains and refer them through S5 and S6 to modulate channel gating. Accordingly, mutations of conserved TRP-domain residues affect multiple modes of TRPV channel activation (Gregorio-Teruel et al.; Teng et al.) .

The TRPV1 structures were solved in complex with various ligands, including vanilloid agonists capsaicin and resiniferatoxin, revealing a vanilloid-binding pocket formed by S4, the S4-S5 linker, and the S6 helix of an adjacent subunit (Cao et al.; Liao et al.) (Figure 1.3 C). In the first high resolution structures (Cao et al.; Liao et al.), the vanilloid molecules could not be unambiguously modelled, but new structures of TRPV1 (Gao et al.) were reported early this year that reveal the molecular details of vanilloid binding. A discussion of those details is included at the end of Chapter 2. The combination of new structural information with biochemical and functional characterization has led to a much more detailed understanding of how TRPV1 works.

1.2.3 Function, Modulation, and Structure of TRPA1

Like TRPV1, TRPA1 is a nonselective cation channel expressed in nociceptor neurons, and it is a molecular receptor for multiple painful stimuli (Barabas et al.; Jordt et al.; Story et al.; Zygmunt & Högestätt). In humans, mutations in TRPA1 are associated with pain pathologies. A TRPA1 variant N855S that displays hyperactivity is associated with familial episodic pain syndrome, a condition characterized by extreme

bouts of upper body pain (Kremeyer et al.). TRPA1 is also known for its role in facilitating neurogenic and inflammatory pain (Andersson et al.; Bautista et al.; Trevisani et al.). As a result, it is also a major target of pharmacological intervention for the development of anti-inflammatory and analgesic therapies (Chen & Hackos; Garrison & Stucky; Trevisan et al.).

In particular, TRPA1 is associated with irritant sensing; the channel is activated by a wide variety of pungent compounds including allyl isothiocyanate (AITC) from wasabi, cinnamaldehyde from cinnamon, and allicin from onions and garlic (Bandell et al.; Bautista et al.; Macpherson et al.). These chemicals have very different structures, but similar chemical characteristics: they are all reactive electrophiles with the ability to form covalent bonds with free nucleophiles (Hinman et al.; Macpherson et al.). Mutagenesis experiments attributed electrophile sensing to cysteines and a lysine in the N-terminus (Cys422, Cys621, Cys641, Cys665, and Lys710 of human TRPA1) (Hinman et al.; Macpherson et al.). This irritant sensing ability of TRPA1 is a property conserved from invertebrates to vertebrates (Kang et al.).

TRPA1 is also a temperature-activated channel. In mice and humans, TRPA1 opens in response to noxious cold, temperatures below 18°C (Bandell et al.; Sawada et al.). However, there is conflicting evidence over the physiological role of TRPA1 in cold sensing. Some studies report that TRPA1-deficient mice no longer respond to burning cold on their extremities (Kwan et al.), while others report normal responses to noxious cold (Chen et al.). Interestingly, TRPA1 in other organisms is a heat-sensitive channel. In pit snakes, TRPA1 is the heat sensor expressed in pits above their nostrils used for infrared detection of prey (Gracheva et al.). Female mosquitoes express a version of

TRPA1 in their antennae, where it mediates heat-seeking feeding behaviors (Wang et al.). In *Drosophila* TRPA1 is involved in setting the preferred temperature range near 25 °C (Hamada et al.).

Additionally, TRPA1 can be activated by a number of non-electrophilic molecules. For example, menthol activates human TRPA1, providing a molecular reason for why mint can seem painfully cold (Karashima et al.; Klement et al.). TRPA1 is also activated by gingerol, an aromatic chemical from ginger (Bandell et al.). Of medical significance, GABA_A-targeting general anesthetics, including propofol, activate TRPA1, resulting in unwanted burning pain at the site of injection (Fischer et al.; Matta et al.). Many of these non-electrophilic TRPA1 agonists are hydrophobic, aromatic molecules.

Since the channel was first cloned in 2003, TRPA1 has been the target of many structure-function studies, leading to accumulation of biochemical and functional knowledge about the channel (Story et al.). In 2015, a high resolution cryoEM structure of TRPA1 was published (Paulsen et al.), allowing biochemical information to be mapped onto a structural scaffold. Like TRPV1, TRPA1 is a tetrameric channel with cytoplasmic N- and C-termini (Figure 1.4). At the N-terminus is the channel's namesake, a large stack of ankyrin repeats. Only the last 6 of 17 predicted repeats could be modelled in this structure; however, evidence of the first 11 repeats could be seen in the cryoEM class averages and 3D construction as a bowl-shaped density beneath the rest of the channel (Paulsen et al.)(Figure 1.4 B). This is consistent with a kink in the ankyrin repeat domain before repeat 12. The ankyrin repeats lead into a linker region which, similar to TRPV1, also participates in forming a small beta-sheet with a part of the C-

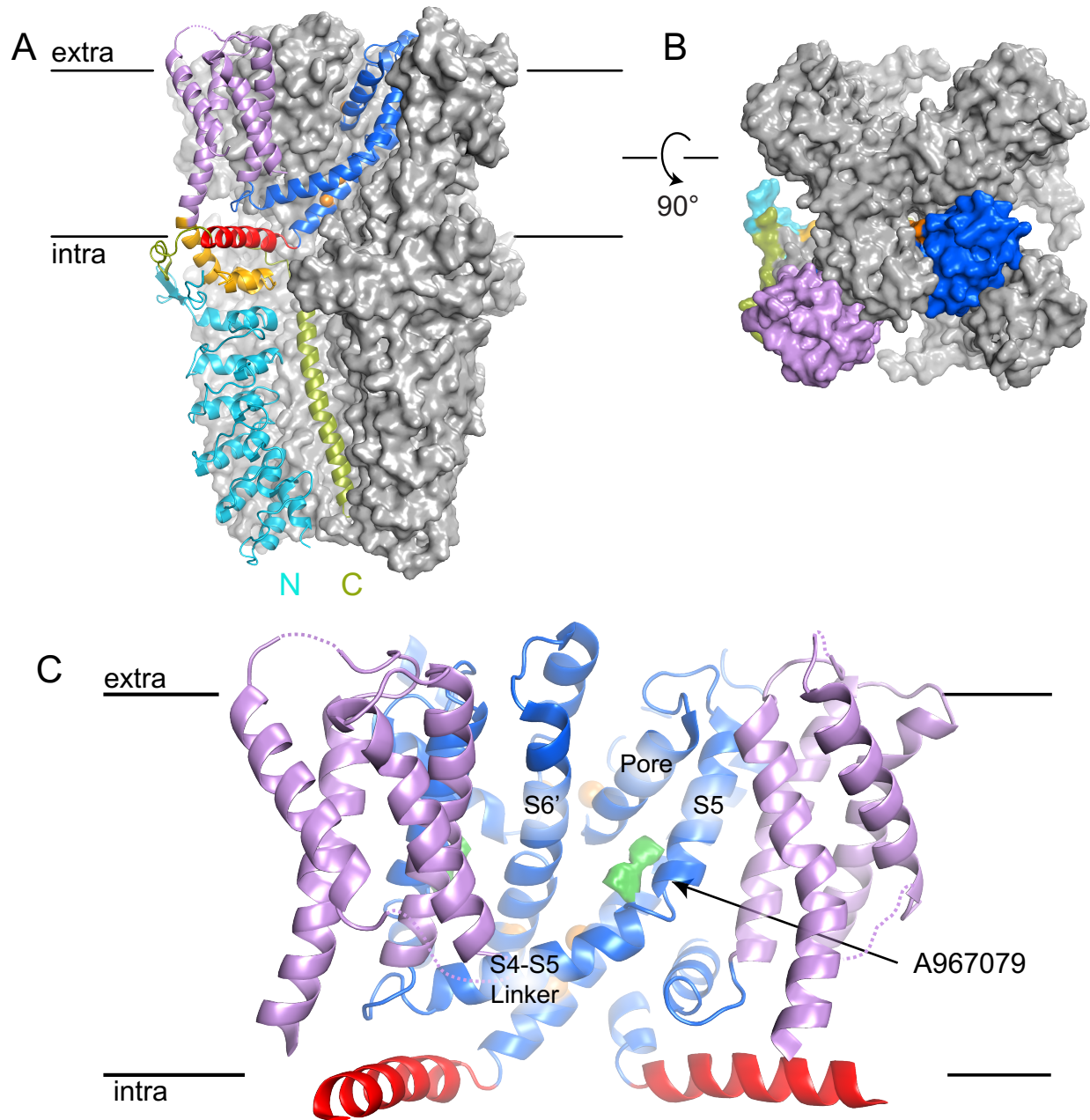


Figure 1.4 High resolution cryoEM structure of TRPA1. (A) TRPA1 (PDB ID: 3j9p) is depicted as a surface with one subunit depicted as a cartoon with the following color scheme from N- to C-terminus: ankyrin repeats, turquoise; linker, gold; preS1, gray; S1-S4, lavender; S5-S6, blue; TRP-box helix, red; C-terminus, forest green. Gate residues, which form the constriction sites of the pore, are indicated as orange spheres. The extracellular and intracellular sides of the membrane are indicated. (B) A surface representation of the channel is shown seen from the extracellular face downwards. One colored subunit illustrates the domain-swapping of the S1-S4 and S5-S6 helices. (C) Channel antagonist, A967079 (green surface), can be seen binding in a cleft between a pore helix and the S5 helix.

terminus before leading into the transmembrane domain (Figure 1.4 A). Ankyrin repeat 17 and the linker also contain three of the cysteines implicated in reactive electrophile sensing (C621, C641, and C665).

The transmembrane domain of TRPA1 is quite similar to that of TRPV1 (Figure 1.5). There is domain-swapping along with the characteristic S1-S4 bundles at the channel periphery. Surprisingly, TRPA1 also has a TRP-domain-like helix, despite a lack of conservation of the classical TRP box motif (EWKFR)(Venkatachalam & Montell). As in TRPV1, the TRPA1 helix runs from the center of the channel beneath the S1-S4 bundles to interact with the linker between S1 and the ankyrin repeats. The proximity of the TRP-domain-like helix to the reactive electrophile associated cysteines of the linker further cements the helix as a potentially important player in gating. Taken together, these observations suggest that a TRP-domain-like helix may be a conserved structural feature in all TRP channels, acting as an integrator and conveyor of signals from the cytoplasmic domains of the channel to the gate (Brewster).

Structure of TRPA1 were also solved in the presence of the synthetic antagonists HC-03003 and A-967079. Surprisingly, the A-967079 molecule binds between the pore helix and S5, a site different than the S4-S5 binding pocket of TRPV1 (Figure 1.5). This reveals a new druggable site for TRPA1 channel modulation in the transmembrane domain that may also be present in other TRP channels.

At the C-terminus of TRPV1 is a tetrameric atypical coiled coil, seated in a cage formed by ankyrin repeats 12-17 (Figure 1.6). Inside the coiled coil, there are two well-conserved glutamines at positions typically occupied by hydrophobic residues like leucine in canonical coiled coils. The outside of the coiled coil is largely hydrophobic,

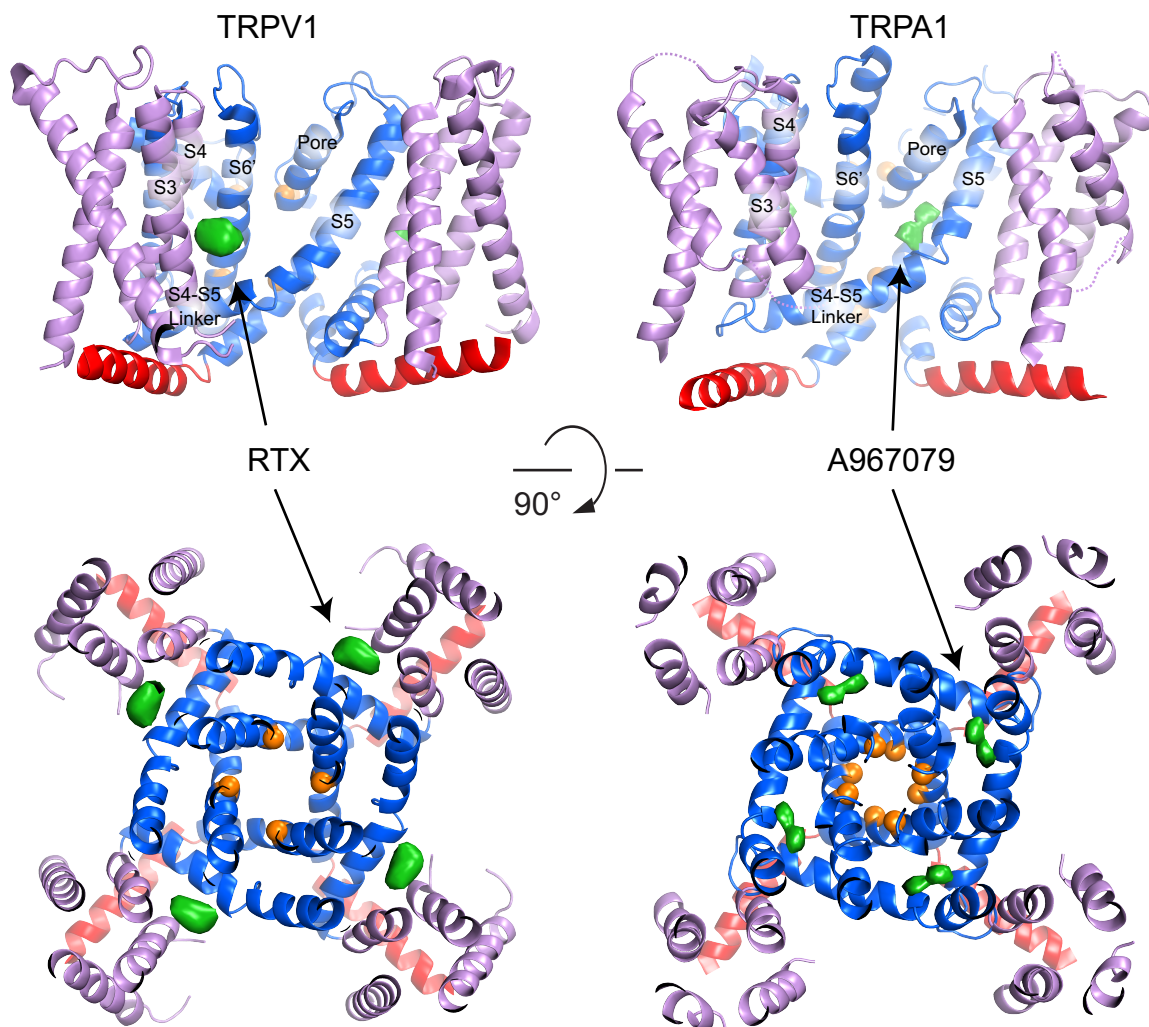


Figure 1.5. Structures of TRPV1 and TRPA1 reveal two binding sites for channel modulators. The transmembrane domains of TRPV1 (PDB ID: 3j5q) and TRPA1 (PDB ID: 3j9p) are depicted as cartoons with the S1-S4 bundles in lavender, S5-S6 in blue, TRP box helices in red, and gate residues as orange spheres. Densities for TRPV1 agonist resiniferatoxin (RTX) and TRPA1 antagonist A9697079 (neon green surfaces) reveal that the molecules do not occupy equivalent sites. Resiniferatoxin binds in the S4-S5 pocket, while the A967079 binds in a cleft between S5 and a pore helix.

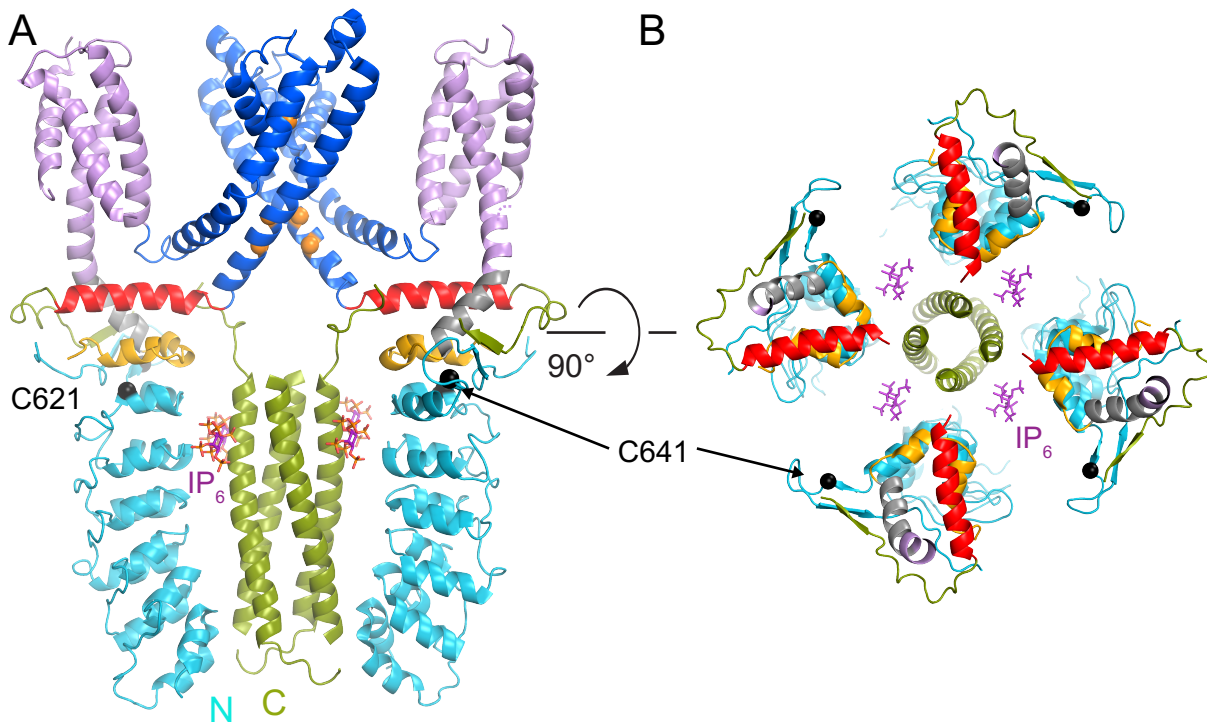


Figure 1.6 TRP-box-like helix of TRPA1 is positioned to propagate cues from the highly interconnected cytoplasmic domains to the channel pore for gating regulation. A cartoon representation of TRPA1 (PDB ID: 3j9p) shows the coiled coil (forest green) of the C-terminus interacting with the last ankyrin repeats (turquoise) through inositol-6-phosphate (purple sticks) in side (A) and in a top down (B) views. For clarity, the transmembrane domains and ankyrin repeats of two subunits were hidden in (A). In B, the entire transmembrane domain has been removed to highlight the packing of the TRP box-like helix (red) with the cytoplasmic domains. TRP box-like helix contacts both the S1-S4 bundle (lavender) and linker (gold), which is in turn stacked directly on top of the ankyrin repeats. This interaction includes C621, one of the residues modified during reactive electrophile activation of the channel. Note that C621 cannot be seen in (B) because it lies directly beneath the linker and TRP box-like helix. The second important cysteine is present on a small β -sheet between subunits. The packing of the membrane-proximal cytoplasmic region suggests a mechanism where the modification status of the cysteine could be propagated through the TRP box-like helix to the channel gates (orange spheres).

with the exception of a patch of positively-charged residues that bind inositol-6-phosphate (IP₆) molecules. These molecules contact both the coiled coil and the ankyrin repeats, bridging the N- and C-terminal domains of TRPV1 (Paulsen et al.). This structural role for IP₆ may be a reason for the observation that phosphate-containing molecules are necessary for TRPA1 activation in excised patches (Kim & Cavanaugh). Phosphate molecules could chelate entrant calcium ions, destabilizing the cytoplasmic domain assemble and acting as a “kill switch” for TRPA1 activity, leading to inactivation (Brewster).

A high-resolution structure of TRPA1 has allowed us to map channel functionalities onto a structural model, providing direction for future studies. The molecular mechanisms behind TRPA1 activation by any of its stimuli are still a mystery. For example, we know where and how the cysteines of TRPA1 sense reactive electrophiles, but we do not yet know the nature of the conformational changes that are propagated to the channel gates to open them. Temperature sensing is even more of a mystery, as multiple regions have been reported as part of the “temperature-sensing domain” (Cordero-Morales et al.) (See Chapter 3 for a more detailed discussion of temperature sensing). More work is necessary to better understand the molecular workings of TRPA1.

1.3 Thesis Outline

This thesis focuses on efforts to combine structural information with biochemical and functional characterization to probe the mechanisms of TRP channel activation. Chapter 2 details the engineering of a capsaicin-sensitive version of chicken TRPV1. We leveraged phylogenetic analysis and knowledge of channel structure to identify

candidate residues responsible for species-specific differences in vanilloid sensitivity. Using mutagenesis and characterization of mutant channels, we identified the minimal set of residues necessary to confer vanilloid sensitivity to chicken TRPV1. New high resolution structures of TRPV1 have allowed us to start assigning physical roles to biochemically-identified determinants of vanilloid sensitivity.

Chapter 3 summarizes experiments to understand temperature sensitivity modulation of TRPA1 isoforms via systematic truncation of a highly temperature sensitive TRPA1 isoform. Through electrophysiology and calcium influx assays, I was able to map the heat-sensitivity promoting region to a small helix in an isoform-specific region of the channel. Furthermore, I propose a structural role for the helix and identify specific residues necessary for the high temperature sensitivity of that TRPA1 isoform.

Appendix A catalogues studies of TRPA1 ankyrin repeat domain fragments. Careful construct design has led to the successful production and purification of various soluble, well-expressed fragments in *E. coli*. Additional work may yield structural information on a yet-to-be seen portion of the TRPA1 ankyrin repeat domain.

1.4 References

- Andersson, D. A., Gentry, C., Moss, S., & Bevan, S. (2008). Transient receptor potential A1 is a sensory receptor for multiple products of oxidative stress. *J Neurosci*, 28(10), 2485-2494.
- Bandell, M., Story, G. M., Hwang, S. W., Viswanath, V., Eid, S. R., Petrus, M. J., Earley, T. J., & Patapoutian, A. (2004). Noxious cold ion channel TRPA1 is activated by pungent compounds and bradykinin. *Neuron*, 41(6), 849-857.
- Barabas, M. E., Kossyrev, E. A., & Stucky, C. L. (2012). TRPA1 is functionally expressed primarily by IB4-binding, non-peptidergic mouse and rat sensory neurons. *PLoS One*, 7(10), e47988.

- Basbaum, A. I., Bautista, D. M., Scherrer, G., & Julius, D. (2009). Cellular and molecular mechanisms of pain. *Cell*, *139*(2), 267-284.
- Bautista, D. M., Movahed, P., Hinman, A., Axelsson, H. E., Sterner, O., Hogestatt, E. D., Julius, D., Jordt, S. E., & Zygmunt, P. M. (2005). Pungent products from garlic activate the sensory ion channel TRPA1. *Proc Natl Acad Sci U S A*, *102*(34), 12248-12252.
- Bautista, D. M., Pellegrino, M., & Tsunozaki, M. (2013). TRPA1: A gatekeeper for inflammation. *Annu Rev Physiol*, *75*, 181-200.
- Brewster, M. S. J. a. G. R. (2015). How the TRPA1 receptor transmits painful stimuli: Inner workings revealed by electron cryomicroscopy. *BioEssays*, *37*(11), 1184--1192.
- Cao, E., Cordero-Morales, J. F., Liu, B., Qin, F., & Julius, D. (2013a). TRPV1 channels are intrinsically heat sensitive and negatively regulated by phosphoinositide lipids. *Neuron*, *77*(4), 667-679.
- Cao, E., Liao, M., Cheng, Y., & Julius, D. (2013b). TRPV1 structures in distinct conformations reveal activation mechanisms. *Nature*, *504*(7478), 113-118.
- Caterina, M. J., Leffler, A., Malmberg, A. B., Martin, W. J., Trafton, J., Petersen-Zeitz, K. R., Koltzenburg, M., Basbaum, A. I., & Julius, D. (2000). Impaired nociception and pain sensation in mice lacking the capsaicin receptor. *Science*, *288*(5464), 306-313.
- Caterina, M. J., Schumacher, M. A., Tominaga, M., Rosen, T. A., Levine, J. D., & Julius, D. (1997). The capsaicin receptor: a heat-activated ion channel in the pain pathway. *Nature*, *389*(6653), 816-824.
- Catterall, W. A., & Swanson, T. M. (2015). Structural Basis for Pharmacology of Voltage-Gated Sodium and Calcium Channels. *Molecular Pharmacology*, *88*(1), 141-150.
- Chen, J., & Hackos, D. H. (2015). TRPA1 as a drug target--promise and challenges. *Naunyn Schmiedebergs Arch Pharmacol*, *388*(4), 451-463.
- Chen, J., Joshi, S. K., DiDomenico, S., Perner, R. J., Mikusa, J. P., Gauvin, D. M., Segreti, J. A., Han, P., Zhang, X. F., Niforatos, W., Bianchi, B. R., Baker, S. J., Zhong, C., Simler, G. H., McDonald, H. A., Schmidt, R. G., McGaraughty, S. P., Chu, K. L., Faltynek, C. R., Kort, M. E., Reilly, R. M., & Kym, P. R. (2011). Selective blockade of TRPA1 channel attenuates pathological pain without altering noxious cold sensation or body temperature regulation. *Pain*, *152*(5), 1165-1172.
- Chuang, H. H., Prescott, E. D., Kong, H., Shields, S., Jordt, S. E., Basbaum, A. I., Chao, M. V., & Julius, D. (2001). Bradykinin and nerve growth factor release the

- capsaicin receptor from PtdIns(4,5)P₂-mediated inhibition. *Nature*, 411(6840), 957-962.
- Clapham, D. E. (2003). TRP channels as cellular sensors. *Nature*, 426(6966), 517-524.
- Cordero-Morales, J. F., Gracheva, E. O., & Julius, D. (2011). Cytoplasmic ankyrin repeats of transient receptor potential A1 (TRPA1) dictate sensitivity to thermal and chemical stimuli. *Proc Natl Acad Sci U S A*, 108(46), E1184-1191.
- Davis, J. B., Gray, J., Gunthorpe, M. J., Hatcher, J. P., Davey, P. T., Overend, P., Harries, M. H., Latcham, J., Clapham, C., Atkinson, K., Hughes, S. A., Rance, K., Grau, E., Harper, A. J., Pugh, P. L., Rogers, D. C., Bingham, S., Randall, A., & Sheardown, S. A. (2000). Vanilloid receptor-1 is essential for inflammatory thermal hyperalgesia. *Nature*, 405(6783), 183-187.
- Fischer, M. J., Leffler, A., Niedermirtl, F., Kistner, K., Eberhardt, M., Reeh, P. W., & Nau, C. (2010). The general anesthetic propofol excites nociceptors by activating TRPV1 and TRPA1 rather than GABAA receptors. *J Biol Chem*, 285(45), 34781-34792.
- Gao, Y., Cao, E., Julius, D., & Cheng, Y. (2016). TRPV1 structures in nanodiscs reveal mechanisms of ligand and lipid action. *Nature*, 534(7607), 347-351.
- Garrison, S. R., & Stucky, C. L. (2011). The dynamic TRPA1 channel: a suitable pharmacological pain target? *Curr Pharm Biotechnol*, 12(10), 1689-1697.
- Gracheva, E. O., Ingolia, N. T., Kelly, Y. M., Cordero-Morales, J. F., Hollopeter, G., Chesler, A. T., Sanchez, E. E., Perez, J. C., Weissman, J. S., & Julius, D. (2010). Molecular basis of infrared detection by snakes. *Nature*, 464(7291), 1006-1011.
- Gregorio-Teruel, L., Valente, P., Gonzalez-Ros, J. M., Fernandez-Ballester, G., & Ferrer-Montiel, A. (2014). Mutation of I696 and W697 in the TRP box of vanilloid receptor subtype I modulates allosteric channel activation. *J Gen Physiol*, 143(3), 361-375.
- Hamada, F. N., Rosenzweig, M., Kang, K., Pulver, S. R., Ghezzi, A., Jegla, T. J., & Garrity, P. A. (2008). An internal thermal sensor controlling temperature preference in *Drosophila*. *Nature*, 454(7201), 217-220.
- Hellmich, U., & Gaudet, R. (2014). High-Resolution Views of TRPV1 and Their Implications for the TRP Channel Superfamily. In B. Nilius & V. Flockerzi (Eds.), *Mammalian Transient Receptor Potential (TRP) Cation Channels* (Vol. 223, pp. 991-1004): Springer International Publishing.
- Hinman, A., Chuang, H. H., Bautista, D. M., & Julius, D. (2006). TRP channel activation by reversible covalent modification. *Proc Natl Acad Sci U S A*, 103(51), 19564-19568.

- Jordt, S. E., Bautista, D. M., Chuang, H. H., McKemy, D. D., Zygmunt, P. M., Hogestatt, E. D., Meng, I. D., & Julius, D. (2004). Mustard oils and cannabinoids excite sensory nerve fibres through the TRP channel ANKTM1. *Nature*, *427*(6971), 260-265.
- Julius, D. (2013). TRP channels and pain. *Annu Rev Cell Dev Biol*, *29*, 355-384.
- Kang, K., Pulver, S. R., Panzano, V. C., Chang, E. C., Griffith, L. C., Theobald, D. L., & Garrity, P. A. (2010). Analysis of *Drosophila* TRPA1 reveals an ancient origin for human chemical nociception. *Nature*, *464*(7288), 597-600.
- Karashima, Y., Damann, N., Prenen, J., Talavera, K., Segal, A., Voets, T., & Nilius, B. (2007). Bimodal action of menthol on the transient receptor potential channel TRPA1. *J Neurosci*, *27*(37), 9874-9884.
- Kim, D., & Cavanaugh, E. J. (2007). Requirement of a soluble intracellular factor for activation of transient receptor potential A1 by pungent chemicals: role of inorganic polyphosphates. *J Neurosci*, *27*(24), 6500-6509.
- Klement, G., Eisele, L., Malinowsky, D., Nolting, A., Svensson, M., Terp, G., Weigelt, D., & Dabrowski, M. (2013). Characterization of a ligand binding site in the human transient receptor potential ankyrin 1 pore. *Biophys J*, *104*(4), 798-806.
- Koplas, P. A., Rosenberg, R. L., & Oxford, G. S. (1997). The role of calcium in the desensitization of capsaicin responses in rat dorsal root ganglion neurons. *J Neurosci*, *17*(10), 3525-3537.
- Kremeyer, B., Lopera, F., Cox, J. J., Momin, A., Rugiero, F., Marsh, S., Woods, C. G., Jones, N. G., Paterson, K. J., Fricker, F. R., Villegas, A., Acosta, N., Pineda-Trujillo, N. G., Ramirez, J. D., Zea, J., Burley, M. W., Bedoya, G., Bennett, D. L., Wood, J. N., & Ruiz-Linares, A. (2010). A gain-of-function mutation in TRPA1 causes familial episodic pain syndrome. *Neuron*, *66*(5), 671-680.
- Kuang, Q., Purhonen, P., & Hebert, H. (2015). Structure of potassium channels. *Cellular and Molecular Life Sciences*, 1-17.
- Kwak, J., Wang, M. H., Hwang, S. W., Kim, T. Y., Lee, S. Y., & Oh, U. (2000). Intracellular ATP increases capsaicin-activated channel activity by interacting with nucleotide-binding domains. *J Neurosci*, *20*(22), 8298-8304.
- Kwan, K. Y., Allchorne, A. J., Vollrath, M. A., Christensen, A. P., Zhang, D. S., Woolf, C. J., & Corey, D. P. (2006). TRPA1 contributes to cold, mechanical, and chemical nociception but is not essential for hair-cell transduction. *Neuron*, *50*(2), 277-289.
- Liao, M., Cao, E., Julius, D., & Cheng, Y. (2013). Structure of the TRPV1 ion channel determined by electron cryo-microscopy. *Nature*, *504*(7478), 107-112.

- Lindemann, B. (2001). Receptors and transduction in taste. *Nature*, 413(6852), 219-225.
- Lishko, P. V., Procko, E., Jin, X., Phelps, C. B., & Gaudet, R. (2007). The ankyrin repeats of TRPV1 bind multiple ligands and modulate channel sensitivity. *Neuron*, 54(6), 905-918.
- Liu, B., Zhang, C., & Qin, F. (2005). Functional recovery from desensitization of vanilloid receptor TRPV1 requires resynthesis of phosphatidylinositol 4,5-bisphosphate. *J Neurosci*, 25(19), 4835-4843.
- Lukacs, V., Yudin, Y., Hammond, G. R., Sharma, E., Fukami, K., & Rohacs, T. (2013). Distinctive changes in plasma membrane phosphoinositides underlie differential regulation of TRPV1 in nociceptive neurons. *J Neurosci*, 33(28), 11451-11463.
- Macpherson, L. J., Dubin, A. E., Evans, M. J., Marr, F., Schultz, P. G., Cravatt, B. F., & Patapoutian, A. (2007). Noxious compounds activate TRPA1 ion channels through covalent modification of cysteines. *Nature*, 445(7127), 541-545.
- Matta, J. A., Cornett, P. M., Miyares, R. L., Abe, K., Sahibzada, N., & Ahern, G. P. (2008). General anesthetics activate a nociceptive ion channel to enhance pain and inflammation. *Proc Natl Acad Sci U S A*, 105(25), 8784-8789.
- Moiseenkova-Bell, V. Y., Stanciu, L. A., Serysheva, I., Tobe, B. J., & Wensel, T. G. (2008). Structure of TRPV1 channel revealed by electron cryomicroscopy. *Proc Natl Acad Sci U S A*, 105(21), 7451-7455.
- Montell, C., & Rubin, G. M. (1989). Molecular characterization of the *Drosophila* trp locus: A putative integral membrane protein required for phototransduction. *Neuron*, 2, 1313-1323.
- Paulsen, C. E., Armache, J. P., Gao, Y., Cheng, Y., & Julius, D. (2015). Structure of the TRPA1 ion channel suggests regulatory mechanisms. *Nature*, 520(7548), 511-517.
- Premkumar, L. S., & Abooj, M. (2013). TRP channels and analgesia. *Life Sci*, 92(8-9), 415-424.
- Rohacs, T., Thyagarajan, B., & Lukacs, V. (2008). Phospholipase C mediated modulation of TRPV1 channels. *Mol Neurobiol*, 37(2-3), 153-163.
- Sawada, Y., Hosokawa, H., Hori, A., Matsumura, K., & Kobayashi, S. (2007). Cold sensitivity of recombinant TRPA1 channels. *Brain Res*, 1160, 39-46.
- Siemens, J., Zhou, S., Piskrowski, R., Nikai, T., Lumpkin, E. A., Basbaum, A. I., King, D., & Julius, D. (2006). Spider toxins activate the capsaicin receptor to produce inflammatory pain. *Nature*, 444(7116), 208-212.

- Stein, A. T., Ufret-Vincenty, C. A., Hua, L., Santana, L. F., & Gordon, S. E. (2006). Phosphoinositide 3-kinase binds to TRPV1 and mediates NGF-stimulated TRPV1 trafficking to the plasma membrane. *J Gen Physiol*, 128(5), 509-522.
- Story, G. M., Peier, A. M., Reeve, A. J., Eid, S. R., Mosbacher, J., Hricik, T. R., Earley, T. J., Hergarden, A. C., Andersson, D. A., Hwang, S. W., McIntyre, P., Jegla, T., Bevan, S., & Patapoutian, A. (2003). ANKTM1, a TRP-like channel expressed in nociceptive neurons, is activated by cold temperatures. *Cell*, 112(6), 819-829.
- Teng, J., Loukin, S. H., Anishkin, A., & Kung, C. (2015). L596-W733 bond between the start of the S4-S5 linker and the TRP box stabilizes the closed state of TRPV4 channel. *Proc Natl Acad Sci U S A*, 112(11), 3386-3391.
- Tominaga, M., & Caterina, M. J. (2004). Thermosensation and pain. *J Neurobiol*, 61(1), 3-12.
- Trevisan, G., Materazzi, S., Fusi, C., Altomare, A., Aldini, G., Lodovici, M., Patacchini, R., Geppetti, P., & Nassini, R. (2013). Novel therapeutic strategy to prevent chemotherapy-induced persistent sensory neuropathy by TRPA1 blockade. *Cancer Res*, 73(10), 3120-3131.
- Trevisani, M., Siemens, J., Materazzi, S., Bautista, D. M., Nassini, R., Campi, B., Imamachi, N., Andre, E., Patacchini, R., Cottrell, G. S., Gatti, R., Basbaum, A. I., Bunnett, N. W., Julius, D., & Geppetti, P. (2007). 4-Hydroxynonenal, an endogenous aldehyde, causes pain and neurogenic inflammation through activation of the irritant receptor TRPA1. *Proc Natl Acad Sci U S A*, 104(33), 13519-13524.
- Venkatachalam, K., & Montell, C. (2007). TRP channels. *Annu Rev Biochem*, 76, 387-417.
- Wang, G., Qiu, Y. T., Lu, T., Kwon, H. W., Pitts, R. J., Van Loon, J. J., Takken, W., & Zwiebel, L. J. (2009). *Anopheles gambiae* TRPA1 is a heat-activated channel expressed in thermosensitive sensilla of female antennae. *Eur J Neurosci*, 30(6), 967-974.
- Winter, Z., Buhala, A., Otvos, F., Josvay, K., Vizler, C., Dombi, G., Szakonyi, G., & Olah, Z. (2013). Functionally important amino acid residues in the transient receptor potential vanilloid 1 (TRPV1) ion channel--an overview of the current mutational data. *Mol Pain*, 9, 30.
- Wu, L. J., Sweet, T. B., & Clapham, D. E. (2010). International Union of Basic and Clinical Pharmacology. LXXVI. Current progress in the mammalian TRP ion channel family. *Pharmacol Rev*, 62(3), 381-404.
- Zhang, W. Y., & Li Wan Po, A. (1994). The effectiveness of topically applied capsaicin. A meta-analysis. *Eur J Clin Pharmacol*, 46(6), 517-522.

Zygmunt, P. M., & Högestätt, E. D. (2014). Trpa1. In B. Nilius & V. Flockerzi (Eds.), *Mammalian Transient Receptor Potential (TRP) Cation Channels* (Vol. 1, pp. 583-630). Heidelberg, Germany: Springer.

Chapter 2

Engineering vanilloid sensitivity into avian TRPV1

2.1 Background and Approach

Since the channel was first cloned and characterized in 1997, TRPV1 has been the target of a staggering amount of biochemistry aimed at understanding the mechanisms behind activation by small molecules like capsaicin and resiniferatoxin (RTX) as well as activation by heat (Winter et al.). Multiple TRPV1 orthologs have been cloned, expressed heterologously, and their activation profiles by various stimuli studied in detail via electrophysiology and calcium influx assays. These studies have highlighted species-specific differences in channel sensitivity, which are now being leveraged to determine which residues play integral roles in TRPV1 activation.

In 2002, Jordt and Julius took advantage of the differing properties of the rat and chicken TRPV1 channels to identify functionally important regions (Jordt & Julius). The rat and chicken TRPV1 orthologs share 68% sequence identity and 79% amino acid sequence similarity. When expressed in *Xenopus* oocytes, both channels respond similarly to heat and pH, but that is not the case for vanilloid sensitivity. While rat TRPV1 is highly capsaicin sensitive with an EC_{50} of 40-200 nM (Caterina et al.; Hayes et al.; McIntyre et al.; Shin et al.; Tominaga et al.), chicken TRPV1 showed little to no response to capsaicin concentrations of up to 100 μ M (Jordt & Julius). The scientists also reported the activity of a chimera in which a region containing S3 and part of S4 of chicken TRPV1, residues 513-558, was replaced with the corresponding residues of rat TRPV1, 505-550 (Jordt & Julius). Unlike chicken TRPV1, the chimera, called V3/C, responded to capsaicin but not as well as rat TRPV1. Two residues, Y511 and S512, by the rat numbering, were confirmed as major contributors to capsaicin sensitivity of the chimera. From their position low on the S3 segment of the channel, Jordt and Julius

proposed that vanilloid molecules bind between S3 and S4 with the vanilloid moiety facing down towards the cytoplasm to interact with the sidechain of Y511 and the agonist tail pointing up towards the extracellular space (Jordt & Julius) . Because the V3/C chimera responded more weakly to capsaicin than wildtype rat TRPV1, we hypothesized that there may be other residues that play important roles in vanilloid sensitivity.

Gavva et al. reported similar studies of rat and rabbit TRPV1. Rabbit TRPV1 is one of the rare mammalian TRPV1 orthologs that is poorly sensitive to capsaicin and resiniferatoxin (Gavva et al.; Glinsukon et al.; Szallasi & Blumberg), despite the fact that rat and rabbit TRPV1 share 86% identity and 91% similarity. Through chimeras and mutagenesis Gavva et al. identified residues M547, T550, and W549 in the S4 helix as important determinants of vanilloid sensitivity. They proposed that W549 may stack with the vanilloid moiety of agonists, suggesting a head-up, tail-down mechanism for binding (Gavva et al.), opposite to what was proposed by Jordt and Julius.

In 2013, the first high resolution cryoEM structures became available, revealing the channel in apo form, bound to capsaicin, or bound to resiniferatoxin and double-knot toxin. Density was too weak for the vanilloid ligands to be unambiguously modelled, but the structures did reveal a pocket between the S4 and S5 helices where vanilloids density was observed. The molecular details of ligand binding were still a mystery, prompting additional biochemical and mutagenesis studies targeting the S4-S5 pocket.

Taking advantage of the number of available TRPV1 ortholog sequences and the TRPV1 structures (Cao et al.; Liao et al.) available at the time, we combined sequence conservation and structural information into a search for residues underlying the

species-specific differences in mammalian and avian TRPV1 vanilloid sensitivity. This generated a short list of candidate residues to evaluate. Rather than mutating mammalian TRPV1 and using loss of sensitivity to determine the necessity of candidate residues for vanilloid modulation, we aimed to engineer vanilloid sensitivity into the normally insensitive chicken TRPV1 homolog using a minimal set of mutations. We identified four residues near the vanilloid-binding pocket that contribute to capsaicin sensitivity, and the chicken TRPV1 quadruple pocket mutant was only 30-fold less sensitive to capsaicin than rat TRPV1. We also investigated residues near the pore regions and observed effects on both capsaicin sensitivity and activation cooperativity. Finally, we also compared the sensitivity of these mutant chicken TRPV1 channels to another vanilloid TRPV1 agonist, resiniferatoxin. Mutations that were able to confer capsaicin sensitivity also conferred resiniferatoxin sensitivity to the chicken TRPV1 channel. The results of these experiments lend information about the sufficiency of the residues to confer vanilloid sensitivity and can help us to understand how well the targeted residues encompass the mechanisms behind TRPV1 vanilloid sensitivity. We have identified a minimal set of mutations required to engineer vanilloid sensitivity into chicken TRPV. Also, in light of new high resolution structures of both TRPV1 and TRPV2, we propose roles for minimal set residues in providing vanilloid sensitivity.

2.2 Experimental Methods

2.2.1 Phylogenetic and structural analysis of TRPV1

In 2014, Eric Zheng, an undergraduate in the Gaudet Lab, curated a database of TRPV1 sequences publicly available from GenBank, manually removing duplicate and incomplete sequences. The 53 sequences of the resulting database were aligned using

ClustalW (Larkin et al.) and the BLOSUM80 matrix (Henikoff & Henikoff) in Geneious 9, and a phylogenetic tree was constructed using the neighbor-joining method with distances calculated by the Jukes-Cantor method (Jukes & Cantor). Mammalian and avian sequence logos were created using WebLogo v. 2.8.2 (Crooks et al.) based on the same multiple sequence alignment described above.

2.2.2 Insect Cell Culture

Sf9 and Sf21 cells were maintained as adherent cultures at 27°C in Hink's TNM-FH medium with L-glutamine, lactalbumin hydrolysate, and yeastolate without insect hemolymph (Corning) supplemented with 10% fetal bovine serum (Sigma-Aldrich) and 10 µg/ml gentamicin (Invitrogen). Cells were passaged by gentle sloughing when they reached 95% confluency and diluted down to 0.3-0.6 x 10⁶ cells/ml.

2.2.3 Plasmids and Cloning

pFastBac-cFLAG was generated from pFastBac1 (Invitrogen) by ligating a short double-stranded oligonucleotide, 5'-

TCGACACTAGTGACGTCGCGGCCGCTGATTACAAGGATGACGACGATAAGTG

A-3' and

'5-GGCCTCACTTATCGTCGTCATCCTTGTAATCAGCGGCCGCGACGTCAGTG-

3', into the Sal I and Not I sites of the vector (Lishko et al.). Mutant chicken TRPV1

plasmids were made by QuikChange (Agilent) site-directed mutagenesis of pFastBac-chicken TRPV1-cFLAG. Table 2.1 lists the templates and primers used to produce the mutants. The pFastBac plasmids for the single, double, and two of the triple pocket mutants as well as all of the pore mutants were generated by Eric Zheng. I cloned the

Table 2.1 Primers for QuikChange Mutagenesis of chicken TRPV1

Mutation	Forward Primer Sequence	Reverse Primer Sequence
A558T	CTGGGCTGGACTAACATGCTATACTACACCCG	CATGTTAGTCCAGCCCGAGCCAAAGGAGAAG
S574A	CATTTACGGCTGTCATGATCGCAAAGATGATCCTAAGAG	ATCATGACAGCGTAAATGCCCATCTGCTGGAAG
A578E	CTGTCATGATCGAAAAGATGATCCTAAGAGACTTATG	ATCTTTTCGATCATGACAGAGTAAATGCCCATCTG
L672A	CTTTTGGTTGCCATGTCATCCTTACGTACATCCTCCTG	GACATAGGCAACCAAAAGGATGACAAACACACAGACTTGAAC
S574A/A578E	CATTTACGCTGTCATGATCGAAAAGATGATCCTAAGAGACTTATG	CTTTTCGATCATGACAGCGTAAATGCCCATCTGCTGGAAG
S6: S664A/V667I/V671I	GGCTGTGTTTATCATCCTTTTGCCTTCTCTATGTCATCCTTACGTACAT	AAGCAAAAGGATGATAAACACACAGCCTTGAACCTGTAGTTCTCTG
Y639S	GTCGTATTCTACCTGCTTGGAACTTTTCAAGTTC	GCAGGTAGAATACAGACTGTTATAGGATGTGCC
L672A with S6	TTTTGCTTgcccTATGTCATCCTTACGTACATCATCCTGCTC	ATGACATAGGcCAAGCAAAAAGGATGATAAACACACAGCCTTGAACC

remaining two triple mutants and also generated combinations of pocket and pore mutants through two-piece Gibson Assembly with a small fragment containing the pore mutant region with desired mutations and a larger fragment consisting of the remainder of the channel and vector with three of the pocket mutations (A558T, S574A, and A578E). Table 2.2 details the templates and primers used to create the fragments for assembly. An additional round of QuikChange (Agilent) mutagenesis using the L672withS6 primer pair (Table 2.1) was needed to introduce the final mutation in constructs including both the S6 mutants and L672A. The open reading frames of all constructs were verified by sequencing.

2.2.4 Baculovirus-mediated Protein Expression

Baculovirus stocks for protein expression were produced as described in the Invitrogen Bac-to-Bac® Expression System Manual (Invitrogen) with minor alterations to ensure viral stock quality and purity. The resulting pFastBac vectors were transformed into DH10Bac *E. coli* cells for recombination of the TRPV1 sequence into bacmids, or viral genomes. Recombination results in disruption of lacZ on the bacmid, enabling an X-gal-based colorimetric detection of colonies with recombinant bacmids. Potentially recombinant colonies were picked and re-streaked on X-gal-containing plates to confirm clonal populations. Bacmids were purified from cultures of the colonies and double-checked for gene insertion via PCR with primers flanking the recombination site. Only recombinant bacmid stocks with no sign of contaminating empty bacmid were used to produce baculovirus stocks. P1 viral stocks were obtained by harvesting the medium of Sf21 cells 7-days post transfection with Cellfectin® II Reagent (ThermoFisher Scientific) and the bacmids of interest via the standard

Table 2.2 Primers for fragment generation for Gibson Assembly of Pocket+S6, Pocket+Y, and Pocket+S6/Y pFastBac vectors

Fragments	Forward Primer Sequence	Reverse Primer Sequence
Gibson Fragment 1 (Pore)	TCCACAGCTGTGGTGACTTT	AAAGTCACCACAGCTGTGGA
Gibson Fragment 2 (Vector and rest of cV1)	TACAAGGATGACGACGATAAG	CTTATCGTCGTCATCCTTGTA

protocol. Viral stocks were amplified by infecting fresh Sf21 cells with the P1 stocks (1 μ l per 0.5×10^6 cells in 1 ml of medium) and incubating at 27°C for an additional 7 days. The medium from that infection was harvested as the P2 viral stocks. P2 stocks were used for all protein expression.

For protein expression, Sf9 or Sf21 were infected with P2 viral stocks (10 μ l viral stock per 0.6×10^6 cells in 1 ml of medium). Cells were plated at 0.5 ml/well in 24-well tissue-culture treated plates for western blots or at 100 μ l/well in clear-bottomed black-walled sterile 96-well assay plates (Grenier) for calcium influx assays. Plates were incubated for 48-60 hours before use in western blots or fluorescence-based calcium influx assays.

2.2.5 Western blot analysis

Forty-eight to 60 hours post-transfection, adherent Sf9 or Sf21 cells were harvested by gentle sloughing. The cells were spun down and washed in cold PBS then lysed in 2X sodium dodecyl sulfate-containing loading dye. After heating the samples for 3 minutes at 60°C, I loaded samples and prestained protein ladder on a 10% polyacrylamide gel and ran the electrophoresis at 200V for 45-60 min. Protein was transferred to a polyvinylidene fluoride (PVDF) membrane via the semi-dry blotting method at 100 mA/hour/gel. Afterwards, I blocked the membrane for 45-60 minutes with 3% bovine serum albumin (BSA) in Tris-buffered saline with Tween-20 (TBST: 50 mM Tris-HCl, pH 7.5, 150 mM NaCl, and 0.1% Tween-20). Then, the membrane was incubated with an alkaline phosphatase-conjugated M2-anti-FLAG antibody (Sigma) diluted 1:2000 in TBST with 1% BSA. After three 10-minute rinses in TBST and a final rinse in TBS, bands were developed using the NBT/BCIP one-step kit (ThermoFisher)

according to the manufacturer's instructions. The reaction was quenched with 1% acetic acid and the blots were rinsed with water and dried before photographs.

2.2.6 Fluorescence-based calcium influx assays

Fluorescence-based calcium influx assays were used to test the activation of the wildtype and mutant TRPV1s in insect cells. For these assays, the standard bath solution consisted of 10 mM HEPES, 150 mM sodium gluconate, 10 mM sodium chloride, 10 mM glucose, 2 mM CaCl₂, and 0.02% Pluronic F-127 adjusted to pH 7.2 with sodium hydroxide. In pH and 2-APB assays, bath solution was modified to contain 1 mM probenecid. To prepare that solution, 200 mM probenecid stock was prepared in 1M NaOH. The probenecid stock was neutralized with an equal volume of 1M MES to form a final concentration of 100 mM probenecid. One milliliter of probenecid stock was added per 100 ml of the standard bath solution before final pH adjustment to 7.2. Forty-eight to sixty hours post infection, infected cells in black-walled assays 96-well plates were loaded with dye by replacing the medium with 100 µl per well of bath solution containing 5 µM Fura-2-AM, a membrane-permeable version of a fluorescent calcium indicator. During all subsequent steps the plates were protected from light to prevent bleaching of the dye. The plates were incubated for 45 minutes to allow dye uptake. Afterwards, the medium was replaced with fresh bath solution without dye to wash the cells. Then, the plates were incubated for an additional hour to allow endogenous esterases to convert the dye to the functional form, Fura-2. The medium was again removed and replaced with a final 50 µl of fresh bath solution for the assay.

Fura-2 is a calcium-sensitive ratiometric dye that can function in cells; when it binds calcium fluorescence from 340 nm excitation increases while fluorescence from

380 nm excitation decreases. As a result, the 340/380 ratio of fluorescence is used to monitor calcium influx into cells. A FLEX Station 3 Multi-mode Microplate Reader (Molecular Devices) was used to measure the fluorescence in 96-well plates seeded with TRPV1-expressing insect cells. During the course of a calcium influx assay, fluorescence at 510 nm from 340 and 380 nm excitation was measured every 5 seconds. After a 60 second baseline, the FLEX station integrated pipetting system added the compound of interest to a range of final concentrations across the plate. Note that pipetting briefly interferes with the fluorescence measurement, leading to a characteristic dip in fluorescent ratio at the time of compound addition. Activation of TRPV1 resulted in an influx of calcium through the channel, causing an increase in the Fura-2 fluorescence ratio. After an additional 120 seconds, ionomycin, an ionophore that facilitates calcium entry into cells, was added as confirmation of cell integrity and assay setup. Data from calcium influx assays are reported as the change in fluorescence ratio from the baseline (delta ratio) against time for a range of compound concentrations. Each trace is an average of three to four technical replicates, and the error bars represent standard error of the mean. The assay was repeated two or three times from independent transfections for each construct.

2.2.7 Dose-response curve analysis

Dose-response curves were generated from the calcium influx assay delta ratio vs. time traces. For the calculations, I considered the maximum response to be the average fluorescent ratio reached 110-120 seconds post addition of the agonist. The time point chosen was late enough after agonist addition to represent the plateau of the fluorescence ratio increase. Dose-response curves were fit to the maximum response

fluorescent ratio vs the log of the agonist concentration data using a 4-parameter sigmoidal model including values for EC_{50} , hill slope, maximum and minimum fluorescent ratios. For each dose-response curve, error bars represent the standard error of the mean for 3-4 technical replicates. EC_{50} values from independent experiments were averaged to get the final value for each TRPV1 construct.

2.3 Results

2.3.1 Choosing candidate residues of TRPV1 to target with mutations

In these experiments, we worked with rat and chicken TRPV1 as our model capsaicin-sensitive and capsaicin-insensitive homologs, respectively. The sequence differences between rat TRPV1 and chicken TRPV1 are spread along the channel (838 and 843 amino acids, respectively) with 275 differences in total. All sites are potential targets for mutagenesis of chicken TRPV1 in our efforts to engineer vanilloid sensitivity. Almost all previous biochemistry on rat TRPV1 (Winter et al.), as well as the available structural information (Cao et al.; Liao et al.) pointed to the transmembrane portion of the channel as the site of vanilloid action, allowing us to restrict the list of residues to 71 candidates from the S1-S6 region of TRPV1. However, only a subset of these residues are expected to underlie the rat and chicken species-specific difference in TRPV1 vanilloid sensitivity. The remaining residue differences reflect the divergence between the specific TRPV1 homologs, but do not necessarily have to be associated with the unique functional properties of the channels. Fortunately, there were over 50 unique sequences of TRPV1 from various organisms publicly available, allowing us to leverage phylogeny and conservation to infer which residues are most likely to be important for differential channel function. Note that the sequences available are skewed towards

mammals given the amount of research focused in model organisms similar to humans and classic neurobiology animal models (Figure 2.1).

Capsaicin sensitivity is a characteristic of not just rodent TRPV1; it has been confirmed in a number of mammalian TRPV1 orthologs including rat, mouse, guinea pig, dog, and human homologs (Caterina et al.; Correll et al.; Hayes et al.; Ohta et al.; Phelps et al.). I therefore assumed that capsaicin sensitivity is conserved throughout the mammalian clade. Similarly, we consider capsaicin insensitivity a feature of most, if not all avian TRPV1s, given the observation that various species of wild and domestic birds can consume chili peppers without adverse effects. I created two sequence logos from the transmembrane domain sequences of 36 mammalian TRPV1 sequences and 9 avian TRPV1 sequences, respectively (Figure 2.2). We then selected residues differentially conserved in the mammalian and avian clades as candidate residues for mutagenesis. For example, in the S4 segment, residue position 558 (chicken TRPV1 numbering) is a well-conserved alanine in avian TRPV1 sequences, but conserved as a threonine in the mammalian sequences (Figure 2.2). The fact that the residue is well conserved suggests that it is important for an element of channel function. Since residues at position 558 are both different in the mammalian and avian clades and conserved within each clade, it is probable that the residue plays a role in a function that also differs between the clades, such as vanilloid sensitivity. Indeed, it had already been identified as a residue important for vanilloid sensitivity (Gavva et al.; Jordt & Julius). Consequently, we included A558 (T550 in rat) in our list of candidate residues to mutate in chicken TRPV1 in the search for the minimum set of residues that confer

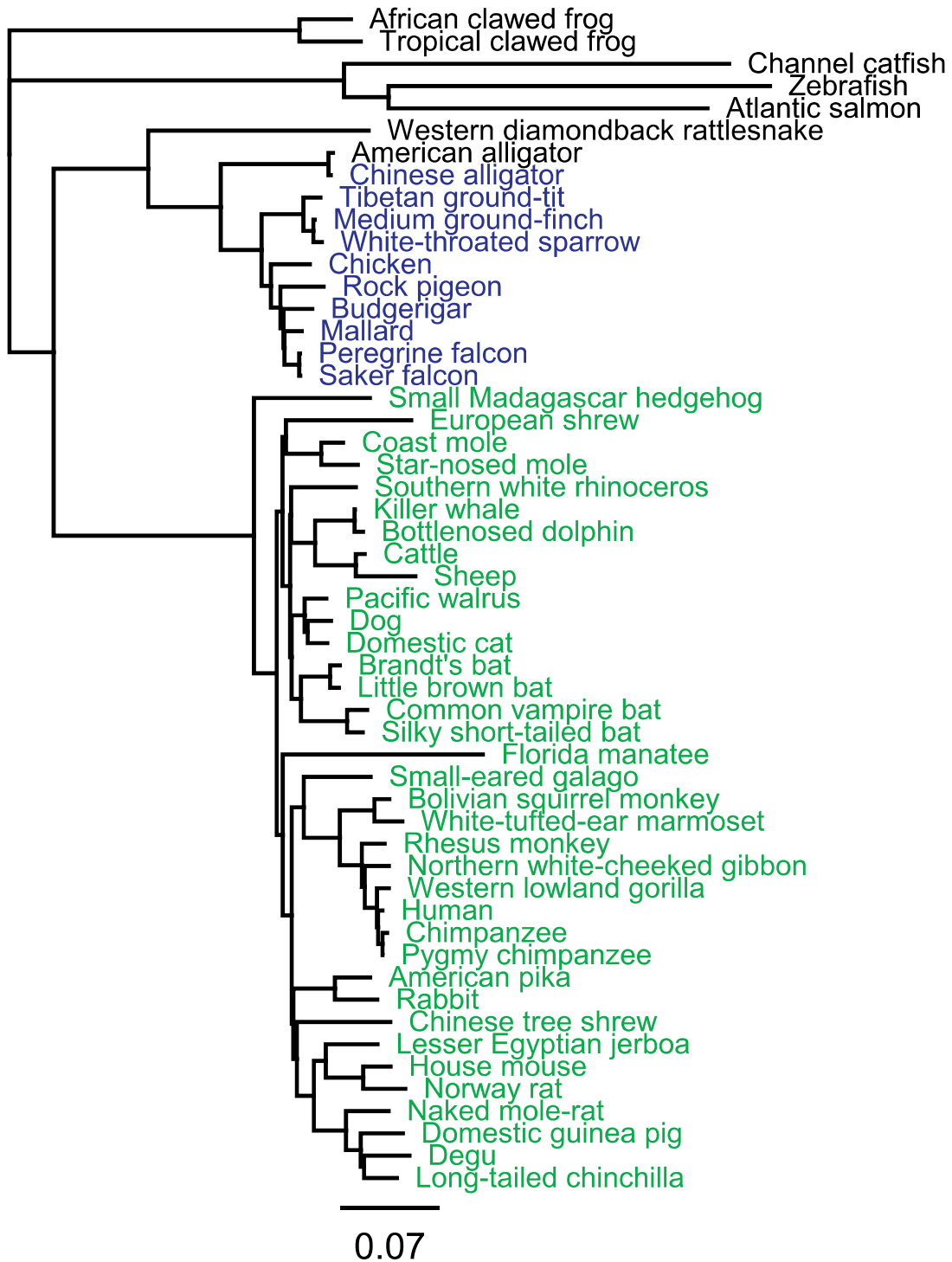


Figure 2.1 TRPV1 phylogenetic tree. Phylogenetic tree was constructed in Geneious 9 (Biomatters Limited) via the neighbor-joining method with all 53 unique TRPV1 sequences available from GenBank in 2014. A scale bar at the bottom indicates genetic distance calculated using the Jukes-Canton method (Jukes). Mammals are represented in green and birds in blue.

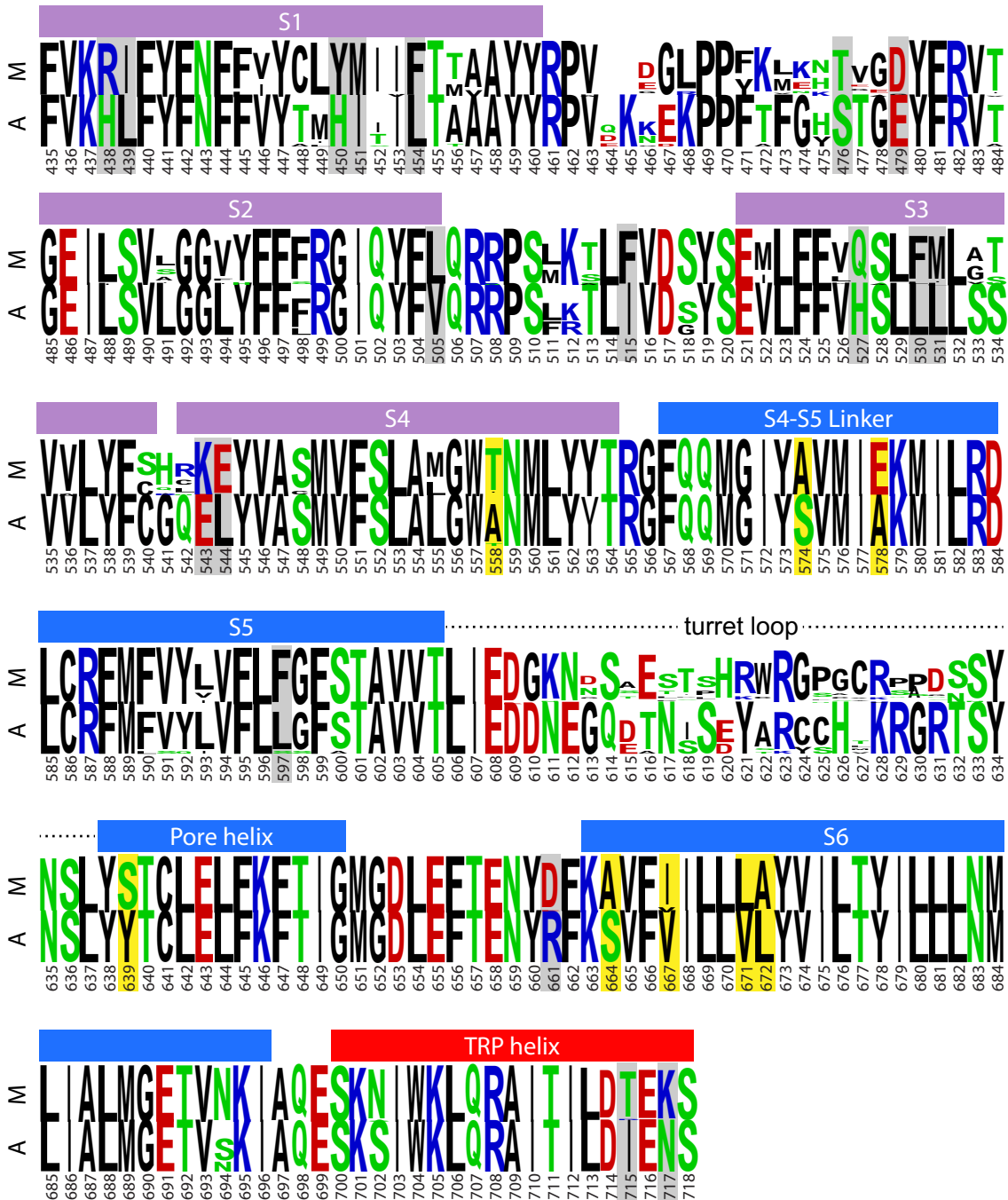


Figure 2.2 Alignment of mammalian and avian TRPV1 sequence logos highlight differentially-conserved residues. Mammalian (M) and avian (A) TRPV1 sequence logos were created using WebLogo (<http://weblogo.berkeley.edu/>) and Clustal W multiple sequence alignments of 36 mammalian sequences and 9 avian sequences. Above the logo, transmembrane helices are indicated with boxes color coded to match the TRPV1 structure color scheme. Chicken TRPV1 residue numbers are included below the logo. Differentially-conserved residues are indicated with gray and yellow boxes. Yellow boxes highlight the candidate residues chosen for mutagenesis.

vanilloid sensitivity. With those criteria, we identified 28 candidate residues in the S1-S6 segments of TRPV1 (Table 2.3).

To further narrow the list of candidate residues, we sought to incorporate structural information, plotting those 28 candidate residues on the available high-resolution structure of rat TRPV1 bound to double-knot toxin and resiniferatoxin, PDB ID: 3j5q (Cao et al.) (Figure 2.3). The majority of the candidate residues are positioned in the extracellular loops or near the periphery of the channel, but there are two apparent clusters of candidate residues: one cluster near the newly-recognized, resiniferatoxin-containing S4-S5 pocket (Gao et al.)(Figure 2.3) and a second cluster near the pore of TRPV1 (Figure 2.3). Clusters of residues are most likely to denote regions of the channel with a specific function, so we focused on the pocket and pore regions. According to the chicken TRPV1 numbering, the “pocket” cluster of residues includes A558 on S4, S574 and A578 on the S4-S5 linker, and L672 from the S6 helix of an adjacent subunit of TRPV1 (Figure 2.3). Those residues correspond to T550, S566, E570, and A665 in rat, respectively. The “pore” cluster of residues includes S664, V667, and V671 on the S6 helix, and Y639 at the top of the pore helix of an adjacent subunit (Figure 2.3). Those residues are A657, I660, I664, and S632 in rat TRPV1. Combining sequence and structure information, we have thus narrowed our candidate list to eight residues. Note that our list of candidate residues shares only one residue, T550, in common with the chimeric region of the V3/C chimera by Jordt and Julius (Jordt & Julius). We focused on these eight residues, mutating them in chicken TRPV1 singly and in combination to determine the minimal set of changes necessary to confer vanilloid sensitivity to the chicken TRPV1 homology. The basic set of chicken

Table 2.3 Candidate residues for minimal set of mutations to confer vanilloid sensitivity to chicken TRPV1

Location	Chicken Residue	Rat Residue
S1 Helix	H438	R432
	L439	I433
	H550	Y444
	I451	M445
	L454	F448
S1-S2 Loop	S476	T468
	E479	D471
S2 Helix	V505	L497
S2-S3 Loop	I515	F507
S3 Helix	H527	Q519
	L530	F522
	L531	M523
S4 Helix	E543	K535
	L544	E536
	A558*	T550
S4-S5 Linker	S574	A566
	A578	E570
S5 Helix	L597	F589
Pore Helix	Y639	S632
S6 Helix	R661	D654
	S664	A457
	V667	I660
	V671	L664
	L672	A665

*Bold residues indicate the final set chosen for analysis

Adapted from (Zheng).

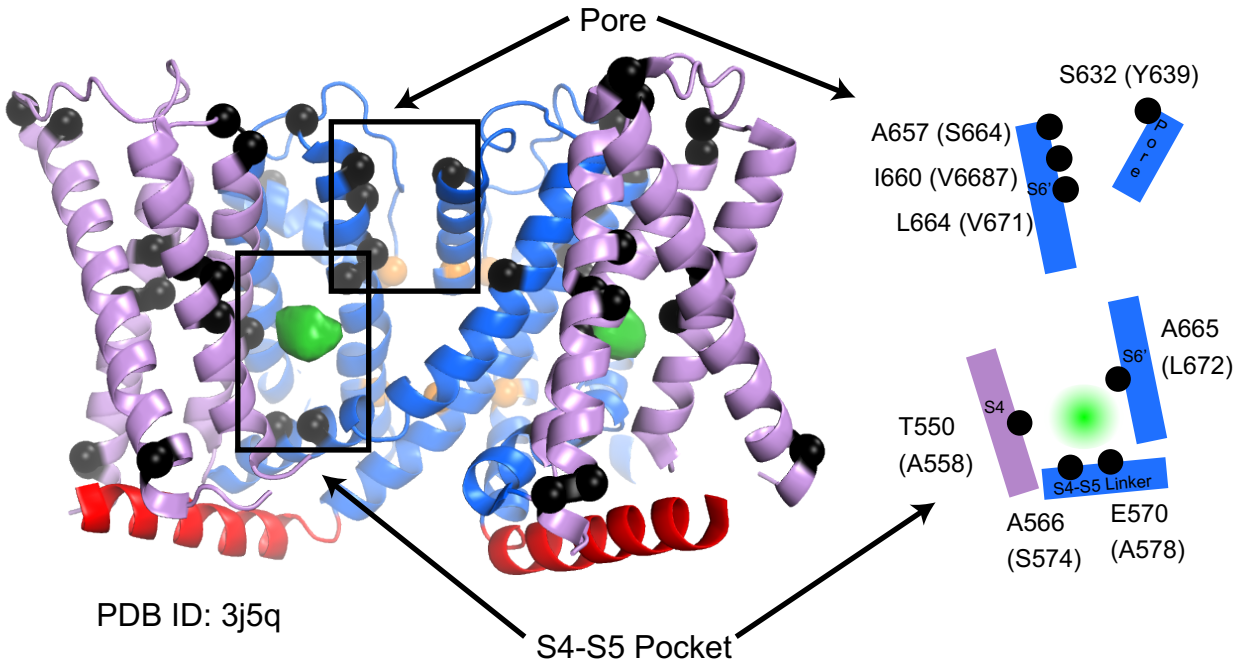


Figure 2.3 Differentially-conserved residues in the TRPV1 transmembrane domain form two clusters of residues near the channel pore and the S4-S5 pocket. The positions of differentially conserved residues in mammalian and avian TRPV1 clades are marked with black spheres on a cartoon representation of the rat TRPV1 transmembrane domain structure (PDB ID 3j5q). The S1-S4 transmembrane segments are illustrated in lavender. The S5-S6 segments and pore helices are in blue and the TRP box helix is shown in red. Gate residues are shown as gold spheres. Density for resiniferatoxin in the S4-S5 pocket is depicted as a neon green surface. The S4-S5 pocket and pore regions are indicated with black boxes. Simplified diagrams of the pocket and pore regions are included on the right with the rat residue numbers, followed by the chicken residue number in parentheses.

TRPV1 mutants near the S4-S5 pocket included all four single mutants (A558T, S574A, A578E, and L672A), upper and lower pocket double mutants (A558T/L672A and S574A/A578E), all possible pocket triple mutants, and the quadruple mutant (A558T/S574A/A578E/L672A). The pore mutation constructs include the S6 triple mutant (S664A/V667I/V671I), and single mutant Y639S, and the combined mutant S6/Y (Y639S/S664A/V667I/V671I). Pocket and pore combination mutants included the S6, Y, and S6/Y constructs combined with the pocket quadruple mutations (Figure 2.4). By analyzing these mutant TRPV1 constructs, we aimed to identify the minimal set of changes necessary to confer vanilloid sensitivity to chicken TRPV1.

2.3.2 All constructs are well-expressed in baculovirus-infected insect cells.

We chose insect cells as our system due to the robust nature of baculovirus-based protein expression. This system had been previously used in our lab to characterize rat TRPV1 via calcium influx assays and electrophysiology (Lishko et al.). To begin, I checked the expression of all of the WT and mutant TRPV1 constructs by western blot against the C-terminal FLAG tag. For all constructs, including the Julius lab V3/C chimera, whole-cell lysates of baculovirus-infected cells showed similar protein expression (Figure 2.5), indicating that they were all suitable for further analysis in calcium influx assays.

2.3.3 Capsaicin sensitivities of rat TRPV1, chicken TRPV1, and the V3/C chimera

The overall goal of these experiments was to engineer vanilloid sensitivity into capsaicin-insensitive chicken TRPV1. So, to begin, we tested the capsaicin sensitivities of chicken TRPV1, rat TRPV1 and the V3/C chimera in insect cells via fluorescence-

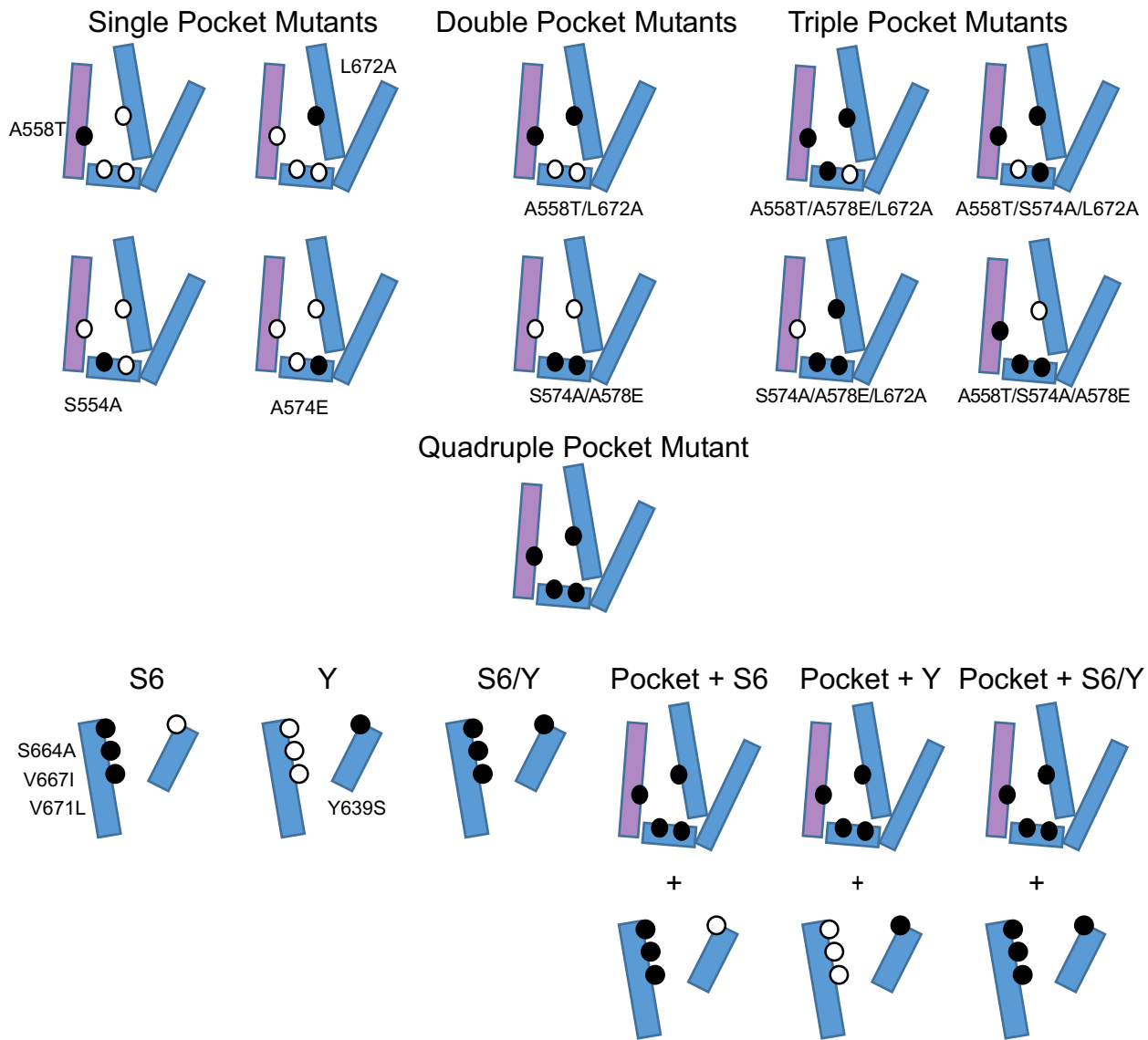


Figure 2.4 Diagrams of all chicken TRPV1 mutant constructs. All the combinations S4-S5 pocket and pore mutations tested in our experiments are diagrammed here. The S4 helix is depicted as a lavender rectangle and the S4-S5 linker, S5, S6, and pore helices are in blue. The eight pocket and pore candidate residue positions are denoted as circles. Black circles indicate the residues mutated in chicken TRPV1 to the corresponding rat TRPV1 residue in each construct.

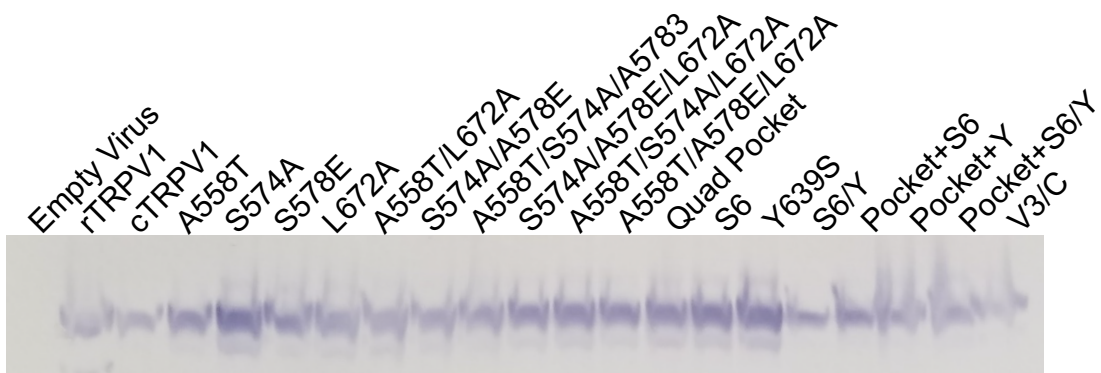


Figure 2.5. All TRPV1 constructs are well-expressed in insect cells. A western blot of whole-cell lysates from baculovirus-infected Sf9 cells against the C-terminal FLAG tag of all constructs show expression of all TRPV1 constructs at similar levels.

based calcium influx assays. In short, during calcium influx assays, channel-expressing insect cells were loaded with a calcium-sensitive fluorescent dye, Fura-2. Upon calcium influx into the cells, the ratio of fluorescence emission due to excitation at 340 and 380 nm increases, creating a way to monitor channel activation. I used a FLEX Station III Fluorescence Microplate Reader to record responses to multiple concentrations of capsaicin for each construct. The data are represented as the change in the fluorescence ratio from the baseline (delta ratio) against time. Dose-response curves were generated from the maximum delta ratio value for multiple concentrations of agonist. In agreement with previous experiments, insect cells expressing rat TRPV1 have robust responses to capsaicin with an EC_{50} of $0.20 \pm 0.05 \mu\text{M}$, while chicken TRPV1-expressing cells and control cells infected with empty virus do not have any response to up to $100 \mu\text{M}$ capsaicin (Figure 2.6A). Interestingly, the V3/C chimera that the Julius lab reported was capsaicin sensitive did not show a response to up to $100 \mu\text{M}$ capsaicin in our insect cell-based calcium influx assays (Jordt & Julius). There was no EC_{50} value reported for the V3/C chimera in the original report, but the relative current amplitudes suggest that the channel is less sensitive to capsaicin than rat TRPV1 (Jordt & Julius). This suggests that our insect-cell based calcium influx assay system may be less sensitive than the electrophysiology-based techniques used by the Julius lab to identify capsaicin-sensitive channels (Jordt & Julius). This suggested that our assay would work well to identify highly vanilloid sensitive channels, but may miss more weakly sensitive channels.

2.3.4 Combinations of mutations in the S4-S5 pocket confers capsaicin sensitivity to chicken TRPV1

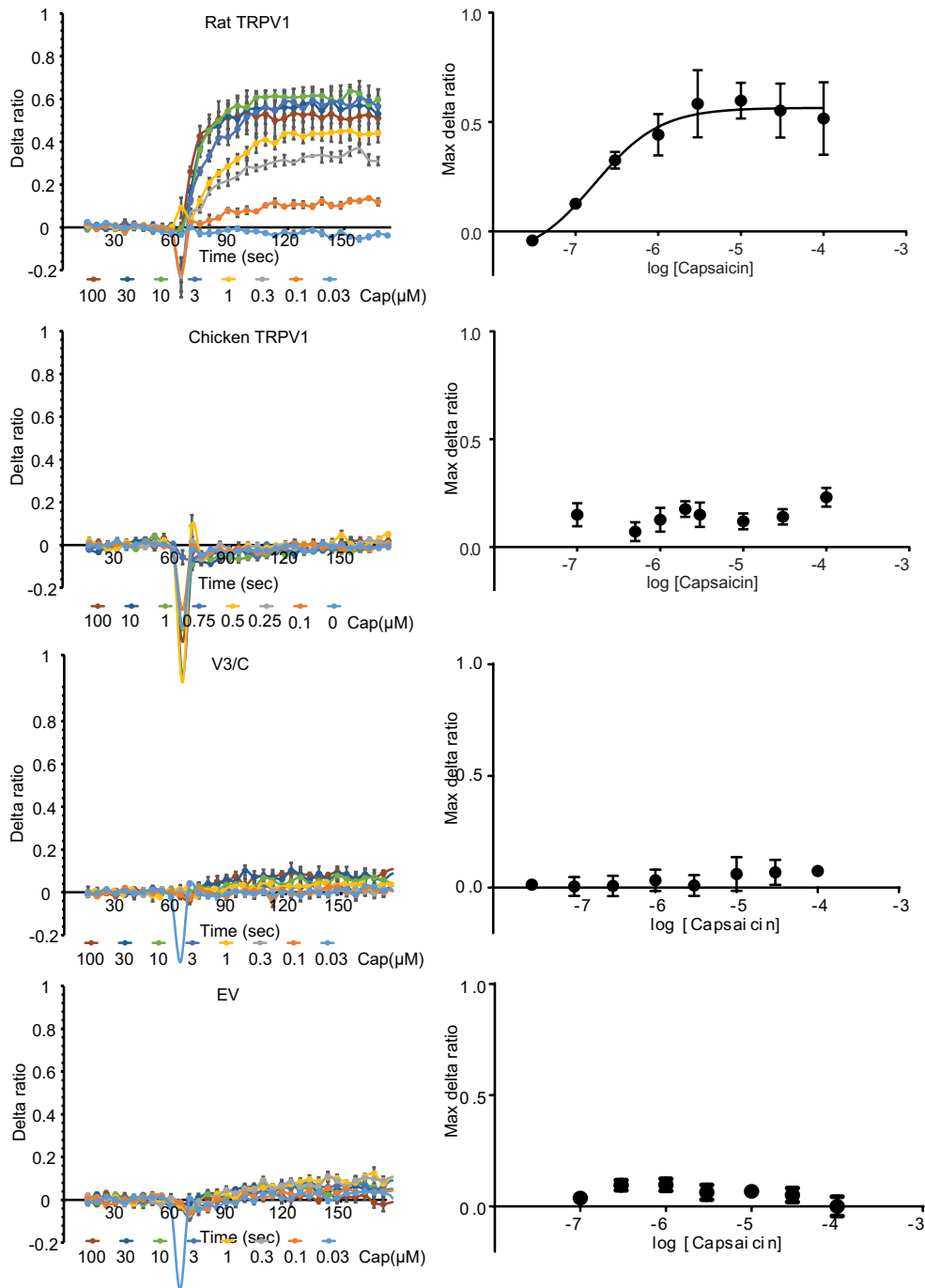


Figure 2.6 Capsaicin responses of rat and chicken TRPV1, V3/C and empty virus-infected insect cells. (Left) Representative calcium influx assay traces are presented as the change in 340/380 fluorescence ratio of a calcium-sensitive dye from the baseline value against time. Capsaicin was added at the indicated concentrations at 60 seconds. Traces are the average of 3-4 replicates with error bars representing standard error of the mean. Only rat TRPV1 is activated by capsaicin, causing an increase in delta ratio. (Right) Max delta ratio responses are plotted for each capsaicin concentration. For rat TRPV1 the data were fit to a 4-parameter sigmoidal model to generate the corresponding dose-response curve.

We initially focused on the four candidate residues of the S4-S5 pocket, which are in close proximity to the proposed vanilloid binding site, and first tested the capsaicin sensitivity of the chicken TRPV1 quadruple pocket mutant (A558T/S574A/A578E/L672A) using the calcium-influx assay. It is activated by capsaicin with an EC₅₀ of 5.9 ± 1.9 μM (Figure 2.7). Table 2.4 summarizes the EC₅₀ values and Hill slopes for all constructs. The apparent sensitivity is at least 100-fold higher than that of the wildtype chicken TRPV1, and only 30-fold lower than rat TRPV1. We have thus succeeded in generating a capsaicin-sensitive chicken TRPV1 variant.

To determine which of the pocket mutations contribute to this dramatic increase in capsaicin sensitivity, we first analyzed the effects of single mutants in the S4-S5 pocket on capsaicin-dependent calcium influx responses. None of the single A558T, S574A, A578E, or L672A mutants responded to even the highest concentration of capsaicin, 100 μM (Figure 2.8). Therefore, single mutations alone were not sufficient to confer capsaicin sensitivity to chicken TRPV1.

Next, we looked at the capsaicin sensitivity of combinations of pocket mutations to see if they would also be sufficient to confer capsaicin sensitivity. We analyzed two double mutants that targeted the upper pocket region or lower pocket region, A558T/L672A and S574A/A578E, respectively. Neither double mutation conferred capsaicin sensitivity to chicken TRPV1 (Figure 2.8).

Conversely, several of the triple mutants within the pocket did respond to capsaicin (Figure 2.7). The capsaicin sensitivities for the triple mutants were too low to generate fully saturating dose response curves due to capsaicin solubility constraints. Nevertheless, comparing the accessible regions of the dose response curves and

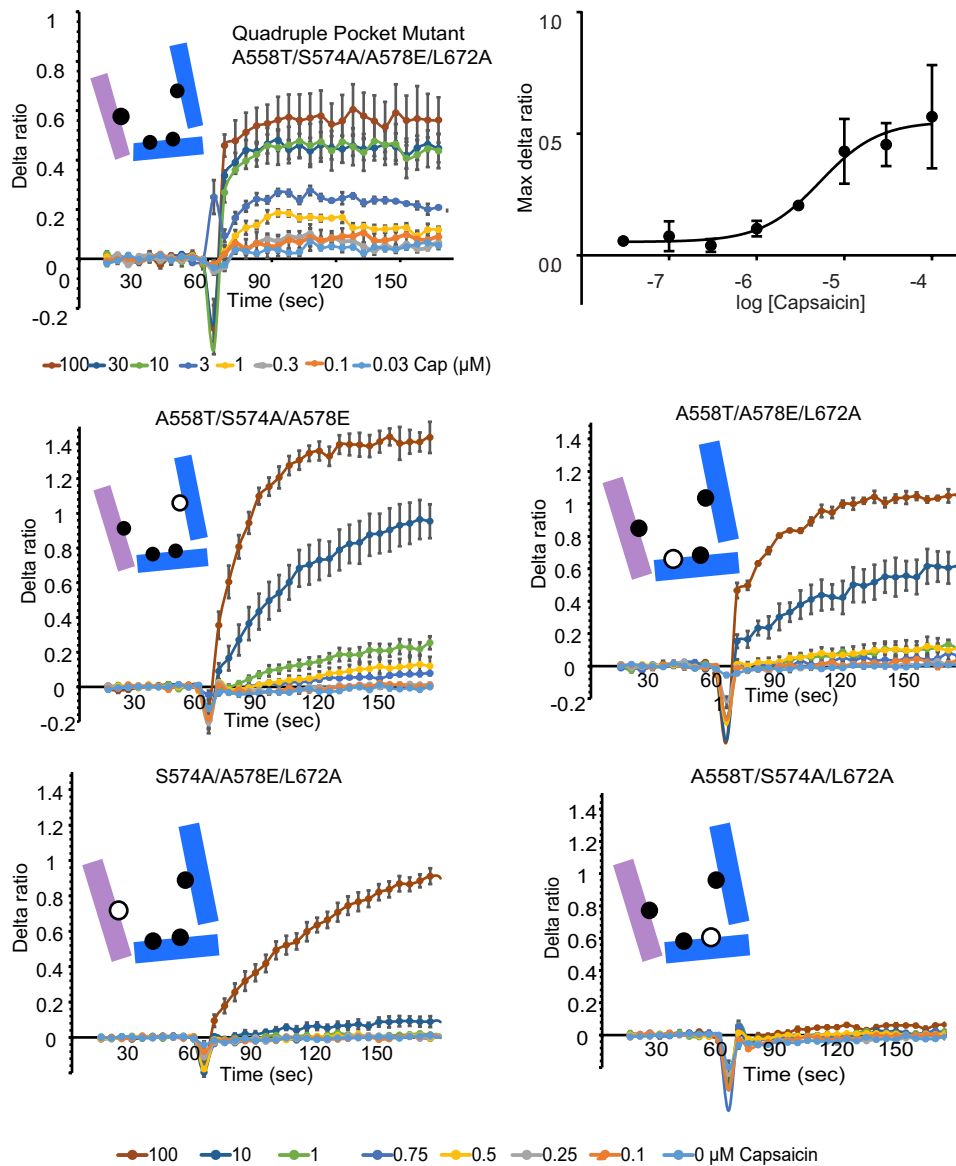


Figure 2.7 Quadruple pocket mutant and three pocket triple mutants respond to capsaicin. Representative calcium influx assay traces are presented as the change in 340/380 fluorescence ratio of a calcium-sensitive dye from the baseline value against time for each construct. Capsaicin was added at the indicated concentrations at 60 seconds. Traces are the average of 3-4 technical replicates and error bars depict standard error of the mean. The quadruple mutant and three of the triple mutants all display increases in fluorescence, signaling channel activation by capsaicin. Only the quadruple pocket mutant traces reached saturation and those data were fit to a 4-parameter sigmoidal model to generate the corresponding dose-response curve.

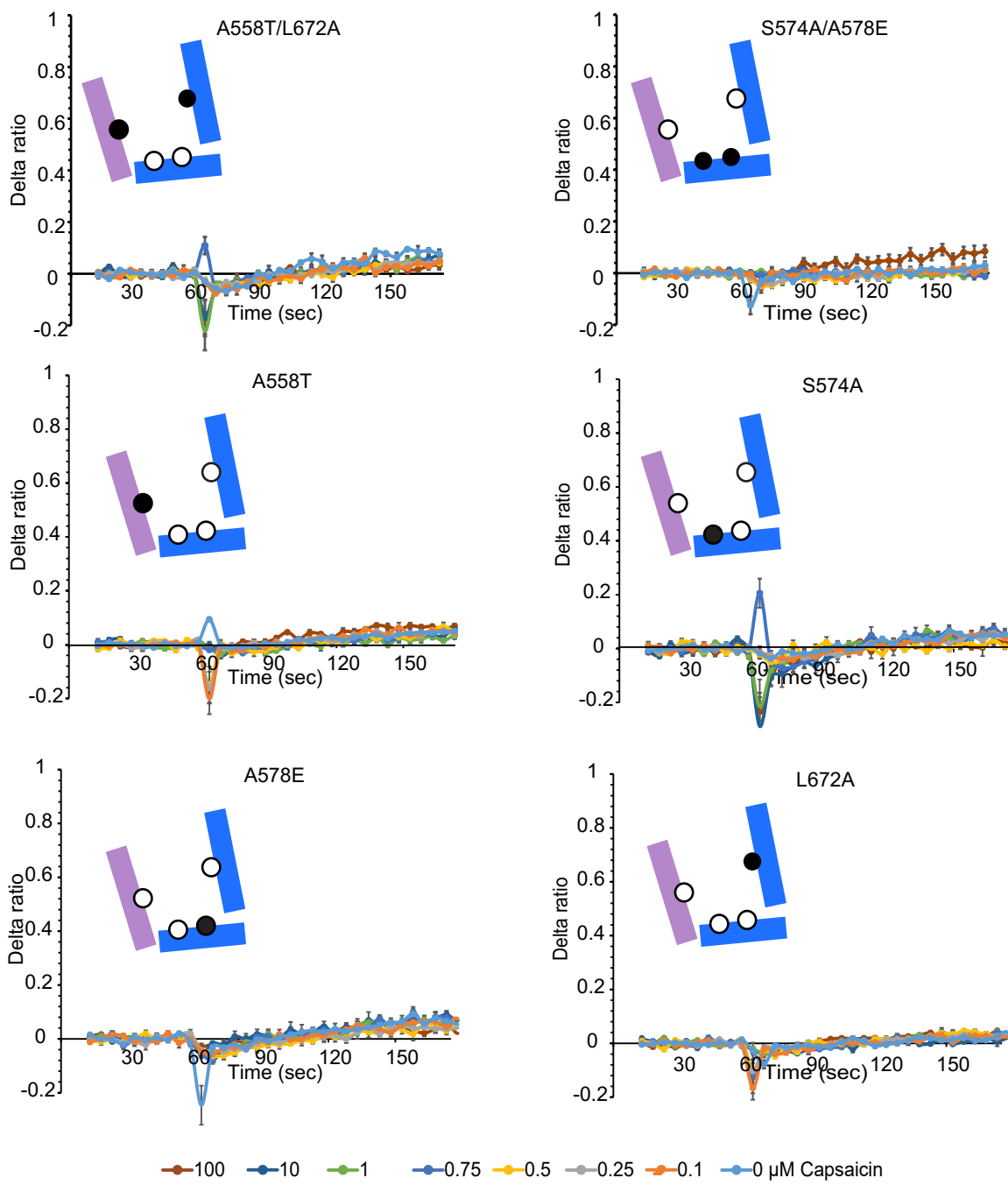


Figure 2.8 Neither single or double pocket mutants respond to capsaicin. Representative calcium influx assay traces are presented as the change in 340/380 fluorescence ratio from the baseline value against time. Capsaicin was added at the indicated concentration at 60 seconds. Traces are the average of 3-4 technical replicates and error bars depict standard error of the mean

estimating lower limits for EC_{50} values allows us to determine the relative sensitivities of pocket mutants and infer the relative importance of each mutation in conferring capsaicin sensitivity. All four pocket triple mutants have a lower sensitivity to capsaicin than the quadruple mutant, confirming that all four mutations assist in boosting capsaicin sensitivity of chicken TRPV1. Not all triple mutants have comparable capsaicin sensitivities, indicating that not all the mutations contribute equally. For example, the A558T/S574A/L672A triple mutant has the lowest sensitivity to capsaicin, displaying no response to 100 μ M capsaicin (Figure 2.7). In this mutant, the EC_{50} for capsaicin is greater than 100 μ M, very different from the sensitivity of the quadruple mutant or any of the other triple mutants. From that we infer that A578E mutation has the highest contribution to capsaicin sensitivity. The S574A/A578E/L672A triple mutant has slightly higher capsaicin sensitivity, responding modestly to 100 μ M capsaicin (Figure 2.7), suggesting that the EC_{50} for capsaicin is much greater than 10 μ M. Compared to the quadruple pocket mutant, S574A/A578E/L672A is missing the A558T mutation, which we thus assign as likely the second-most important change for conferring capsaicin sensitivity. The remaining triple mutants A558T/A574A/L672A and A558T/S574A/A578E have the highest capsaicin sensitivities, although their EC_{50} values were still above 10 μ M (Figure 2.5). This indicates that, of the four pocket mutations, S574A and L672A contribute the least. Written in terms of rat TRPV1 residues, restoring the equivalent of E570 has the most effect on capsaicin sensitivity, followed by T550, and then A566 and A665.

2.3.3 Pore mutations boost the capsaicin sensitivity of the pocket quadruple mutant

Unlike the pocket residues, the four candidate pore residues, Y639, S664, V667, and V671, are not near the proposed vanilloid binding site (Figure 2.3) and have not previously been linked to vanilloid sensitivity by biochemical experiments. Based on the relative position of the pore candidate residues, we tested the vanilloid sensitivity of, an S6 triple mutant (S664A/V667I/V671I), the Y639S mutant, and the pore quadruple mutant S6/Y (Y639S/S664A/V667I/V671I). Neither the S6 triple mutant, the Y639S single mutant, nor the S6/Y pore quadruple mutant responded to 100 μ M capsaicin (Figure 2.9). On their own, the pore mutants were unable to confer capsaicin sensitivity singly or in combination.

The candidate pore residues originally stood out for their strong differential conservation in mammalian and avian TRPV1, suggesting they may still play an indirect role in their differential chemical agonist sensitivity. Therefore we tested whether mutating those pore residues in the background of the already capsaicin-sensitive quadruple pocket chicken TRPV1 mutant had any effect on the capsaicin response. We found that combining some or all of the four pore mutations with the four mutations in the S4-S5 pocket modestly increased the capsaicin sensitivity above that of the quadruple pocket mutant alone (Figure 2.6). The most sensitive mutants were the pocket+S6 and pocket+S6/Y (i.e. full octuple mutant), which have EC_{50} values of 2 ± 1 μ M and 2.1 ± 0.7 μ M, respectively, just 10-fold less than that of rat TRPV1 (Table 2.4).

The pore mutations also affected the Hill slope, or steepness, of the capsaicin responses (Table 2.4). For example, rat TRPV1 and the quadruple pocket chicken TRPV1 mutant have similar Hill slopes of 1.2 ± 0.6 and 1.3 ± 0.4 , respectively. In contrast, Hill slopes for the Pocket+Y, and pocket+S6/Y mutants are slightly higher at

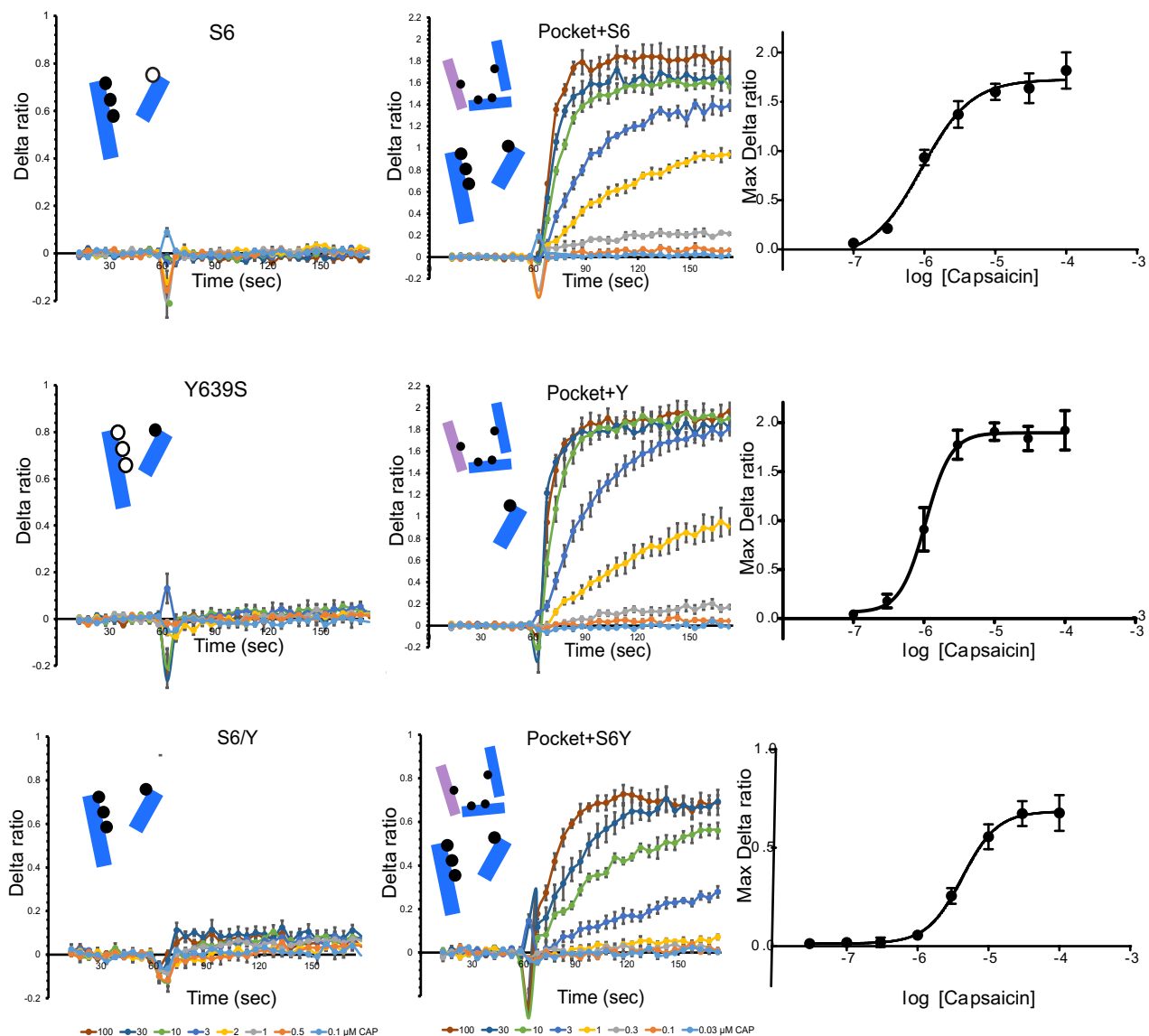


Figure 2.9 Pore mutations enhance the capsaicin sensitivity when combined with pocket mutations. (Left and Middle) Representative calcium influx assay traces are presented as the change in 340/380 fluorescence ratio from the baseline value against time. Capsaicin was added at the indicated concentrations at 60 seconds. Traces are the average of 3-4 technical replicates and error bars depict standard error of the mean. While the pore mutants do not confer capsaicin activation on their own, they do boost capsaicin sensitivity (Right) Max delta ratio responses are plotted for each capsaicin concentration. The data were fit to a 4-parameter sigmoidal model to generate the corresponding dose-response curve.

1.7 ± 0.8 and 1.7 ± 0.6 , respectively. This suggests that the Y639S mutation may affect the cooperativity of activation.

2.3.6 Mutations that confer capsaicin sensitivity also confer sensitivity to resiniferatoxin

Given the success in creating capsaicin-sensitive chicken TRPV1 channel constructs, we also tested whether our mutants could be activated by another vanilloid agonist, resiniferatoxin. Analogous to the case for capsaicin, rat TRPV1 expressed in insect cells was highly sensitive to resiniferatoxin, with an EC_{50} value of 80 ± 10 nM (Figure 2.10). Our resiniferatoxin EC_{50} value is a bit higher than the reported range of 0.3-11 nM (Shin et al.; Szallasi & Blumberg). In contrast, chicken TRPV1-expressing cells did not respond to the highest resiniferatoxin concentration tested, 3 μ M. Interestingly, all capsaicin-responsive chicken TRPV1 mutant constructs also responded to resiniferatoxin, supporting a case for a shared binding pocket for both vanilloid molecules. The quadruple pocket mutant responded well to resiniferatoxin with an EC_{50} of 230 ± 15 nM, demonstrating that mutations in the S4-S5 pocket also confer resiniferatoxin sensitivity. Interestingly, adding the pore mutants seemed to hamper resiniferatoxin sensitivity, as evidenced by the EC_{50} of the Pocket+S6/Y mutant, 400 ± 90 nM. This is the opposite of what was observed for capsaicin sensitivity, which suggests that, while similar, there are differences in mechanism between capsaicin and resiniferatoxin activation of TRPV1. Of note, a small response to 3 μ M resiniferatoxin was also observed for A558T/S574A/L672A, the pocket triple mutant that did not respond to 100 μ M capsaicin. This supports the idea that this mutant channel is

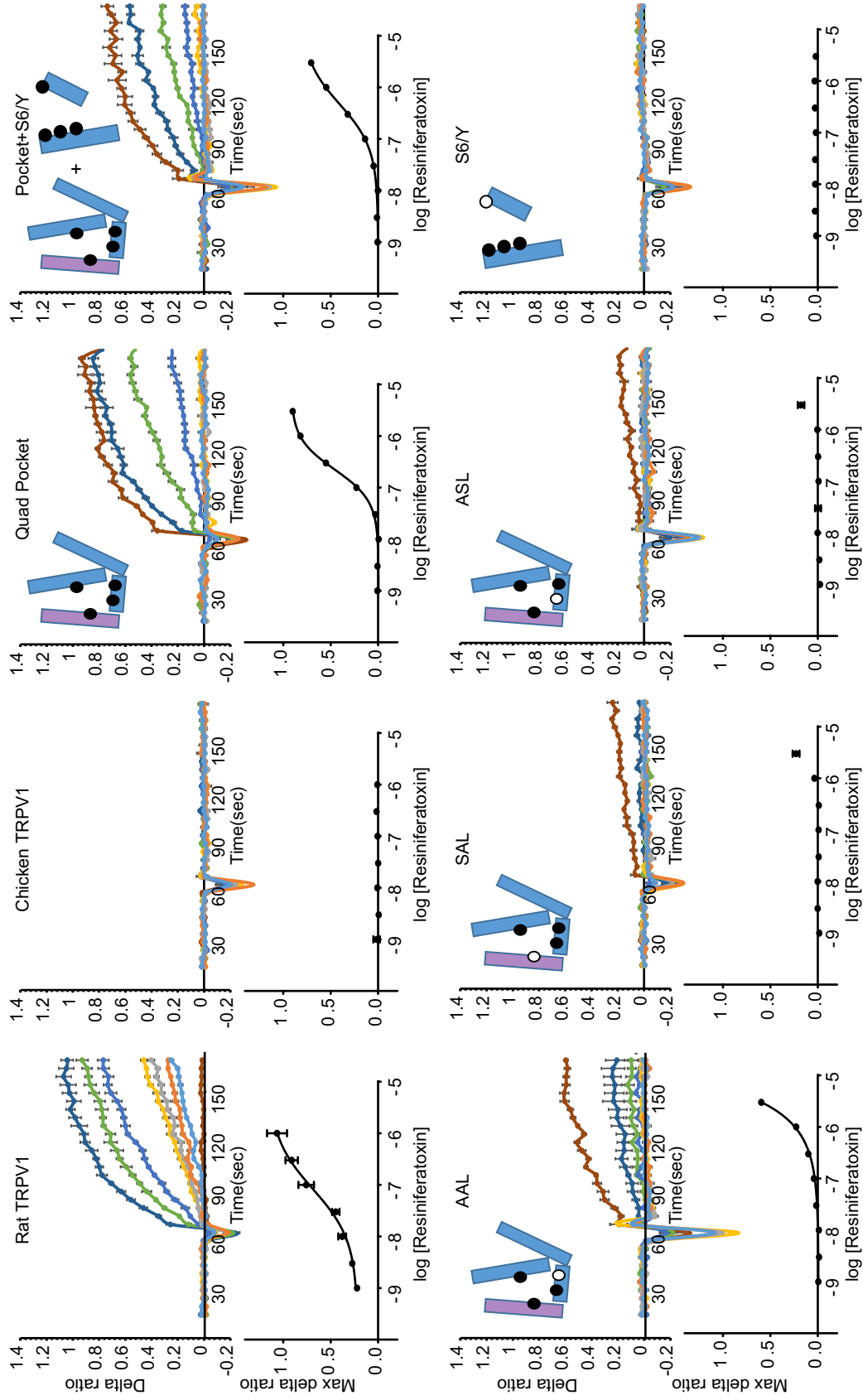


Figure 2.10 Pocket and pore mutations confer resiniferatoxin sensitivity in calcium influx assays. Representative calcium influx assay traces are presented as the change in 340/380 fluorescence ratio from the baseline value (delta ratio) against time. Capsaicin was added at the indicated concentration at 60 seconds. Traces are the average of 3-4 technical replicates and error bars depict standard error of the mean. Below the traces, max delta ratio responses are plotted for each capsaicin concentration. The data were fit to a 4-parameter sigmoidal model to generate the corresponding dose-response curves.

functional and just weakly responsive to vanilloid compounds, although these data are preliminary as additional replicates are necessary for improved confidence.

2.3.7 Testing channel activation by non-vanilloid activators

Many of the chicken TRPV1 mutants we tested were unresponsive to both capsaicin and resiniferatoxin. If we could show that these channels respond to another stimulus, such a finding would confirm that they were not simply misfolded, mislocalized, or otherwise non-activatable and that the lack of vanilloid response is, in fact, indicative of low vanilloid sensitivity. Testing heat sensitivity is unfortunately not an option due to endogenous heat-activated currents in insect cells (Lishko et al.). We thus attempted to test whether the channels could be activated by an independent stimulus like acidic pH, or the general TRP channel activator, 2-aminoethoxydiphenyl borinate (2-ABP), which activates rat TRPV1 (Hu et al.). Rat and chicken TRPV1 expressed in *Xenopus* oocytes or HEK cells do respond to low pH (Caterina et al.; Jordt & Julius). I attempted to use the insect-cell based calcium influx assay to test the pH responses of each of our TRPV1 channels. After the 60-second baseline, bath solution containing HCl was added such that the final solution in each well had a pH of 5.5-6.4 (The pH of the resulting solution measured with a pH meter after replicating the dilution in larger volumes of bath solution). I modified the standard assay bath solution to include 1 mM probenecid, an inhibitor of organic anion transporters, after noticing that lowering the pH prompted TRPV1-independent decreases in fluorescence ratio (Di Virgilio et al.). At pH 5.5 even empty virus-infected cells showed a response in the calcium influx assay, so I also tried altering the buffering system from HEPES to Bis-Tris, which has a buffering range that covers the low pH being tested. While I was able

to see a response above the background for rat TRPV1, I did not observe any significant chicken TRPV1-specific pH response in insect cells (Figure 2.11). They were likely obscured by the large endogenous pH responses in insect cells. As a result, acidic activation is not a viable option for screening my constructs.

Next, I tried activation of TRPV1 by 2-APB, a molecule reported to activate a range of TRPV channels expressed in HEK cells (Hu et al.). No responses to either 100 or 300 μM 2-APB were seen in rat or chicken TRPV1-expressing insect cells (Figure 2.12). The heterologous system-dependent activation of TRPV1 by 2-APB would be consistent with the molecule being an indirect activator of TRPV1.

Even in the absence of an independent method to verify channel function, we can still confidently make conclusions based on our chicken TRPV1 mutants. For example, it is clear that introducing certain mutations causes capsaicin sensitivity, but we cannot claim that a lack of capsaicin sensitivity seen in any chicken TRPV1 mutant is a direct result of a missing mutation. That would require some form of confirmation that the channel is at all functional before posing hypotheses on why the channel is capsaicin insensitive.

2.4 Discussion

2.4.1 The significance of engineering a capsaicin-sensitive avian TRPV1

The combined phylogenetic and structural approach to selecting candidate residues responsible for the vanilloid sensitivity difference between rat TRPV1 and chicken TRPV1 proved highly successful. By identifying differentially-conserved

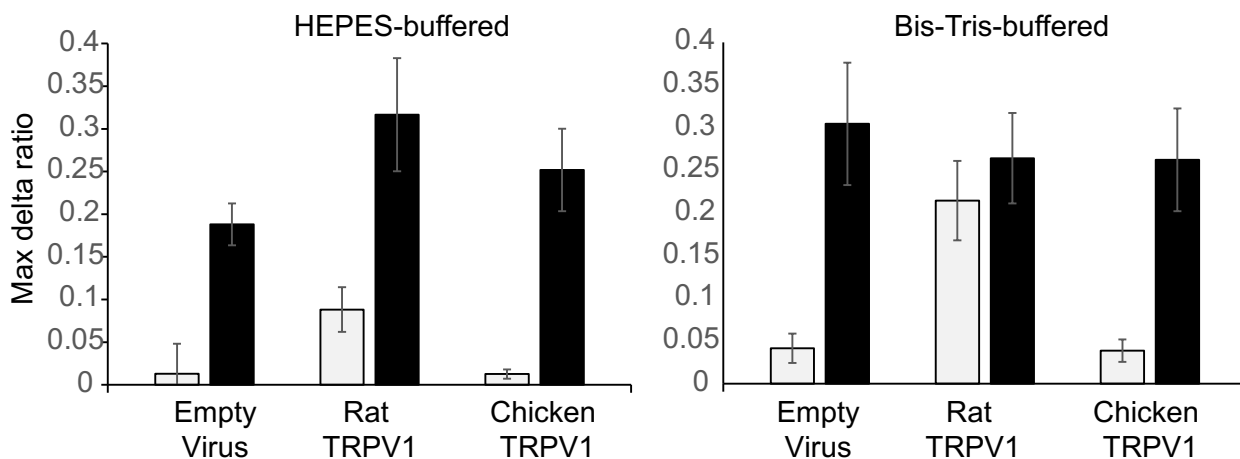


Figure 2.11 Insect cells show endogenous pH responses that mask potential chicken-TRPV1-dependent responses. Bars indicate the the maximum fluorescence ratio change seen in calcium influx assays in response to a shift from pH 7.2 to 6.4 (gray) or 6.0 (black) in either HEPES-buffered (Left) or Bis-Tris-buffered bath solution. Max delta ratio values are the average of 4-8 technical replicates and error bars indicate standard error of the mean. Only rat TRPV1 showed clear activation above background levels at pH 6.4.

residues in the mammalian and avian clades and restricting the search area to clusters of residues in the transmembrane region, we were able to narrow down the list to just eight potential residues. Interestingly, a number of the residues on the list had not yet been defined as important for capsaicin sensitivity, providing a unique opportunity to study new contributors to vanilloid sensitivity. From the testing of single and combinations of mutations in chicken TRPV1, we found that the minimal set of mutations necessary to confer high capsaicin sensitivity involves residues in the S4-S5 pocket. A quadruple mutation of the pocket, A558T/S574A/A578E/L762A, in chicken TRPV1 decreases the capsaicin EC₅₀ to 6 ± 2 μM, just 30-fold lower than that of rat TRPV1. The same mutations also convert chicken TRPV1 to a resiniferatoxin-sensitive channel with an EC₅₀ of 400 ± 90 nM, only 5-fold lower than that of rat TRPV1 in our experiments. From our analysis of the capsaicin sensitivity of pocket triple mutants, we inferred that all four pocket mutations contribute to sensitivity, with A558T and A578E most contributory.

Wildtype chicken TRPV1 is unable to bind resiniferatoxin (Jordt & Julius), but since our pocket quadruple mutant is now vanilloid sensitive, it points to the four pocket residues as directly binding to vanilloid molecules or lining the binding pocket. This is consistent with the S4-S5 pocket being the binding site for vanilloid molecules in TRPV1 (Cao et al.; Gao et al.; Liao et al.). In addition, we found mutations near the TRPV1 pore that further boost the sensitivity of the pocket quadruple mutant to capsaicin, but decreased sensitivity to resiniferatoxin, indicating similar but distinct activation mechanisms for the two vanilloid compounds.

Our findings that engineering capsaicin sensitivity into chicken TRPV1 involves restoring residue A558 (equivalent to T550 of rat TRPV1) agree with previous work on the molecular basis of capsaicin sensitivity in mammalian TRPV1s. T550 was one of the residues included in the V3/C chimera conferring weak capsaicin sensitivity to chicken TRPV1 (Jordt & Julius). In 2004, Gavva et al. discovered that mutating two residues in poorly capsaicin-sensitive rabbit TRPV1 to their rat TRPV1 equivalents to resulted in vanilloid sensitivity near what was observed for rat TRPV1 (Gavva et al.) Those two residues corresponded to T550 and M547 in rat TRPV1.

Selection of our candidate residues for vanilloid sensitivity was based on clade-specific differential conservation; the residues chosen are representatives of potentially important differences between mammalian and avian TRPV1s, rather than just differences between rat and chicken TRPV1 sequences. As a result, we would expect the minimal set of mutations needed to confer vanilloid sensitivity to chicken TRPV1 to be able confer similar sensitivity to other avian TRPV1 channels as well. Also, because of the structural similarity of other TRP channel members to TRPV1, (Paulsen et al.; Saotome et al.; Zubcevic et al.) the same residues and mutations are likely to be integral to engineering vanilloid sensitivity into other members of the channel superfamily.

Recent reports of the engineering vanilloid sensitivity into TRPV2 allow us now to compare our minimal set of residues with those uncovered by other labs attempting to engineer vanilloid sensitivity into another vanilloid-insensitive TRPV family member, TRPV2. Yang et al. created a mutant mouse TRPV2 that binds and is activated by to resiniferatoxin by introducing the following mutations: F467S, S498F, L505T, and

Q525E (Yang et al.). Those mutations convert the mouse TRPV2 residues to their equivalent TRPV1 residues S512, F543, T550, and E570 by the rat numbering. Similarly, Zhang et. al. reported engineering rat TRPV2 to be vanilloid sensitive by making the following mutations: F472S, L507M, L510T, and Q530E (Zhang et al.). These correspond to S512, M547, T550, and E570 by the rat numbering. Note that these minimal sets share three residues with each other, S512, T550, and E570. Our experiments also marked T550 and E570 residues as important for conferring vanilloid sensitivity. S512 and F543 are conserved between rat and chicken TRPV1, explaining why those residues were not identified as part of our minimal set. M457, however, is a leucine in chicken TRPV1. Combining minimal set residues from our studies with that of Yang et al and Zhang et al, could result in creation of TRPV2 channels with even stronger vanilloid sensitivities.

2.4.2 What are potential roles for residues in our minimal set?

Early in 2016, David Julius and Yifan Chang's labs published new higher resolution cryoEM structures of rat TRPV1 in nanodiscs (Gao et al.), small discs of phospholipid bilayer bundled by scaffolding proteins (Bayburt & Sligar). The TRPV1 structures include the channel without ligand, with resiniferatoxin and double-knot toxin agonists, or with the antagonist capsazepine. The new structures of TRPV1 with and without ligands provides atomic details needed to unambiguously assign roles to some of the important residues identified through biochemistry on TRPV1 channels (Gao et al.). In the resiniferatoxin and double-knot toxin-bound structure, the channel gates are open and resiniferatoxin can be clearly resolved binding in the S4-S5 pocket in a head-down, tail-up configuration previously proposed (Jordt & Julius). The T550 residue

implicated by us and in numerous other studies as important for vanilloid binding and sensitivity is oriented to form a hydrogen bond with a carboxyl group in the neck of resiniferatoxin, a motif also present in capsaicin. The aromatic vanilloid head of resiniferatoxin is involved in edge-on pi-stacking with the Y511 sidechain, which also may form a hydrogen bond with part of the resiniferatoxin “tail” (Figure 2.13). Such interactions would lock the resiniferatoxin in place, providing a physical reason for why mutations of Y511 to smaller residues perturb resiniferatoxin binding and increase deactivation (Kumar et al.; Winter et al.; Zhang et al.). The vanilloid moiety also takes part in a hydrogen bonding network linking the molecule to R557 and E570, a previously predicted interaction (Boukalova et al.), as well as S512. This structure implicates both T550 and E570, which we identified as strong contributors to capsaicin sensitivity in our chicken TRPV1 mutants, as key parts of a hydrogen bonding network with vanilloid ligands. Of the two, only T550 directly interacts with resiniferatoxin and the residue likely plays a key role in ligand binding. E570’s lack of direct interaction with resiniferatoxin and positioning closer to the S5 suggest that it may play a role in communicating with the TRPV1 gate rather than ligand binding.

The potential role of the specific pore residues is still a mystery. They have not been previously implicated in vanilloid sensitivity, likely due to their distance from the vanilloid binding site. Three of the four mutations in our pore mutant constructs, A664, V667I, and V671L, merely convert one small hydrophobic amino acid to another, making it difficult to predict how the mutations might affect channel function. The high-resolution structures of TRPV1 did reveal that the pore region is a site of channel modulation. The apo TRPV1 structure reveals multiple lipids bound in the clefts

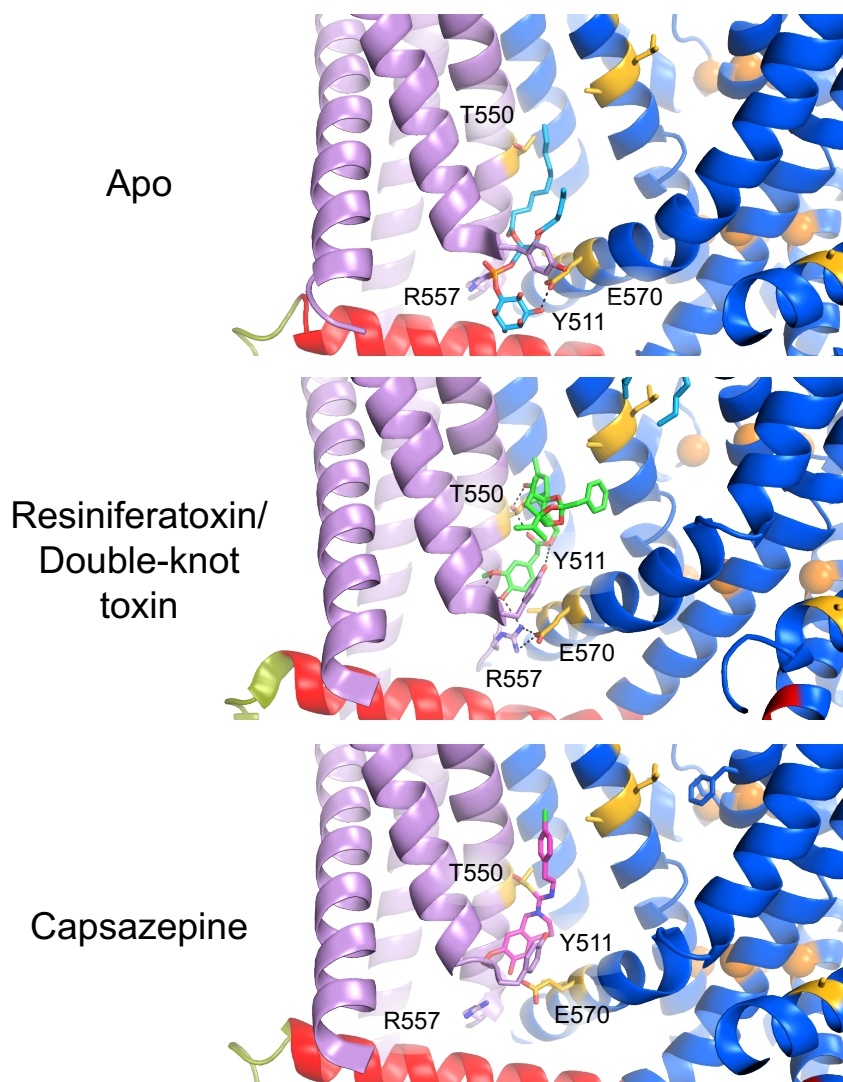


Figure 2.13 High resolution structures of ligand bound TRPV1 reveal roles for biochemically-determined determinants of vanilloid sensitivity. Structures of apo (PDB ID: 5IRZ), resiniferatoxin and doubleknot toxin-bound (PDB ID: 5IRX), and capsazepine-bound (PDB ID:5IS0) TRPV1 are depicted according to the following scheme: S1-S4, lavender; S5-S6, blue; TRP box helix, red; C-terminus, green; gate residues, gold spheres. Key residue sidechains are depicted as sticks, with our minimal set residues in yellow. A phosphatidylinositol molecule is present in the pocket of the apo structure. In the open resiniferatoxin (lime green sticks) and double-knot toxin bound structure, the vanilloid moiety participates in a network of hydrogen bonds (black dashed lines) including residues R557, E570, and S512. This network is not present in the apo or capsazepine (magenta)-bound structures. In addition T550 forms a hydrogen bond with the carbonyl of resiniferatoxin and the Y511 sidechain flips up to also hydrogen bond with the ligand.

between transmembrane helices, including the site of our interesting pore residues, between the S6 and pore helices (Figure 2.14). Also, the resiniferatoxin/double-knot toxin-bound structure shows that a loop of the toxin binds in a similar location at the top of the S6 helix (Figure 2.14) (Gao et al.). It would be interesting to look at resiniferatoxin binding in the Pocket and Pocket+S6/Y mutants to determine whether the pore mutations exert their effects on vanilloid binding allosterically or if they are primarily involved in gating. This could be done using the classic radiolabeled resiniferatoxin binding assays (Szallasi & Blumberg; Yang et al.; Zhang et al.). In addition, investigating the effects of pore mutations on TRPV1 activation by non-vanilloid stimuli, such as heat or pH, may also shed light on the roles of those pore residues.

2.4.3 Future Directions

Armed with high-resolution structures and a wealth of biochemistry, we are at the stage where rational design can be employed to investigate and validate hypotheses on the mechanisms of TRP channel activation. From all of the structure-function studies and mutagenesis, we have a short list of residues that are important for conferring vanilloid sensitivity to TRPV1-related channels: Y511, S512, T550, E570, and also A566 and A665 as minor contributors.

Even though all of our chicken TRPV1 mutants analyzed could be expressed in insect cells, we were unable to observe activation with other non-vanilloid stimuli. Sf9 and Sf21 insect cells are not conducive for testing the pH ranges expected to activate chicken TRPV1; even empty virus-infected cells show extremely large responses to pHs below 6.5 (Figure 2.11) likely due to the action of endogenous pH-activated transporters or channels. Additionally, testing of the temperature sensitivity of the channels was not

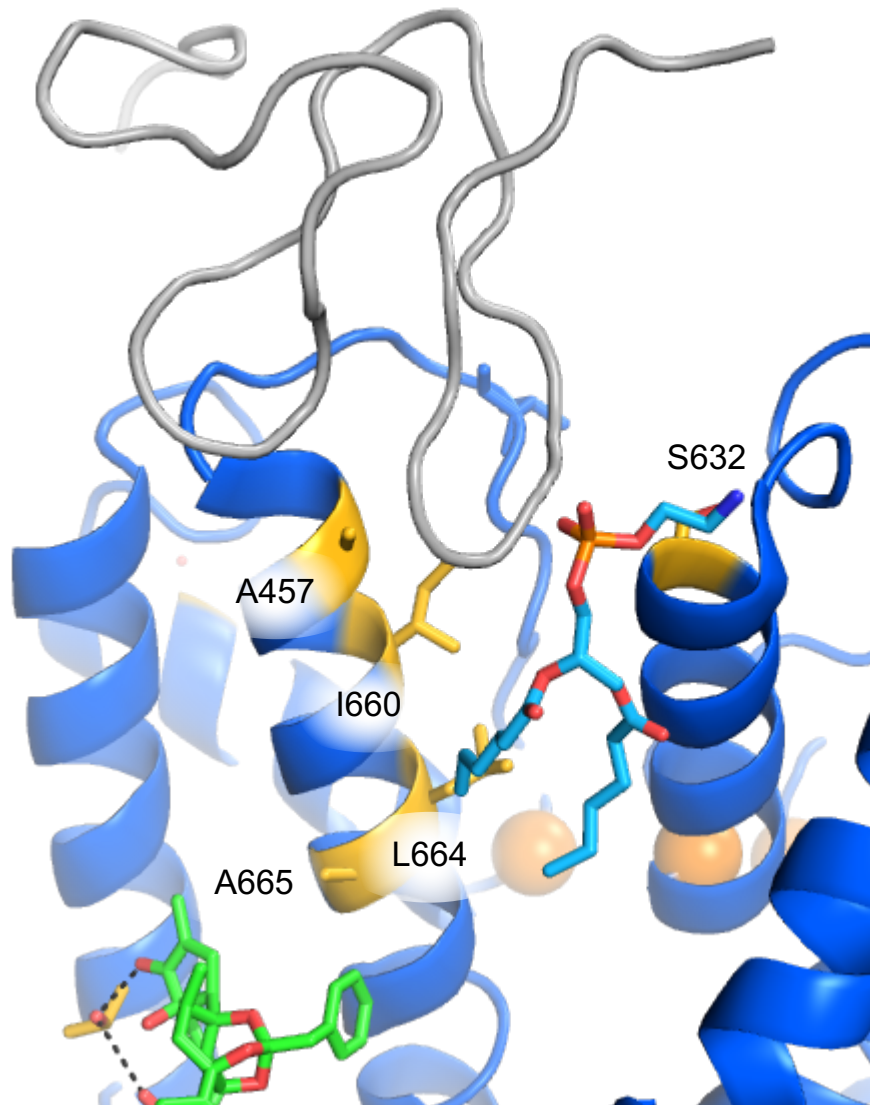


Figure 2.14 Pore mutants that boost capsaicin sensitivity are positioned near the binding site of double-knot toxin and a lipid. The pore region of resiniferatoxin and double-knot toxin-bound TRPV1 (PDB ID:5IRX) structure is depicted in cartoon representation with gate residues represented as orange spheres. Side chains sticks are shown and labelled for the residues corresponding to our capsaicin-sensitivity enhancing pore mutation sites (A665, V667, V671, and Y639 in chicken TRPV1) Loops of the agonist double-knot toxin (gray) along with a lipid (cyan) bind in the cleft between the S6 helix, containing A457, I660, and I664, and the pore helix, which contains S632. This site may be important for gating given its proximity to the channel upper gate.

possible due to endogenous heat-activated channels in insect cells. Moving the channels to a mammalian cell or oocyte expression system would be a worthwhile endeavor to confirm channel function and also determine whether the mutant chicken TRPV1s have the same properties in another heterologous system. Much of the original characterization of TRPV1 channels were done in either HEK293 cells or oocytes (Caterina et al.; Koivisto & Pertovaara; Lishko et al.; Tominaga et al.), so there are established protocols for testing pH, capsaicin, resiniferatoxin, 2-APB, and heat responses by electrophysiology and by calcium influx assays. It could would enable us to investigate other routes of activation and, perhaps, start to understand where they converge to cause channel gating.

References

- Bayburt, T. H., & Sligar, S. G. (2010). Membrane protein assembly into Nanodiscs. *FEBS letters*, 584(9), 1721-1727.
- Boukalova, S., Marsakova, L., Teisinger, J., & Vlachova, V. (2010). Conserved residues within the putative S4-S5 region serve distinct functions among thermosensitive vanilloid transient receptor potential (TRPV) channels. *J Biol Chem*, 285(53), 41455-41462.
- Cao, E., Liao, M., Cheng, Y., & Julius, D. (2013). TRPV1 structures in distinct conformations reveal activation mechanisms. *Nature*, 504(7478), 113-118.
- Caterina, M. J., Schumacher, M. A., Tominaga, M., Rosen, T. A., Levine, J. D., & Julius, D. (1997). The capsaicin receptor: a heat-activated ion channel in the pain pathway. *Nature*, 389(6653), 816-824.
- Correll, C. C., Phelps, P. T., Anthes, J. C., Umland, S., & Greenfeder, S. (2004). Cloning and pharmacological characterization of mouse TRPV1. *Neurosci Lett*, 370(1), 55-60.
- Crooks, G. E., Hon, G., Chandonia, J.-M., & Brenner, S. E. (2004). WebLogo: a sequence logo generator. *Genome research*, 14(6), 1188-1190.

- Di Virgilio, F., Steinberg, T. H., & Silverstein, S. C. (1990). Inhibition of Fura-2 sequestration and secretion with organic anion transport blockers. *Cell Calcium*, 11(2-3), 57-62.
- Gao, Y., Cao, E., Julius, D., & Cheng, Y. (2016). TRPV1 structures in nanodiscs reveal mechanisms of ligand and lipid action. *Nature*, 534(7607), 347-351.
- Gavva, N. R., Klionsky, L., Qu, Y., Shi, L., Tamir, R., Edenson, S., Zhang, T. J., Viswanadhan, V. N., Toth, A., Pearce, L. V., Vanderah, T. W., Porreca, F., Blumberg, P. M., Lile, J., Sun, Y., Wild, K., Louis, J. C., & Treanor, J. J. (2004). Molecular determinants of vanilloid sensitivity in TRPV1. *J Biol Chem*, 279(19), 20283-20295.
- Glinsukon, T., Stitmunnaithum, V., Toskulkao, C., Buranawuti, T., & Tangkrisanavinont, V. (1980). Acute Toxicity of Capsaicin in Several Animal Species. *Toxicol*, 18(2), 215-220.
- Hayes, P., Meadows, H. J., Gunthorpe, M. J., Harries, M. H., Duckworth, D. M., Cairns, W., Harrison, D. C., Clarke, C. E., Ellington, K., Prinjha, R. K., Barton, A. J., Medhurst, A. D., Smith, G. D., Topp, S., Murdock, P., Sanger, G. J., Terrett, J., Jenkins, O., Benham, C. D., Randall, A. D., Gloger, I. S., & Davis, J. B. (2000). Cloning and functional expression of a human orthologue of rat vanilloid receptor-1. *Pain*, 88(2), 205-215.
- Henikoff, S., & Henikoff, J. G. (1993). Performance evaluation of amino acid substitution matrices. *Proteins*, 17(1), 49-61.
- Hu, H. Z., Gu, Q., Wang, C., Colton, C. K., Tang, J., Kinoshita-Kawada, M., Lee, L. Y., Wood, J. D., & Zhu, M. X. (2004). 2-aminoethoxydiphenyl borate is a common activator of TRPV1, TRPV2, and TRPV3. *J Biol Chem*, 279(34), 35741-35748.
- Jordt, S. E., & Julius, D. (2002). Molecular basis for species-specific sensitivity to "hot" chili peppers. *Cell*, 108(3), 421-430.
- Jukes, T. H., & Cantor, C. R. (1969). *Evolution of protein molecules* (Vol. 3).
- Koivisto, A., & Pertovaara, A. (2015). Transient Receptor Potential Ankyrin 1 Channel Antagonists for Pain Relief. In A. Szallasi (Ed.), *TRP channels as therapeutic targets: from science to clinical use* (pp. 146-158): Academic Press.
- Kumar, R., Hazan, A., Basu, A., Zalcman, N., Matzner, H., & Priel, A. (2016). Tyrosine Residue in the TRPV1 Vanilloid Binding Pocket Regulates Deactivation Kinetics. *J Biol Chem*, 291(26), 13855-13863.
- Larkin, M. A., Blackshields, G., Brown, N. P., Chenna, R., McGettigan, P. A., McWilliam, H., Valentin, F., Wallace, I. M., Wilm, A., Lopez, R., Thompson, J. D., Gibson, T. J., & Higgins, D. G. (2007). Clustal W and Clustal X version 2.0. *Bioinformatics*, 23(21), 2947-2948.

- Liao, M., Cao, E., Julius, D., & Cheng, Y. (2013). Structure of the TRPV1 ion channel determined by electron cryo-microscopy. *Nature*, *504*(7478), 107-112.
- Lishko, P. V., Procko, E., Jin, X., Phelps, C. B., & Gaudet, R. (2007). The ankyrin repeats of TRPV1 bind multiple ligands and modulate channel sensitivity. *Neuron*, *54*(6), 905-918.
- McIntyre, P., McLatchie, L. M., Chambers, A., Phillips, E., Clarke, M., Savidge, J., Toms, C., Peacock, M., Shah, K., Winter, J., Weerasakera, N., Webb, M., Rang, H. P., Bevan, S., & James, I. F. (2001). Pharmacological differences between the human and rat vanilloid receptor 1 (VR1). *Br J Pharmacol*, *132*(5), 1084-1094.
- Ohta, T., Komatsu, R., Imagawa, T., Otsuguro, K., & Ito, S. (2005). Molecular cloning, functional characterization of the porcine transient receptor potential V1 (pTRPV1) and pharmacological comparison with endogenous pTRPV1. *Biochem Pharmacol*, *71*(1-2), 173-187.
- Paulsen, C. E., Armache, J. P., Gao, Y., Cheng, Y., & Julius, D. (2015). Structure of the TRPA1 ion channel suggests regulatory mechanisms. *Nature*, *520*(7548), 511-517.
- Phelps, P. T., Anthes, J. C., & Correll, C. C. (2005). Cloning and functional characterization of dog transient receptor potential vanilloid receptor-1 (TRPV1). *Eur J Pharmacol*, *513*(1-2), 57-66.
- Saotome, K., Singh, A. K., Yelshanskaya, M. V., & Sobolevsky, A. I. (2016). Crystal structure of the epithelial calcium channel TRPV6. *Nature*, *534*(7608), 506-511.
- Shin, J. S., Wang, M. H., Hwang, S. W., Cho, H., Cho, S. Y., Kwon, M. J., Lee, S. Y., & Oh, U. (2001). Differences in sensitivity of vanilloid receptor 1 transfected to human embryonic kidney cells and capsaicin-activated channels in cultured rat dorsal root ganglion neurons to capsaicin receptor agonists. *Neurosci Lett*, *299*(1-2), 135-139.
- Szallasi, A., & Blumberg, P. M. (1993). [3H]resiniferatoxin binding by the vanilloid receptor: species-related differences, effects of temperature and sulfhydryl reagents. *Naunyn Schmiedeberg's Arch Pharmacol*, *347*(1), 84-91.
- Tominaga, M., Caterina, M. J., Malmberg, A. B., Rosen, T. A., Gilbert, H., Skinner, K., Raumann, B. E., Basbaum, A. I., & Julius, D. (1998). The cloned capsaicin receptor integrates multiple pain-producing stimuli. *Neuron*, *21*(3), 531-543.
- Winter, Z., Buhala, A., Otvos, F., Josvay, K., Vizler, C., Dombi, G., Szakonyi, G., & Olah, Z. (2013). Functionally important amino acid residues in the transient receptor potential vanilloid 1 (TRPV1) ion channel--an overview of the current mutational data. *Mol Pain*, *9*, 30.

- Yang, F., Vu, S., Yarov-Yarovoy, V., & Zheng, J. (2016). Rational design and validation of a vanilloid-sensitive TRPV2 ion channel. *Proc Natl Acad Sci U S A*, 113(26), E3657-3666.
- Yang, F., Xiao, X., Cheng, W., Yang, W., Yu, P., Song, Z., Yarov-Yarovoy, V., & Zheng, J. (2015). Structural mechanism underlying capsaicin binding and activation of the TRPV1 ion channel. *Nat Chem Biol*, 11(7), 518-524.
- Zhang, F., Hanson, S. M., Jara-oseguera, A., Krepiy, D., & Bae, C. (2016). Engineering vanilloid-sensitivity into the rat TRPV2 channel. *eLife*, 1--36.
- Zubcevic, L., Herzik, M. A., Jr., Chung, B. C., Liu, Z., Lander, G. C., & Lee, S. Y. (2016). Cryo-electron microscopy structure of the TRPV2 ion channel. *Nat Struct Mol Biol*, 23(2), 180-186.

Chapter 3

Dissecting the role of the insect TRPA1 N-termini in temperature modulation

3.1 Background

3.1.1 InsectTRPA1 isoforms

In insects, TRPA1 is involved in both innocuous temperature sensing and irritant avoidance. In mosquitos, TRPA1 is expressed in the antennae of females, where it is thought to mediate feeding-associated heat-seeking behaviors (G. Wang et al.). TRPA1 is also responsible for setting the preferred temperature range of *Drosophila* near 25°C (Hamada et al.). Citronellal, the lemon-scented chemical found in many bug repellents, triggers avoidance in both *Drosophila melanogaster* and *Anopheles gambiae* through activation of TRPA1 (Du et al.; Kwon et al.). The key to TRPA1's apparently disparate roles in both innocuous temperature sensing and noxious chemical sensing is the fact that insects have multiple TRPA1 isoforms with unique expression patterns (Kang et al.; Zhong et al.). Kang et al. reported the temperature and chemical sensing properties of two such TRPA1 isoforms, A and B, in both *D. melanogaster* and *A. gambiae*. The A and B isoforms are the result of alternative promotor choice affecting the first exon (Kang et al.). As a result the A and B isoforms differ at a small region of the N-terminus, but the remainder of the channels is identical (Figure 3.1). Both isoforms are activated by reactive electrophiles, but only the B isoform displays robust activation by heat. In *Drosophila*, the A isoform is expressed in the proboscis where it primarily acts as a chemosensor, prompting avoidance of irritants in food. The B isoform is expressed in neurons deep in the fly brain, effectively sequestered away from possible exposure to external reactive chemicals and allowing the channel to function primarily as a thermosensor in this location (Kang et al.).

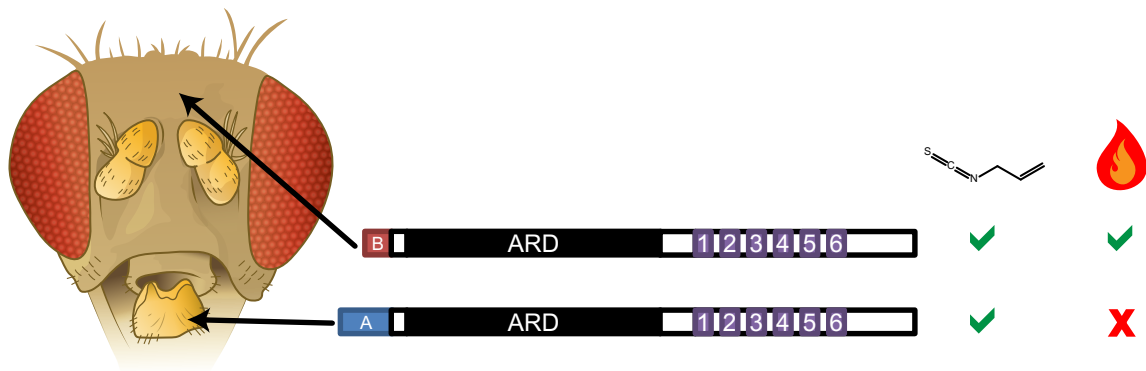


Figure 3.1 Drosophila TRPA1 A and B isoforms have different temperature sensitivities and expression patterns. The A and B isoforms of TRPA1 differ only at the N-terminus. Both isoforms can be activated by reactive electrophiles like allyl isothiocyanate. The A isoform is poorly temperature sensitive and expressed in the proboscis to act as a chemosensor. The B isoform is highly temperature sensitive and is expressed in the brain where it acts primarily as a thermosensor.

The insect A and B isoforms differ only at a small region of the N-terminus, but they have extreme differences in temperature sensitivity. This prompts many questions, and provides an optimal system for studying how the insect TRPA1 N-termini modulate channel temperature sensitivity. For instance, how temperature sensitive is the channel without the N-terminus? Is the A N-terminus working to suppress temperature sensitivity of the remainder of the channel or is the B N-terminus responsible for promoting temperature sensitivity? Or are both possibilities true? More specifically, what residues in the A or B N-terminus are essential for that temperature modulation? We aimed to answer those questions by analyzing the properties of N-terminally truncated A and B isoforms of insect TRPA1s using calcium influx assays and electrophysiology.

3.2 Experimental Methods

3.2.1 Mammalian cell culture

HEK293 cells were maintained in a 5% CO₂ incubator at 37°C in DMEM containing 10% (vol/vol) fetal bovine serum, 20 mM GlutaMax (Gibco), and 100 units/ml penicillin and streptomycin.

3.2.2 Plasmids and Cloning

D. melanogaster and *A. gambiae* isoform A and B sequences (provided by Paul Garrity) were amplified via PCR and cloned into the NdeI and NotI sites of the pcDNA3-cFLAG vector. The pcDNA3-cFLAG vector was modified from pcDNA3.1 to change the multiple cloning site to allow gene insertion using NdeI and NotI and an NdeI site from the backbone was removed. Oligos were used to introduce the sequence of the C-

terminal FLAG tag in-frame with the NotI site (Amino acid sequence added: AAADYDDDDK). Primers used to generate full length and N-terminally truncated TRPA1 plasmids are listed in Table 3.1. Site-directed mutagenesis was used to generate mutants of interest in the *Drosophila melanogaster* B isoform channel via the QuikChange (Agilent) protocol. Table 3.2 lists the template DNA and primers used to generate each mutant construct. The open reading frames of all constructs were sequenced to verify clone identity and quality.

3.2.3 Transient transfection of HEK 293 cells and protein expression

HEK cells were transfected using Lipofectamine 2000 Reagent (ThermoFisher) according to the manufacturer's protocol, or transfected by a calcium phosphate-based protocol. For the calcium phosphate transfections for calcium influx assays, 1.5 µg of DNA was mixed with 450 µl of 250 mM CaCl₂. The DNA-CaCl₂ solution was then added dropwise to 500 µl of 2X HEPES-buffered solution (50 mM HEPES, 10 mM KCl, 12 mM dextrose, 280 mM NaCl, 1.5 mM Na₂PO₄, adjusted to 7.05 with HCl). The complete transfection mixture was added dropwise to 7.5 x 10⁵ cells in 4 ml of complete DMEM medium with gentle agitation. Transfection mix was plated at 200 µl per well in 96-well back-walled clear bottom poly-lysine-coated assay plates. After 12-16 hours of incubation at 37°C, the medium was exchanged for fresh DMEM and the cells were moved to 30°C for protein expression. For electrophysiology, 7.5 x 10⁵ cells were cotransfected with 1.5 µg of pcDNA-TRPA1-cFLAG and 0.75 µg of pcDNA-eGFP in 10 ml of medium and plated at 800 µl/well on coverslips in a 24-well plate. After 12-16 hours of incubation at 37°C, the medium was exchanged and cells were moved to a 30°C incubator for protein expression.

Table 3.1 Primers for cloning truncated insect TRPA1 constructs into pcDNA-cFLAG

Construct Name	Forward Primer Sequence	Reverse Primer Sequence
AgaTRPA1 A	CGGCAGCCATATGCCTACTCCGCTGTACTT	AAGACTGGGGCCGCTTTGCCAATAGATTTGTTGAAG
AgaTRPA1 B	CGGCAGCCATATGTGGCGCAACTGTGCAC	AAGACTGGGGCCGCTTTGCCAATAGATTTGTTGAAG
AgaTRPA1 sp-end	CGGCAGCCATATGGCGGCAGAAAGCCGGTAAT	AAGACTGGGGCCGCTTTGCCAATAGATTTGTTGAAG
AgaTRPA1 ANK1-end	GCGTTGTACATATGTCGGTGAAGGATAGCAAGGG	AAGACTGGGGCCGCTTTGCCAATAGATTTGTTGAAG
DmeTRPA1 A	CGGCAGCCATATGATTACAGCTCCGGCCA	AAGACTGGGGCCGCTTTGCCAATAGATTTGTTGAAG
DmeTRPA1 B	CGGCAGCCATATGACTTCGGGCGACAAGG	AAGACTGGGGCCGCTTTGCCAATAGATTTGTTGAAG
DmeTRPA1 sp-end	CGGCAGCCATATGGCGGCTGAGTCCGGAAAC	AAGACTGGGGCCGCTTTGCCAATAGATTTGTTGAAG
DmeTRPA1 ANK1-end	GCGTTGTACATATGGCTTTAAAGGATGCGAAAGGAC	AAGACTGGGGCCGCTTTGCCAATAGATTTGTTGAAG
DmeTRPA1 A NΔ19	CGGCAGCCATATGCCCAAGCTCTACAACG	AAGACTGGGGCCGCTTTGCCAATAGATTTGTTGAAG
DmeTRPA1 A NΔ35	CGGCAGCCATATGTGCGCCACCTGACCTCATG	AAGACTGGGGCCGCTTTGCCAATAGATTTGTTGAAG
DmeTRPA1 A NΔ59	CGGCAGCCATATGGGCGGGAACAGCAAGTATG	AAGACTGGGGCCGCTTTGCCAATAGATTTGTTGAAG
DmeTRPA1 A NΔ99	CGGCAGCCATATGCCGCCGCGGAGGTCT	AAGACTGGGGCCGCTTTGCCAATAGATTTGTTGAAG
DmeTRPA1 A NΔ110	CGGCAGCCATATGCCCTTCAGGATATTGCGGG	AAGACTGGGGCCGCTTTGCCAATAGATTTGTTGAAG
DmeTRPA1 B NΔ21	CGGCAGCCATATGGGCGGCTGTGCCCGCGG	AAGACTGGGGCCGCTTTGCCAATAGATTTGTTGAAG
DmeTRPA1 B NΔ38	CGGCAGCCATATGCTGCCCAAAAAGTGGGCAC	AAGACTGGGGCCGCTTTGCCAATAGATTTGTTGAAG
DmeTRPA1 B NΔ48	CGGCAGCCATATGCTCTCGACGCCCAAAGA	AAGACTGGGGCCGCTTTGCCAATAGATTTGTTGAAG

Table 3.2 QuikChange parameters for the B isoform N-terminus mutagenesis

Mutations	Template	Forward Primer	Reverse Primer
R45E/R48E	DmeTRPA1 B	GTGGGCAGAGATCCTGGAGA TGCCTCGACGCCAAAGATAC CAATCGTGGACTATC	GACATCTCCAGGATCTCTGCCCA CTTTTTGGGCAGGTTAAGCGGC
K41E/K42E/ R45E/R48E	DmeTRPA1 B R45E/R48E	CTGCCCCGAGGAGTGGGCAGA GATCCTGGAGATG	CTGCCCACTCCTCGGGCAGGTT AAGCGGCGC
D70R/D71R	DmeTRPA1 B	GAAACCTTCGCCGCTTCAAGC GACTCTTCATGGCGGACAAC	CTTGAAGCGGCGAAGGTTTCCG GACTCAGCCGCTCC
D59R/E62R	DmeTRPA1 B	CGTGCGCTATCTGCGGCGCG CTGAGTCCGAAACC	GCCCGCAGATAGCGCACGATTG GTATCTTTGGCGACGAG
R45E/R48E/ D70R/D71R	DmeTRPA1 B R45E/R48E	GAAACCTTCGCCGCTTCAAGC GACTCTTCATGGCGGACAAC	CTTGAAGCGGCGAAGGTTTCCG GACTCAGCCGCTCC

3.2.4 Western Blot Analysis

Forty-eight hours post-transfection, I harvested HEK293 cells by scraping in cold 1X PBS. Cells were spun down and washed once more in cold PBS then lysed in 2X sodium dodecyl sulfate-containing loading dye. After heating the samples for 3 minutes at 60°C, I loaded samples and prestained protein ladder on a 10% polyacrylamide gel and ran the electrophoresis at 200V for 45-60 min. Protein was transferred to a polyvinylidene fluoride (PVDF) membrane via the semi-dry blotting method at 100 mA/hour/gel. Afterwards, I blocked the membrane for 45-60 minutes with 3% bovine serum albumin (BSA) in Tris-buffered saline with Tween-20 (TBST: 50 mM Tris-HCl, pH 7.5, 150 mM NaCl, and 0.1% Tween-20). Then, the membrane was incubated with an alkaline phosphatase-conjugated M2-anti-FLAG antibody (Sigma) diluted 1:2000 in TBST with 1% BSA. After three 10-minute rinses in TBST and a final rinse in TBS, bands were developed using the NBT/BCIP one-step kit (ThermoFisher) according to the manufacturer's instructions. The reaction was quenched with 1% acetic acid and the blots were rinsed with water and dried before photographing.

3.2.5 Fluorescence-based calcium influx assays

I conducted calcium influx assays 24 to 72 hrs post-transfection. Plate preparation and assay setup were the same as described in section 2.2.4.

3.2.6 Whole-cell patch-clamp electrophysiology

We conducted whole-cell patch-clamp electrophysiology measurements of GFP-expressing transiently-transfected HEK293 cells as previously described (Lishko et al.), using an Axopatch 200B amplifier controlled by a Digidata 1322 and pClamp 9.2

software (Molecular Devices). HEK293 cells had been cotransfected with a GFP vector, so GFP-positive cells were chosen for measurements. Temperature was controlled using an in-line Peltier device and CL-100 bipolar temperature controller. The intracellular solution contained 150 mM Cs-methanesulfonate, 10 mM HEPES, 10 mM EGTA, and 2.5 mM NaCl, pH adjusted to 7.2 with CsOH. The extracellular solution contained 150 mM NaCl, 10 mM HEPES, 5 mM KCl, 2 mM CaCl₂, 1 mM MgCl₂, 10 mM glucose, pH adjusted to 7.2 with NaOH. Voltage ramps occurred every 5 seconds sweeping from -100 to +100 in 1500 ms with the holding potential at -60 mV. For Q₁₀ measurements, voltage ramp was shortened to 325 ms and frequency was increased to a sweep every second. Graphs and calculations were done with Graph Pad Prism 7.

3.3 Results

3.3.1 *Drosophila melanogaster* TRPA1 constructs respond to AITC in calcium influx assays

To begin to understand which form of the N-terminus, A or B, plays an active role in modulating TRPA1 temperature sensitivity, I designed constructs of the channel missing all of the isoform-specific regions. I cloned two versions each of N-terminally truncated *A. gambiae* TRPA1 (AgaTRPA1) and *D. melanogaster* TRPA1 (DmeTRPA1) with C-terminal FLAG tags into a pcDNA vector. One construct, called sp-end, removes all of the residues from the N-terminus up until the splice site; the second construct, ANK1-end removes an additional 17 residues, beginning just before the ANK1, the first predicted ankyrin repeat (Figure 3.2).



Figure 3.2 Diagram of the WT and truncated insect TRPA1 constructs. In the topology diagrams, the A and B isoform-specific regions are indicated in blue and red, respectively. The ankyrin repeat domain (ARD), consisting of ankyrin repeats 1-17, is shown in black and the transmembrane segments are numbered and in purple. Two constructs were designed missing the isoform-specific regions. The sp-end construct starts just after the splice site, while the ANK1-end construct begins with ankyrin repeat 1. All channels include a C-terminal FLAG tag.

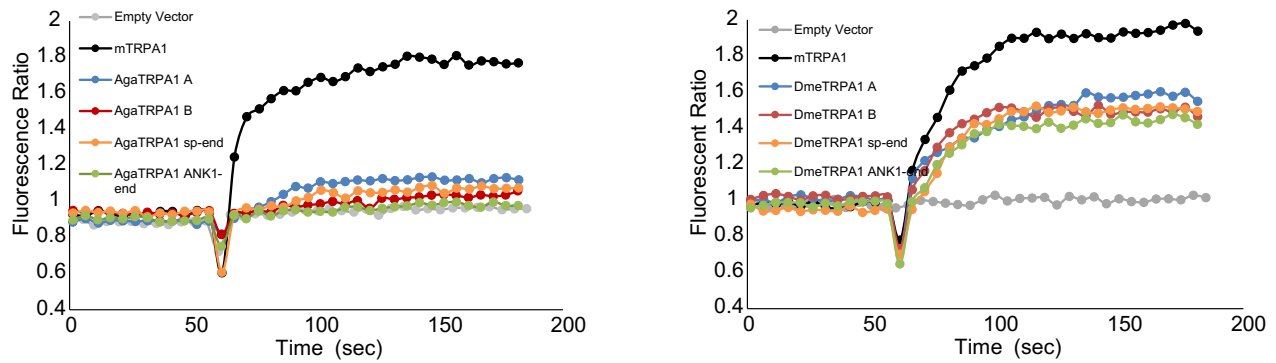
To test expression of all constructs, HEK293 cells were transiently transfected with pcDNA vectors encoding full-length or truncated *D. melanogaster* and *A. gambiae* A or B isoform TRPA1 with a C-terminal FLAG tag. Mouse TRPA1-cFLAG was also included as a benchmark for a well-expressed channel. After 48 hours, western blots of whole-cell lysates confirmed that all channels were expressed as well, if not better than mouse TRPA1 (Figure 3.3 A).

Next, the AITC responses of the channels were measured in HEK293 cell-based calcium influx assays to check for channel function for all constructs. In agreement with the original characterization of the channels (Kang et al.), both the A and B isoforms showed responses to 1 mM AITC, a presumed saturating concentration of agonist. Barely any AITC responses were detected for any of the *AgaTRPA1* constructs (Figure 3.3 A).

Western blots against the C-terminal FLAG tags of all TRPA1 constructs confirmed that *A. gambiae* constructs were expressed at least as well as their *D. melanogaster* counterparts and the benchmark, mouse TRPA1 (Figure 3.3 B). The deficit in AITC response of the *A. gambiae* channels was not remedied by changing transfection variables, such as the amount of DNA used, or by changing the protein expression period from 48 hours to 24 or 72 hours. Consequently, I used *D. melanogaster* TRPA1 channels for all future calcium influx assays and electrophysiology.

3.3.2 Complete removal of the isoform-specific N-terminus leads to small heat responses.

A



B

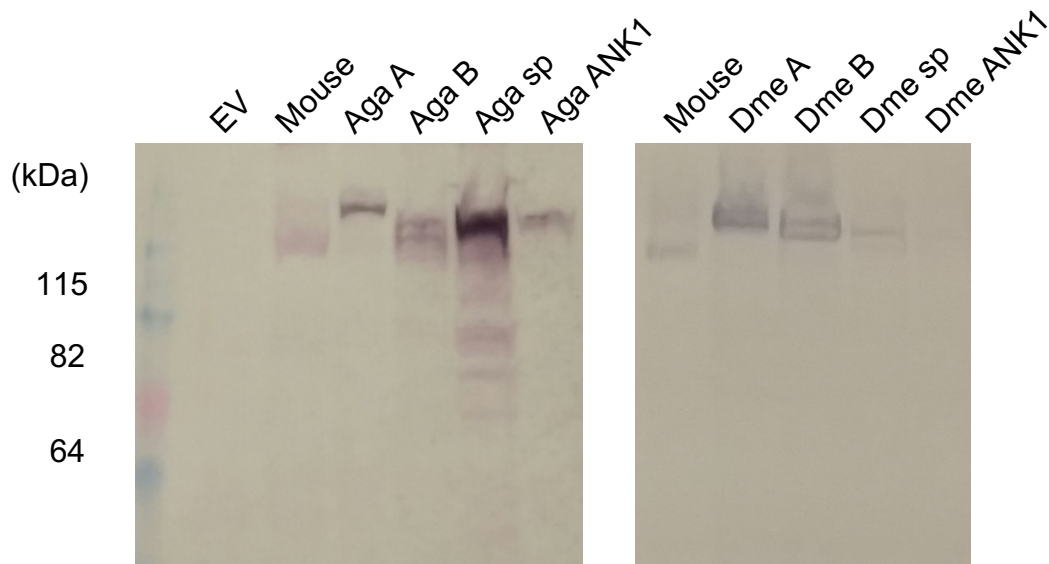


Figure 3.3 *Drosophila* TRPA1 isoforms respond to AITC in calcium influx assays. (A) Only mouse TRPA1 and *D. melanogaster* TRPA1 channels responded to 1 mM AITC in fluorescence-based calcium influx assays. Fura-2 340/380 fluorescent ratios are plotted against time. The sharp dip in delta ratio at 60 seconds is an artifact of an addition by the plate reader's liquid handling system. Allyl isothiocyanate (AITC) was added to a final concentration 1 mM at 60 seconds. (B) Western blots of HEK293 cell lysate samples against the C-terminal FLAG-tag confirm expression for the the full length A and B isoforms and the truncated sp-end and ANK1-end *D. melanogaster* and *A. gambiae* constructs.

Alongside Postdoctoral Fellow Jeff McArthur, I tested the temperature and AITC activation of the wildtype DmeTRPA1 A and B isoforms as well as channels missing the isoform-specific N-termini via whole-cell patch clamping. As in the calcium influx assays, both the A and B isoforms were robustly activated by AITC. In addition, both isoforms display the characteristic outward rectification of TRPA1, as evidenced by the much larger outward currents compared to the inward currents (Figure 3.4). Both the sp-end and the ANK1-end channels have much smaller responses to temperature. These results are consistent with a model where the B isoform N-terminus is acting to increase the temperature sensitivity of the remainder of the channel, but it does not rule out the possibility that the A N-terminus also acts as a suppressor of temperature sensitivity.

3.3.3 Truncations of the B isoform N-terminus reveal residues 39-48 are important for high temperature sensitivity

Since the B isoform N-terminus promotes high temperature sensitivity, we dissected the B isoform N-termini with finer truncations to locate the active elements. We used secondary structure predictions to guide construct design, selecting start sites that occur in unstructured regions. We thus generated the N Δ 21, N Δ 38, N Δ 48 constructs, which are all longer than the sp-end and ANK1-end constructs, deleting 21, 38 and 48 residues, respectively, from the N-terminus. Using a similar consideration of the A isoform N-terminus, we designed the A N Δ 23, N Δ 51, N Δ 89, N Δ 99, N Δ 110 constructs, but those channels have yet to be characterized in detail (Figure 3.5).

I screened all constructs screened by western blot and in calcium influx assays, confirming both channel expression and AITC activation before patch-clamp electrophysiology measurements. Based on the properties of the sp-end and the ANK1-

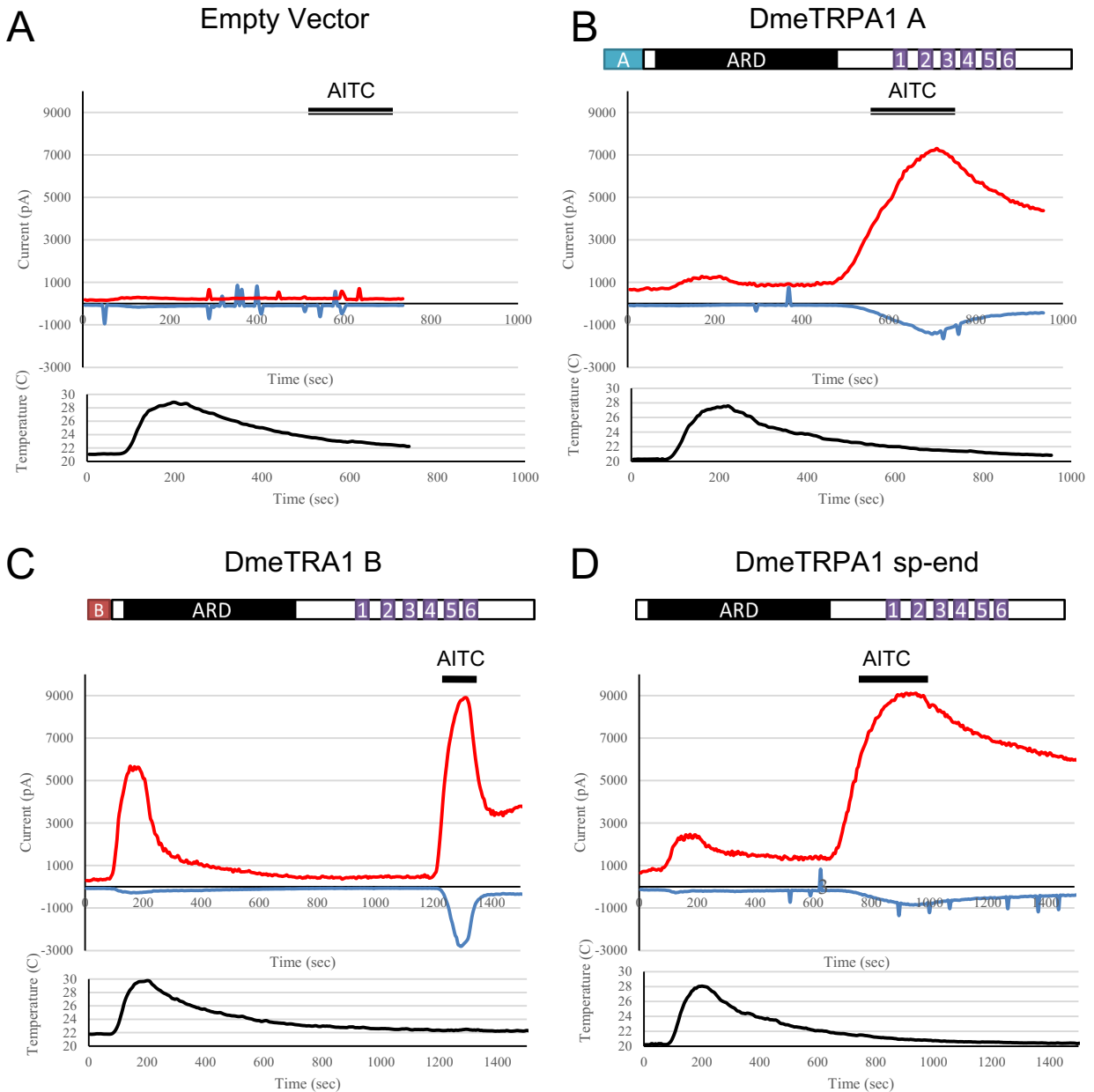


Figure 3.4 DmeTRPA1 A and DmeTRPA1 without the N-terminus have a small heat responses. Representative traces of whole-cell patch clamping recordings of HEK293 cells expressing WT or truncated *D. melanogaster* TRPA1 constructs. The B isoform has a large response to both heat and capsaicin, while the A isoform and sp-end constructs have reduced heat response amplitudes. Currents at +60 mV (red) and -60 mV (blue) were extracted from 0.5 second voltage ramps from -100 mV to +100 mV every 5 seconds. Temperature is plotted beneath the current graphs. Application of AITC is indicated by the black bars.

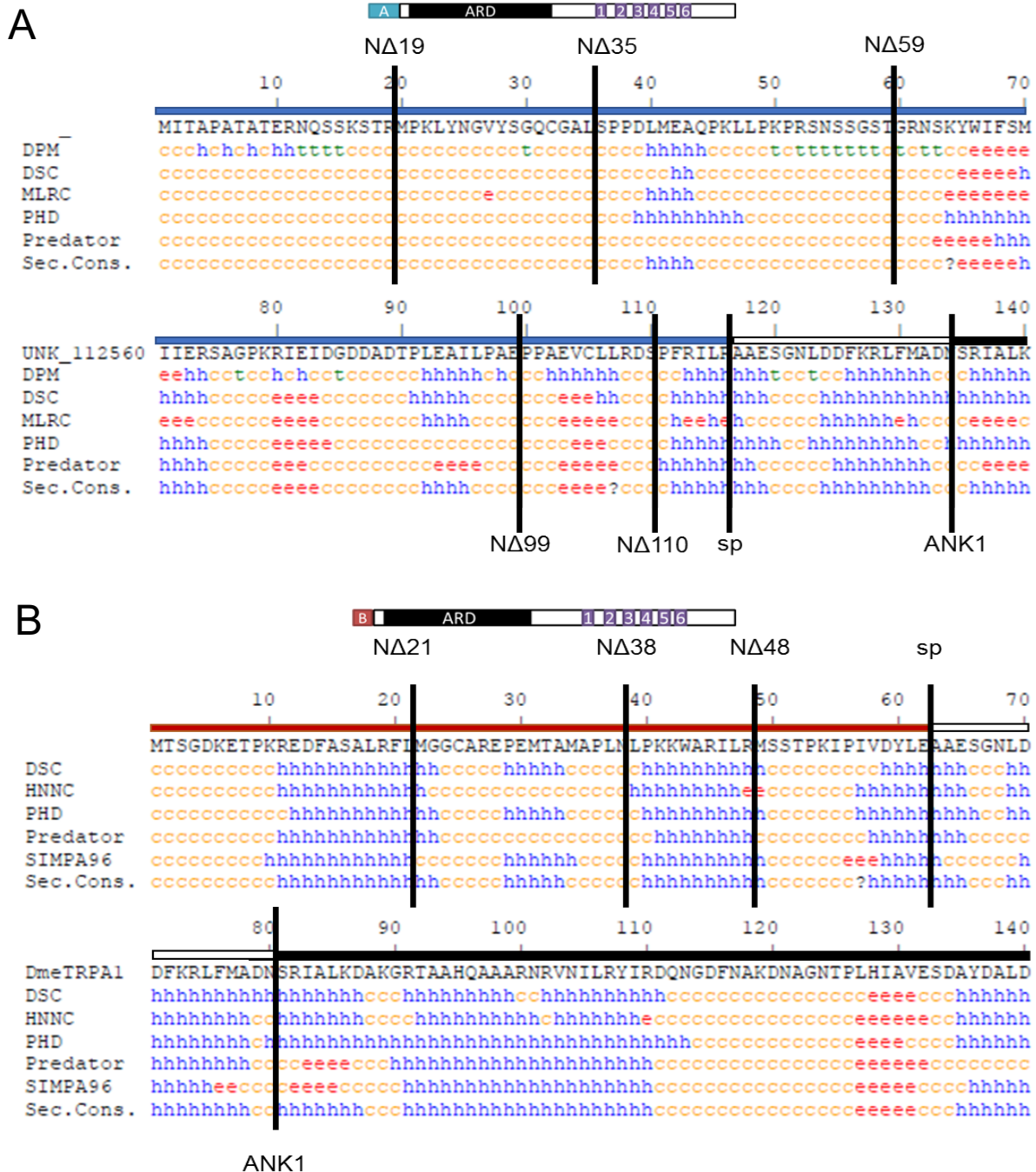


Figure 3.5 Secondary structure predictions were used to choose N-terminal truncation sites. The sequences of *Drosophila melanogaster* TRPA1 A and B were analyzed with the NPS@ Consensus Secondary Structure Predictor (Combet et al. 2000). Predicted helical residues are marked as “h,” beta strands as “e,” and unstructured coil as “c.” For orientation, the residue numbers and a color coded bar are included above the sequence that matches the construct diagram. The blue or red bar corresponds to the isoform-specific region. The black bar indicates the beginning of the predicted ankyrin repeat domain (ARD) from repeat one. The white bar is the region just after the splice site, but before ankyrin repeat one. Vertical lines indicate the start sites and names of N-terminal truncations designed not to disrupt any predicted secondary structure.

end constructs, we focused on characterizing the temperature responses of the B isoform N-terminally-truncated constructs. Both the B isoform N Δ 21 and N Δ 38 constructs retained the characteristic large heat responses of the full-length B isoform TRPA1; however, N Δ 48 had only small temperature responses (Figure 3.6). This result implicates residues 39-48 as the part of the B isoform N-terminus involved in promoting high temperature sensitivity.

3.3.4 Quantifying temperature sensitivity

We first considered using maximum heat response normalized to maximum AITC response ($I_{\max \text{ heat}}/I_{\max \text{ AITC}}$) as a way compare the temperature sensitivity of different TRPA1 constructs. However, there were large discrepancies in the relative temperature sensitivities of the channels depending on whether outward currents at +60 mV or inward currents at -60 mV were used for the calculations (Figure 3.7 A). Based on the outward currents, $I_{\max \text{ heat}}/I_{\max \text{ AITC}}$ values for the B isoform, N Δ 21, and N Δ 38 channels are 0.54, 0.58, and 0.52, respectively, indicating similar high heat sensitivities. The values for the A isoform, B N Δ 48, sp-end, and ANK1-end constructs are lower, 0.17, 0.28, 0.27, and 0.26, indicating lower or intermediate temperature sensitivity. The $I_{\max \text{ heat}}/I_{\max \text{ AITC}}$ values calculated from the small, inward currents at -60 mV, do not follow the same pattern. All of the inward current $I_{\max \text{ heat}}/I_{\max \text{ AITC}}$ values are much lower, likely reflecting a loss of rectification seen during strong AITC responses. TRPA1 channels are also known to be inactivated by permeant calcium ions (Y. Y. Wang et al.), therefore it is possible that AITC responses may be affected by preceding heat responses. As a result, the AITC response after heat activation may not be a suitable normalization factor.

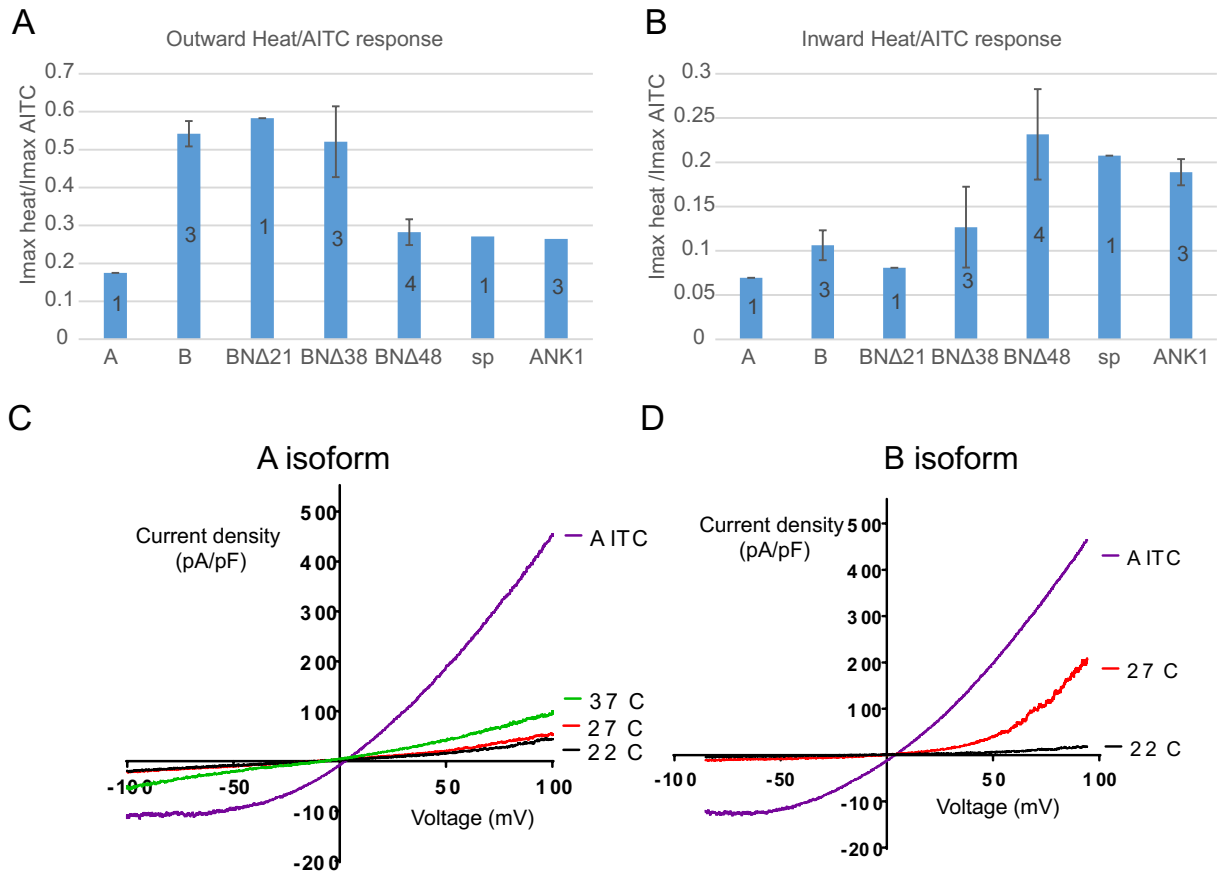


Figure 3.7 Outward and inward current $I_{max\ heat}/I_{max\ AITC}$ suggest conflicting temperature channel sensitivities. Currents at at +60 mV (A) and -60 mV (B) were used to calculate $I_{max\ heat}/I_{max\ AITC}$ as a normalized measure of temperature sensitivity. The number of traces used for each calculation is included on the bar. Error bars represent standard error of the mean. Example I-V curves for the A isoform (C) and B isoform (D) are demonstrate changes in rectification undergone by the channel when activated by 300 μ M AITC.

We thus switched to calculating Q_{10} values, the fold increase in current when temperature is raised by 10 degrees. In this case, no normalization is required, and the AITC response only served as confirmation of TRPA1 expression. Rather than holding the potential at a single value (-60 mV) during the entire temperature ramp, we opted to keep the fast, periodic voltage sweeps, extracting current values during the sweeps for Q_{10} calculations. This allowed continuous monitoring of the instantaneous current-voltage curves for TRPA1-characteristic features to ensure seal integrity during the entire recording. Continuous monitoring of the current-voltage curve was necessary ensure there was no leaks or drift could obscure the relatively low amplitude of inward currents. We then created Arrhenius plots by graphing the natural logarithm of current at -60 mV against inverse absolute temperature. The slope of the linear range of the plot was used to calculate the Arrhenius Q_{10} using the formula below as previously described (Kang et al.; Vyklický et al.).

$$Q_{10} = e^{S_{arr} \left(\frac{10}{T_1 T_2} \right)}$$

I also calculated the Q_{10} (27-73) values for a specific temperature range, 27-37 as a standard reference using a second formula, the ratio of rates.

$$Q_{10} = \left(\frac{R_2}{R_1} \right)^{\frac{10}{T_2 - T_1}}$$

Example traces of temperature ramp recordings and the resulting Arrhenius curves are included in Figure 3.10 Table 3.3 contains a summary of both the Arrhenius and 27-37°C therme;a Q_{10} values In line with previous channel chracterizaions, the B isoform is strongly activated by heat, while the A isoform is not. The B channel has a modest Q_{10} (27-37°C) of 6.

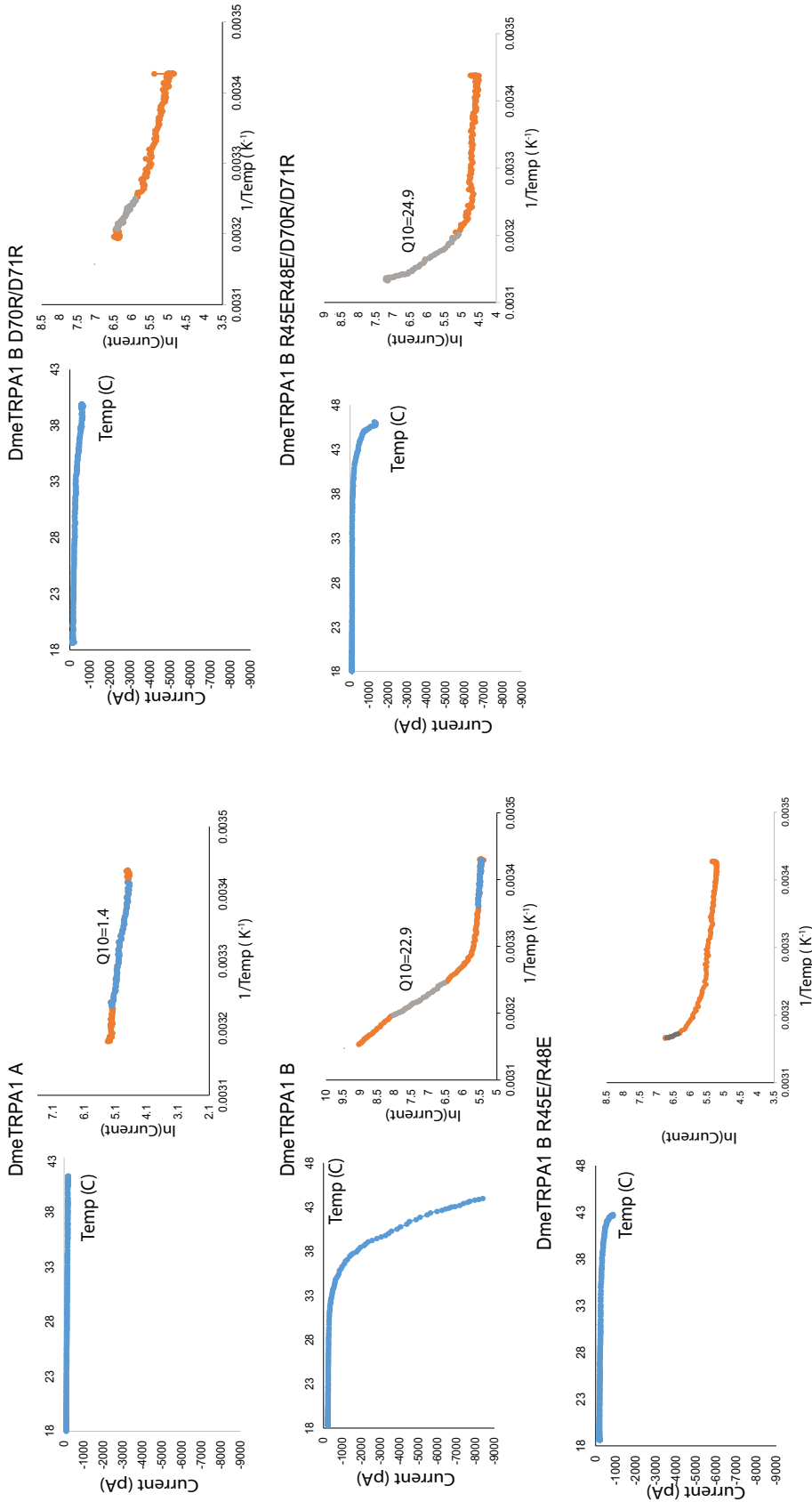


Figure 3.9 Charge replacement mutants on Helix 3 and ANK0 have varying effects on temperature sensitivity and threshold. HEK293 cells expressing wildtype or mutated insect TRPA1 constructs were analyzed by whole-cell patch-clamp electrophysiology. Voltage ramps were applied every second and the current at -60 mV was extracted during a temperature ramp from about 20 °C to 45°C. Current is plotted against temperature for the graphs on the left and Arrhenius plots are included on the right. The high-temperature linear regions of the Arrhenius plots used for Q10 calculations are shown in grey. Both the B isoform and the R45E/R48E/D70R/D71R mutant have high Q10 values, indicative of high heat sensitivity. The D70R/D71R mutant has a very flat Arrhenius plot at both high and low temperatures, suggesting that it is not a very temperature sensitive channel. The R45E/R48E containing mutants appear to have a temperature activation threshold shifted towards higher temperatures.

3.3.5 A potential electrostatic interface in the B N-terminus

Secondary structure predictions for the B isoform (Figure 3.5) revealed that residues 39-48, which were implicated as important for high temperature sensitivity in our patch-clamp electrophysiology experiments, make up a short predicted helix, the third one from the N-terminus. Plotting the residues as a helical wheel, it becomes apparent that Helix 3 is amphipathic with one positively-charged face, including residues K41, K42, R45, and R48 (Figure 3.8). Just after Helix 3 in sequence, but before ANK1, there is a helix-turn-helix motif reminiscent of a capping, or terminal, ankyrin repeat (Figure 3.5). We refer to the motif as ANK0 due to its position before ANK1 in the canonical 17 ankyrin repeat domain of TRPA1. When ANK0 is modelled a capping ankyrin repeat, it has both the hydrophobic face necessary to pack against ANK1 and a hydrophilic face typical of solvent-exposed region (Figure 3.8). The hydrophilic face of ANK0 has a number of negatively charged residues, including D59, D62, D70, and D71. Since the charges on Helix 3 and exposed face of ANK0 are complementary, we propose that there is an electrostatic interaction between the two elements. Furthermore, we hypothesize that the interaction between Helix 3 and ANK0 is necessary for the high temperatures sensitivity of the B isoform.

3.3.6 Integrity of the potential electrostatic interface in the B N-terminus correlates with high temperature sensitivity

Given the importance of Helix 3 to temperature sensitivity, we proceeded to target the potential Helix 3-ANK0 interaction for disruption by mutating charged residues

at the proposed interface. I introduced charge replacement mutations into Helix 3 or ANK0. For the Helix 3 charge replacement mutations, I generated R45E/R48E, which reversed the charge on the most conserved positively-charged residues, and K41E/K42E/R45E/R48E, which changes all of the positively-charged residues of Helix 3 to negatively-charged glutamates. The constructs with charge reversal mutations on ANK0 were D70R/D71R (the completely conserved residues), D59R/E62R, and D59R/E62R/D70R/D71R. I also generated the R45E/R48E/D70R/D71R mutant, a potential rescue construct that switches the placement of the positive and negative charges on proposed Helix 3 and ANK0 interface. Based on residue conservation, we focused on first characterizing the R45E/R48E and D70R/D71R constructs. Jeff McArthur tested the heat and AITC responses of the channels by whole cell patch-clamping. To quantify temperature sensitivity of the channels we calculated both the Q_{10} in a fixed physiological temperature window, 27-37°C as well as the Q_{10} Arrhenius where possible. Example traces of temperature ramp recordings and the resulting Arrhenius curves are included in Figure 3.10. Table 3.3 contains a summary of both the Arrhenius and 27-37°C Q_{10} values. In line with previous channel characterizations, the B isoform is strongly activated by heat, while the A isoform is not. The B channel has a modest Q_{10} (27-37°C) of 6, but its Q_{10} Arrhenius value is over 20. This is because the Arrhenius value is calculated from the linear or steepest part of the Arrhenius plot, reflecting the Q_{10} at the most sensitive temperature range for the channel. In effect, the 27-37°C temperature window is actually too low to describe the maximum Q_{10} of the channel. The A isoform channel reports, Q_{10} (27-37°C) and Q_{10} Arrhenius values of 1.31 ± 0.04 and 1.74 ± 0.70 . The similarity of those values, and the completeness and

Table 3.3 Summary of WT and mutant *D. melanogaster* TRPA1 temperature sensitivity

Construct	# Replicates	Q ₁₀ (27-37°C)	Q ₁₀ Arrhenius	Approximate Temperature Range for Q ₁₀ Arrhenius
DmeTRPA1 A	3	1.31 ± 0.04	1.7 ± 0.8	36-41°C
DmeTRA1 B	1	6.4	22.8	35-39°C
R45E/R48E	5	1.6 ± 0.3		
D70R/D71R	2	1.8 ± 0.9		
R45E/R48E/D70R/D71R	3	1.7 ± 0.7	21 ± 4	39-44°C

flatness of the curve seen in Figure 3.10 suggest that even near its optimal range for temperature-related activation, the A isoform is poorly heat sensitive. Interestingly, the charge replacement and reversal mutants all have relatively low Q_{10} (27-37°C) values (Table 3.5). However, the raw data point to different reasons for these low values. The current-temperature graphs associated with D70R/D71-expressing cells show hardly any response to temperature ramps that reach almost 45°C; The D70R/D71R Q_{10} (27-37°C) value is 1.76 ± 0.90 . In addition, the Arrhenius curve is similar to that of the A isoform, very flat and missing a clear inflection point that signifies a temperature-related switch from a poorly-conducting to a highly conducting channel. This indicates that the D70R/D71R mutant has reduced temperature sensitivity. In the case of the R45E/R48E and R45E/R48E/D70R/D71 channels, their current-temperature graphs seem to be shifted to the right compared to the B isoform. Their Arrhenius plots still show evidence of a transition, but it occurs at such a high temperature that a full Arrhenius plot could not be observed. Even so, the R45E/R48E/D70R/D71R mutant has an approximate Arrhenius Q_{10} value of 20.6 ± 4.0 , suggesting that with complementary mutations at the potential interface, near B isoform-level heat sensitivity is retained, but the threshold for activation has been shifted to higher temperatures. The linear region of that mutant's Arrhenius plot occurs between 39 and 44 °C, quite removed from the 35-39°C linear range of the B isoform channel's heat response. Based on these results, altering residues at the proposed Helix 3-ANK0 interface can hamper channel heat sensitivity. In particular the D70 and D71 residues seem to be involved. The fact that the Helix 3 mutant construct R45E/R48E appears to still have residual heat sensitivity, suggests that there may be other important residues on Helix 3 and in the immediate vicinity. It

would be interesting to next look at the temperature sensitivity of K41E/K42E/R45E/R48E, in which all the positively-charged residues of Helix 3 are changed, to determine whether additional charge replacement mutations on Helix 3 hampers temperature sensitivity (Q_{10}) or shifts the temperature activation threshold.

3.4 Discussion

3.4.1 How do the N-termini exert their effects on temperature sensitivity?

From our experiments with N-terminally-truncated or mutant channels, we have identified an element of the B isoform N-terminus, predicted Helix 3 and ANK0, involved in temperature sensitivity modulation. Removal of the entire N-terminus reduced temperature sensitivity to levels near that of the A isoform, pointing to the B N-terminus as a promoter of temperature sensitivity. Finer truncations narrowed down the major component to residues 39-48 of the B N-terminus, a helix that potentially forms an electrostatic interaction with capping ankyrin repeat ANK0. Additionally, some of the mutations targeted to disrupt the interaction also appear to reduce temperature sensitivity of the channel.

The molecular mechanism behind temperature sensing itself is poorly understood; however, in 2011, David Clapham and Christopher Miller proposed a thermodynamic framework describing how an ion channel could be temperature sensitive (Clapham & Miller). In short, a large change in molar heat capacity between closed and open conformation of a channel would result in favorable opening at both high and low temperatures due to the opposing effects of temperature on the entropic and enthalpic components of Gibbs free energy. Clapham and Miller also proposed that the difference

in heat capacity of a channel in different conformations could be the result of burial of charged residues or the exposure of hydrophobic ones as part of the transition (Clapham & Miller). Based on this reasoning, there need not be a defined temperature sensor, instead the sensor theoretically could be delocalized across the channel. The importance of a change in heat capacity to temperature sensitivity is supported by experimental evidence, including the rational design of temperature sensitivity into the Shaker channel (Chowdhury et al.). Perhaps, the insect TRPA1 B N-terminus is a temperature-sensitive module provides charged and hydrophobic residues that contribute to a high change in heat capacity associated with high temperature sensitivity. Our current data speak more towards the importance of a potential electrostatic interaction rather than changes in heat capacity. Rather than eliminating or increasing the number of charges at the interface, we changed the complementarity across the potential interface. Creating charge neutralization mutations or switching large hydrophobic residues to small ones at the interface and analyzing the Q_{10} of resulting channels may help determine whether the interface makes sizeable contributions to the change in molar heat capacity during channel opening. These biophysical measurements may also be able to be conducted on soluble channel fragments.(See appendix A).

Based on thermodynamic principles alone, Clapham and Miller concluded that all heat-sensing channels are also cold-sensing channels and could have similar architecture. Only practical obstacles, such as the flatness of the free energy curve and experimentally accessible temperature range, are thought to prevent the observation of both the low and high temperature arms of channel activation (Clapham & Miller). If this is the case, insect or snake TRPA1 and mammalian TRPA1 may share the same general

temperature-sensing architecture, but modulation of channel properties leads to the observation of opposite temperature activation properties. Therefore, studies of heat-activated insect TRPA1 channels may also be relevant to cold-activated mammalian TRPA1 channels. The principles discovered through these TRPA1 studies may be applicable to thermosensitive TRP channels in general.

3.4.2 Q₁₀ values and temperature sensitivity

The Q₁₀ values we measured for our channels are lower than those originally reported from *Xenopus* oocytes (Kang et al.). This may reflect a difference in temperature sensitivity when the channels are expressed in different heterologous systems. Consequently, it would be prudent to also test the heat responses of our truncated and mutated channels expressed in the original expression system, *Xenopus* oocytes. These measurements could be completed as part of our ongoing collaboration with Paul Garrity at Brandeis University, whose lab conducted the original characterization of the wildtype channels (Kang et al.). In addition, some of these mutant channels could be expressed in *Drosophila* gustatory bristles, allowing electrophysiological recordings to be conducted with channels in native cells (Kang et al.). As an alternative, my mutated or truncated channels could be used to rescue TRPA1 isoform B-deficiency in *Drosophila* AC neurons in the brain. By measuring the temperature preference of the resulting flies we could determine whether Q₁₀ of the channel correlates with the ability to restore the normal preference for 25 °C, a behavioral readout for channel temperature sensitivity (Kang et al.).

3.4.3 Future Directions

The exact mechanism of action of the B N-terminus is unknown and the role of the A N-terminus has yet to be tested. I created five truncations of the DmeTRPA1 A N-terminus. A similar analysis of the Q_{10} values would determine whether the A isoform N-terminus suppresses temperature sensitivity. If so, further mutation or dissection of the N-terminus based on secondary structure and conservation could reveal the residues responsible for that action. Structural or biophysical characterization of fragments of the insect TRPA1 N-termini and ankyrin repeat domain may help further elucidate the mechanisms behind temperature sensitivity modulation. Do the N-termini have temperature-related structural changes themselves? What effects do the insect N-termini have on the stability of surrounding areas of the ankyrin repeat domain? Do these effects correlate with temperature sensitivity? To answer some of these questions, I have designed and attempted to purify various fragments of the insect N-terminus and ankyrin repeat domain for biophysical and structural characterization. Thus far, however, protein expression, purification, and crystallization of such fragments has proven difficult (See Appendix A). Continued work on this front may yield structures that reveal the structural workings of the insect N-termini. Additionally, if practical obstacles can be overcome, techniques such as differential scanning calorimetry could be used to directly measure the change in heat capacity of isolated N-terminal fragments from either the A or B isoforms and tie fragment properties to full channel function.

References

Chowdhury, S., Jarecki, B. W., & Chanda, B. (2014). A molecular framework for temperature-dependent gating of ion channels. *Cell*, 158(5), 1148-1158.

- Clapham, D. E., & Miller, C. (2011). A thermodynamic framework for understanding temperature sensing by transient receptor potential (TRP) channels. *Proc Natl Acad Sci U S A*, *108*(49), 19492-19497.
- Du, E. J., Ahn, T. J., Choi, M. S., Kwon, I., Kim, H. W., Kwon, J. Y., & Kang, K. (2015). The Mosquito Repellent Citronellal Directly Potentiates Drosophila TRPA1, Facilitating Feeding Suppression. *Mol Cells*, *38*(10), 911-917.
- Hamada, F. N., Rosenzweig, M., Kang, K., Pulver, S. R., Ghezzi, A., Jegla, T. J., & Garrity, P. A. (2008). An internal thermal sensor controlling temperature preference in Drosophila. *Nature*, *454*(7201), 217-220.
- Kang, K., Panzano, V. C., Chang, E. C., Ni, L., Dainis, A. M., Jenkins, A. M., Regna, K., Muskavitch, M. A., & Garrity, P. A. (2012). Modulation of TRPA1 thermal sensitivity enables sensory discrimination in Drosophila. *Nature*, *481*(7379), 76-80.
- Kwon, Y., Kim, S. H., Ronderos, D. S., Lee, Y., Akitake, B., Woodward, O. M., Guggino, W. B., Smith, D. P., & Montell, C. (2010). Drosophila TRPA1 channel is required to avoid the naturally occurring insect repellent citronellal. *Curr Biol*, *20*(18), 1672-1678.
- Lishko, P. V., Procko, E., Jin, X., Phelps, C. B., & Gaudet, R. (2007). The ankyrin repeats of TRPV1 bind multiple ligands and modulate channel sensitivity. *Neuron*, *54*(6), 905-918.
- Vyklický, L., Vlachová, V., Vitásková, Z., Dittert, I., Kabát, M., & Orkand, R. K. (1999). Temperature coefficient of membrane currents induced by noxious heat in sensory neurones in the rat. *The Journal of physiology*, *517*(1), 181-192.
- Wang, G., Qiu, Y. T., Lu, T., Kwon, H. W., Pitts, R. J., Van Loon, J. J., Takken, W., & Zwiebel, L. J. (2009). Anopheles gambiae TRPA1 is a heat-activated channel expressed in thermosensitive sensilla of female antennae. *Eur J Neurosci*, *30*(6), 967-974.
- Wang, Y. Y., Chang, R. B., Waters, H. N., McKemy, D. D., & Liman, E. R. (2008). The nociceptor ion channel TRPA1 is potentiated and inactivated by permeating calcium ions. *J Biol Chem*, *283*(47), 32691-32703.
- Zhong, L., Bellemer, A., Yan, H., Ken, H., Jessica, R., Hwang, R. Y., Pitt, G. S., & Tracey, W. D. (2012). Thermosensory and nonthermosensory isoforms of Drosophila melanogaster TRPA1 reveal heat-sensor domains of a thermoTRP Channel. *Cell Rep*, *1*(1), 43-55.

Appendix

**Expression and purification of TRPA1 ankyrin repeat domain
fragments for structural and biophysical characterization**

A.1 Introduction

A.1.1 Ankyrin repeat domains act as protein and small molecule interaction domains.

As discussed in 1.2.3, TRPA1 is named after the 17 ankyrin repeats predicted at its cytoplasmic N-terminus. An ankyrin repeat is a ~33 amino acid structural fold. Each repeat consists of two short helices followed by a β -hair pin loop. Consecutive repeats pack together with hydrophobic residues to form a stack that can be compared to a left hand, with the inner helices of the repeat forming the concave surface of the “palm” and loops forming the “fingers” (Gaudet)(Figure A1 A). There is a slight twist and offset between repeats that results in large stacks of ankyrin repeats forming a spiral around a central axis (Michaely et al.; Wang et al.) (Figure A1).

Traditionally, ankyrin repeat domains are known as interaction domains. There are numerous examples of ankyrin repeats forming specific interactions with proteins and small molecules. For example, in ankyrinR, a scaffolding protein associated with the cytoskeleton, the extended ankyrin repeat domain binds an auto-inhibitory fragment from the protein C-terminus (Wang et al.) (Figure A1B). In another case, the ankyrin repeats of NF κ B inhibitor I κ B β are responsible for binding the nuclear localization sequence of the transcription factor and preventing NF κ B translocation into the nucleus (Malek et al.)(Figure A1C). The ankyrin repeats of TRPV1 are the binding site of ATP, a modulator of channel sensitivity (Lishko et al.)(Figure A1D). In all of these examples, the

protein and small molecule interactions occurred with the “palm” inner helices and loops.

A1.2 The TRPA1 ankyrin repeat domain is involved in chemical- and temperature-based activation of the channel

The sequence of the TRPA1 ankyrin repeat domain is unique, and not all of the repeats are equivalent. Specifically, repeats near ankyrin repeat 10 (ANK10) are quite different from the consensus ankyrin repeat sequence (Figure A2 A). Based on this information, we suspected there may be a kink in the ankyrin repeat domain in that area. The recent cryo-EM structure of TRPA1 confirmed that there is a break in the ankyrin repeat domain before ANK12, the first repeat modelled in the structure (Paulsen et al.). As of yet, there is no structural information available for the N-terminus and the first 11 repeats of TRPA1.

With the exception of recently-identified, structurally important inositol hexakisphosphate (Paulsen et al.) (Figure 1.6), no endogenous protein or small molecules are known to bind to the TRPA1 ankyrin repeat domain, suggesting that the domain is more than just an interaction site. The cysteines necessary for TRPA1 activation by reactive electrophiles are present in ankyrin repeat 17 and the linker that immediately follows. The new high-resolution structure of TRPA1 reveals that ankyrin repeat 17, the linker, and the TRP helix are packed against one another (Paulsen et al.), providing a physical link between the electrophile-sensing part of the cytoplasmic domains and the TRP box-like helix, a potential molecular handle to open the channel.

Some determinants of the directionality of TRPA1 temperature activation (cold-activated vs. heat-activated) lie in the ankyrin repeat domain. Cordero-Morales et al.

reported that swapping ankyrin repeats 3-8 or 10-15 of cold-activated human TRPA1 with the corresponding repeats from heat-activated rattlesnake TRPA1 resulted in chimeric channels that were also heat-activated. They concluded that the TRPA1 ankyrin repeat domain contains two portable temperature sensing modules, ankyrin repeats 3-8, and repeats 10-15 (Cordero-Morales et al.).

In another study, Jabba et al. reported point mutations in ankyrin repeats that are able to convert cold-activated mouse TRPA1 to a heat-activated channel. The mutations, S250N, M258L, and D261G, are part of ankyrin repeat 6 of mouse TRPA1 (Figure A2B). The existence of small amino acid changes that can flip the temperature response of TRPA1 is in line with ideas in the thermodynamics-based framework for temperature sensing discussed by Clapham and Miller (Clapham & Miller). It is empirical evidence that cold-activated and heat-activated channels can have largely similar molecular architecture. Analyzing the structure and biophysical properties of this region in the presence and absence of these mutations may shed light on how TRP temperature sensitivity parameters are set.

A1.2 A divide-and-conquer approach to studying the TRPA1 ankyrin repeat domain

Taken together, the structural and biochemical information points to the ankyrin repeats and adjacent regions (See chapter 2) as important elements in chemical and temperature sensing. At the start of this project there was no structure available for any portion of the TRPA1. Even now, with the release of the high resolution TRPA1 structure (Paulsen et al.), the structure of over two-thirds of the ankyrin repeat domain

remains a mystery. Structures containing more of the ankyrin repeat domain may reveal some molecular mechanisms behind temperature sensing.

To approach this problem, I took a divide-and-conquer approach. I designed, expressed and purified fragments of the TRPA1 ankyrin repeat domain spanning regions of interest. These fragments were used in structural determination efforts along with biochemical and biophysical analyses. By analyzing the structure and behavior of TRPA1 fragments in response to heat and other conditions, we aimed to correlate fragment properties with the properties of the full-length channel.

A2 Methods

A2.1 Cloning

The mouse TRPA1 ankyrin repeat domain fragment library was created by a previous lab member. Briefly, a vector pET-ANK was created by inserting an oligo that encodes an N-terminal 6x-histidine tag and the N- and C- terminal capping repeats into a pET21b vector. For the library, PCR was used to amplify the ankyrin repeat sequence of interest from mouse TRPA1 and introduce NdeI and NotI sites for cut-and-paste insertion into pET-ANK. Plasmids created included every possible choice of three or more consecutive repeats, for a total of 120 plasmids. Primer and construct details are included in Table A1. The open reading frames of all plasmids were previously confirmed by sequencing.

A plasmid encoding mouse TRPA1 ankyrin repeats 1-11 with a C-terminal 6x-histidine tag was created by PCR of a mouse TRPA1 template with primers MmTRPA1 F1 and MmTRPA1 R11 followed by cut-and-paste with NdeI and NotI into a pET21-C6H vector (Jin et al.). QuikChange (Agilent) site-directed mutagenesis was used to

generate plasmids encode mouse TRPA1 ankyrin repeats with the following mutations: S250N, M258L/D261G, and S250N/M258L/D261G. Primers used are listed in Table 2A.

Plasmids encoding *A. gambiae* or *D. melanogaster* TRPA1 ankyrin repeat domain fragments were generated by PCR amplification of the fragment of interest and subsequent cut-and-paste cloning into the pET21-C6H vector. A list of the plasmids created and primers used is included in Table A3.

A2.2 Small-scale Protein Expression and Solubility Tests

For small-scale expression and solubility tests, 5 ml cultures BL21 (DE3) *E. coli* were induced with 500 μ M IPTG for 3 hours at 25 or 37°C. Equal amounts of cells were spun down from each culture and lysed by sonication in 20 mM Tris pH 7.5, 200 mM NaCl. Samples of cleared lysate and cell pellets were run side-by-side on Tris-glycine or Tris-tricine polyacrylamide gels. Expression and solubility was assessed by comparing the amount of the expressed protein in the supernatant and pellet samples.

A2.3 Large-scale Protein Expression and Purification

For large-scale protein purification, BL21(DE3) *E. coli* were grown at 37°C to an OD₆₀₀ of ~0.2 then switched to 20°C. Protein expression was induced with 100 μ M isopropyl β -D-1-thiogalactopyranoside (IPTG) at an OD₆₀₀ of ~0.4. Cells were harvested after 8-12 hours of expression and frozen in liquid nitrogen.

For purification, cells were lysed by sonication in lysis buffer containing 20 mM Tris pH 7.5 or 8.0, 300 mM NaCl, 20 mM imidazole, 0.1% Triton X-100, 0.5 mM phenylmethylsulfonyl fluoride (PMSF), 2 mM benzamidine, 0.2 mg/ml lysozyme, 0.08

mg/ml RNaseA, and 0.04 mg/ml DNase I. Cleared lysate was applied to a nickel-nitrilotriacetic acid column (Qiagen). After washes (20 mM Tris pH 7.5 or 8.0, 300 mM NaCl, 20 mM imidazole, 0.375 mM PMSF, 1.25 mM benzamidine, 5.3 mM β -mercaptoethanol), protein was eluted with a step gradient of imidazole (25, 50, 100, 150, 250 mM). After adding EDTA and dithiothreitol (DTT) to 10 and 1 mM, respectively, eluted protein was dialyzed into a low salt buffer, (10 mM Tris pH 7.5 or 8.0, 80 mM NaCl, 1mM DTT). Fractions containing the protein of interest were loaded onto a Resource Q column (GE Healthcare) and eluted with a sodium chloride gradient. Fractions containing the expressed protein were pooled and run on a Superdex 75 or 200 16/60 column (GE Healthcare) in 20 mM Tris pH 7.5 or 8.0, 150 mM NaCl, and 1 mM DTT. Fractions deemed pure by analysis on Coomassie-stained SDS polyacrylamide gels were pooled and concentrated to >10 mg/ml when possible.

A2.4 Limited Proteolysis

Purified protein was incubated with trypsin, chymotrypsin, elastase, endopeptidase GluC, or papain at a 1:500 w:w ratio on ice for 5-30 minutes. The digestions were stopped by adding reducing SDS PAGE sample dye and boiling for 5 minutes. Samples of the digests were analyzed by SDS PAGE and western blots as described in Chapter 2 with an alkaline phosphatase-conjugated anti-His antibody. For sequencing, protein was transferred from the SDS PAGE gel to a PVDF membrane. Ponceau red stain was used to visualize the bands so they could be excised. Protein sequencing was performed by the Harvard Mass Spectrometry and Proteomics Research Laboratory.

A2.5 Thermofluor Assay

The Thermofluor Assay was used to generate protein melting curves and screen for stabilizing additives. For each 10 μ l reaction, 0.1-0.2 mg/ml protein with was mixed with SYPRO Orange (5X Final concentration) in various buffers with different additives in low-profile white-walled PCR plate sealed with optically clear caps (Biorad). After a twenty minute incubation on ice, fluorescence of each well was measured on the Bio-Rad Opticon 2 RT-PCR machine operated by MJ Opticon Monitor software. Data was analyzed in the Opticon Monitor software to calculate melting temperatures.

A2.6 Crystallization Trials

Crystallization trials were all done in sitting-drop vapor diffusion configuration. Protein was mixed at various ratios with reservoir solution. A variety of protein concentration and protein:precipitant ratios were sampled for each construct. Drops were set either by hand or using an NT8 (Formulatrix) dropsetter. A range of protein concentrations, protein:precipitate ratios, and two incubation temperatures (4°C and room temperature) were sampled for each construct. Crystallization screens included homemade grid screens as well as commercial screens from Hampton and Nextal. Trays were scored by hand or imaged with a Rock Imager automated hotel.

A3 Results

A3.1 Screening of a mouse TRPA1 ankyrin repeat domain fragment library identified a soluble, well-expressed construct containing repeats 1-11

To identify suitable TRPA1 ankyrin repeat domain fragments for structural and biochemical studies, I screened a large library of constructs created previously by Alejandra Beristain-Barajas for expression and solubility in *E. coli*. The library consists of 120 constructs including every possible option of 3 or more consecutive ankyrin

repeats. Each construct also includes capping ankyrin repeats, which are designed with a hydrophobic face to shield the free hydrophobic ends of the ankyrin repeat fragment and a hydrophilic face to be stable when exposed to solvent (Binz et al.) All constructs have a C-terminal 6x-histidine tag for purification. The constructs were expressed in 5 ml cultures of BL21 (DE3) *E. coli* at 25 or 37°C. After harvesting equal amounts of cells from each culture, the cells were lysed by sonication. The lysate was cleared by centrifugation and samples of the supernatant and pellets were run on SDS-polyacrylamide gels to judge expression and solubility of each construct. The full results are included in Figure A3. One of the largest soluble constructs identified included ankyrin repeats 1-11 of mouse TRPA1 (MmTRPA1 ANK1-11). The fragment was well-expressed in large scale preparations and could be easily purified via nickel affinity chromatography, anion exchange chromatography, and size exclusion chromatography (Figure A4). A version of the ANK 1-11 construct without the capping repeats was also soluble and could be purified by the same method.

Given the promise of the ANK1-11 fragment, I also introduced the temperature activation flipping mutations reported by Jabba et. al to create three more versions of the construct, S250N, M258L/D261G, and S250N/M258L/D261G. All three constructs could be purified by the same protocol yielding over 100 milligrams of protein per liter of culture.

A3.2. Efforts to crystallize mouse TRPA1 ANK1-11 have not been successful

Capped, capless, and mutant versions of mouse TRPA1 ANK1-11 were subjected to sitting-drop vapor diffusion crystallization trials to find conditions that promote the formation of high-quality crystals. Concentrated protein (1-30 mg/ml) was

mixed one-to one with solutions in commercial crystallization screens and allowed to equilibrate against a reservoir of precipitant solution in sealed crystallization trays at room temperature or at 4°C. The commercial screens used included ProComplex, Salt Rx (Hampton), Anions (Hampton), Cations (Hampton), Index (Hampton), Classics (Nextal), and Classics Lite (Nextal), which sample a wide range of precipitants, salts, and pH conditions. Despite these efforts, the mouse TRPA1 ANK1-11 fragments forms noncrystalline precipitation in most conditions.

A3.3 Small-scale expression tests of insect TRPA1 ankyrin repeat domain constructs identify soluble constructs containing all 17 ankyrin repeats.

I moved on from working with mouse TRPA1 fragments to working with insect TRPA1 ankyrin repeat domain fragments in the hopes that the new homolog might be more conducive to X-ray crystallography. In addition, the fact that N-terminal regions of insect TRPA1 A and B isoforms can modulate channel temperature sensitivity (Kang et al.) made them interesting targets in their own right for structural, biochemical, and biophysical analysis. By comparing the properties of these fragments (conformation, stability, I aimed to gain insight into the roles of the A and B N-termini and uncover what properties are associated with the increased temperature sensitivity of the B isoform version of the channel.

Based on what we know from the mouse TRPA1 ankyrin repeat domain screening, I designed constructs that span various regions of the ankyrin repeat domains of the A and B isoform versions of *A. gambiae* and *D. melanogaster* TRPA1 (Figure A5). This includes constructs containing just the isoform-specific region (N-splice site) all the way through to constructs containing the full isoform N-termini and all

17 ankyrin repeats (N-ANK17). All constructs had a C-terminal 6x-histidine tag for later purification. First, I tested the constructs in the same *E. coli* small-scale expression and solubility screen. (Figure A6). In general the *A. gambiae* constructs were better expressed and soluble than the *D. melanogaster* constructs. Surprisingly, both the A and B isoform version of N-ANK17 from *A. gambiae* TRPA1 appeared well-expressed and soluble (Figure A6). Since the N-ANK17 constructs contain isoform specific N-termini and all 17, I focused my efforts on expressing and purifying those fragments on a large scale for further study.

A3.5 Purified mosquito TRPA1 constructs containing all 17 ankyrin repeats have limited solubility that is not improved by stabilizing additives

Both the A and B isoform N-ANK17 constructs from *A. gambiae* could be expressed and purified on a large scale (Figure A7); however the proteins had relatively low solubility. Similar to my other purifications, the ankyrin repeat domain fragments were purified via a combination of nickel-affinity chromatography, anion exchange chromatography, and size exclusion chromatography. Even at the nickel column stage, solutions containing the N-ANK17 proteins were very viscous and formed skins. In addition, neither A ANK-17 nor B ANK17 could be concentrated higher than 1 mg/ml in standard buffer containing 20 mM Tris pH 8.0, 150 mM NaCl, and 1 mM DTT. Circular dichroism measurements of the A and B N-ANK17 fragments show minima near 208 and 222 nm, confirming the high helical content expected for a folded ankyrin repeat domain (Figure A8); therefore the poor behavior is not likely to be caused by gross misfolding of the protein.

To improve the behavior and solubility of the A and B N-ANK17 fragments I searched for additives that may stabilize the N-ANK17 constructs. For this I used a high through-put differential scanning fluorimetry (ThermoFluor) (Ericsson et al.; Vedadi et al.). The assay uses SYPRO Orange, a dye that fluoresces when bound to hydrophobic regions of proteins, to monitor protein unfolding in response to increasing temperature in a qPCR machine. I performed this assay using the AgaTRPA1 A N-ANK17 and discovered that the fragment is most stable around pH 8 and that quaternary amines like choline and trimethylamine N-oxide increased fragment stability. Additionally, sugars, including sorbitol, were able to increase the melting temperature of the fragment in the assay (Figure A9). Unfortunately, adding choline and sorbitol during fragment purification did not have a dramatic effect on N-ANK17 fragment solubility.

A3.6 Limited proteolysis identified a stable truncation of the A N-ANK17 fragment

Next I conducted limited proteolysis experiments on the A and B N-ANK17 constructs to identify the most stable and well-folded regions within the fragments. Small amounts of trypsin, chymotrypsin, elastase, or endoproteinase GluC were incubated with A or B N-ANK17 for 5 10 or 20 minutes on ice. Limited proteolysis with A N-ANK17 and GluC indicated a single major cleavage product. (Figure A9) A western blot against the C-terminal histidine tag of the construct revealed that A N-ANK17 was being cleaved from the N-terminus. A similar result was obtained in limited proteolysis experiments using trypsin. Edman degradation was used to confirm the cut sites in the N-terminus and inform the design of new truncated constructs.

A3.7 N-terminal truncation of the mosquito A and B N-ANK17 constructs improved protein behavior.

Based on the results of the limited proteolysis experiments, I designed truncations of the A and B N-ANK17 constructs, trying to find a construct that is more soluble and better behaved than the full-length versions. Specifically, start sites were chosen to remove regions that are predicted to be disorder, as that may improve the overall stability of the protein. I created four truncations of A N-ANK17: A N Δ 23, A N Δ 51, A N Δ 65, A N Δ 87. Two more constructs were made based on B N-ANK17: B N Δ 26 and B N Δ 31. In addition, I also made smaller constructs that include just the isoform-specific N-termini or only the ankyrin repeat domain. I expressed and attempted to purify these constructs on a large scale for crystallization trials. A summary of the results is included as Table 4. Truncation of the A ANK1-17 construct resulted in a more soluble constructs less prone to precipitation and skin formation. All constructs that could be purified were subjected to crystallization trials; however, there have been no initial hits.

A4 Discussion

Based on our knowledge of ankyrin repeats, we were able to express and purify multiple fragments of the TRPA1 ankyrin repeat domain from *E. coli*. One successfully purified construct spans ankyrin repeats 1-11 of mouse TRPA1, which corresponds to most of the unseen N-terminal residues in the TRPA1 cryo-EM structure {Paulsen}. We've also produced an ankyrin repeat domain containing all 17 repeats; however its solubility is still problematic. Further structural and biochemical work with these fragments may yet yield important information.

In an effort to find a crystallization chaperone for mouse TRPA1 ankyrin repeat domain, we have collaborated with Dr. Emily Liman at UCSF to create intrabodies,

antibody-like evolved binding proteins based on the fibronectin fold. We provided purified mouse TRPA1 ANK1-11 for intrabody generation and received plasmids for 9 intrabodies against the fragment. These intrabodies have yet to all be expressed and purified for binding trials. A tight-binding intrabody may provide the necessary stabilization and contacts to promote crystallization that is not possible for the ankyrin repeat domain fragment alone. In addition other techniques, like seeding with other small crystals have yet to be tried.

Many of the fragments produced may be useful for other structural and biochemical analyses that don't require crystallization. For example, small angle X-ray scattering. Unlike X-ray crystallography, these measurements are conducted in solution. SAXS does not provide atomic detail, but it does give a low resolution envelope of the molecule. This may be enough detail to begin to appreciate differences in conformation between key fragments. This would be especially well suited for the mouse TRPA1 ANK1-11 constructs, both the wildtype fragment and the fragments containing mutations that flip the temperature activation of TRPA1. These constructs are quite stable and can easily be obtained at the quantities and concentrations necessary for SAXS measurements.

In addition, ankyrin repeat domain fragments can be used in differential scanning calorimetry measurements and melting curves, allowing direct calculation of the change in heat capacity during temperature ramps. Given the biochemically supported role of these fragments in temperature sensing {Cordero-Morales} as well as the thermodynamic between heat capacity and temperature sensitivity {Clapham and Miller}, measuring the change in heat capacity of fragments from both hot and cold-

activated channels may help us understand more about the molecular mechanisms behind temperature sensing.

A5 References

- Binz, H. K., Stumpp, M. T., Forrer, P., Amstutz, P., & Pluckthun, A. (2003). Designing repeat proteins: well-expressed, soluble and stable proteins from combinatorial libraries of consensus ankyrin repeat proteins. *J Mol Biol*, 332(2), 489-503. doi:10.1016/S0022-2836(03)00896-9
- Clapham, D. E., & Miller, C. (2011). A thermodynamic framework for understanding temperature sensing by transient receptor potential (TRP) channels. *Proc Natl Acad Sci U S A*, 108(49), 19492-19497. doi:10.1073/pnas.1117485108
- Cordero-Morales, J. F., Gracheva, E. O., & Julius, D. (2011). Cytoplasmic ankyrin repeats of transient receptor potential A1 (TRPA1) dictate sensitivity to thermal and chemical stimuli. *Proc Natl Acad Sci U S A*, 108(46), E1184-1191. doi:10.1073/pnas.1114124108
- Ericsson, U. B., Hallberg, B. M., DeTitta, G. T., Dekker, N., & Nordlund, P. (2006). Thermofluor-based high-throughput stability optimization of proteins for structural studies. *Analytical biochemistry*, 357(2), 289-298.
- Gaudet, R. (2008). A primer on ankyrin repeat function in TRP channels and beyond. *Mol Biosyst*, 4(5), 372-379. doi:10.1039/b801481g
- Jin, X., Touhey, J., & Gaudet, R. (2006). Structure of the N-terminal ankyrin repeat domain of the TRPV2 ion channel. *Journal of Biological Chemistry*, 281(35), 25006-25010.

- Kang, K., Panzano, V. C., Chang, E. C., Ni, L., Dainis, A. M., Jenkins, A. M., Regna, K., Muskavitch, M. A., & Garrity, P. A. (2012). Modulation of TRPA1 thermal sensitivity enables sensory discrimination in *Drosophila*. *Nature*, *481*(7379), 76-80. doi:10.1038/nature10715
- Lishko, P. V., Procko, E., Jin, X., Phelps, C. B., & Gaudet, R. (2007). The ankyrin repeats of TRPV1 bind multiple ligands and modulate channel sensitivity. *Neuron*, *54*(6), 905-918. doi:10.1016/j.neuron.2007.05.027
- Malek, S., Huang, D.-B., Huxford, T., Ghosh, S., & Ghosh, G. (2003). X-ray crystal structure of an I κ B β ·NF- κ B p65 homodimer complex. *Journal of Biological Chemistry*, *278*(25), 23094-23100.
- Michaely, P., Tomchick, D. R., Machius, M., & Anderson, R. G. (2002). Crystal structure of a 12 ANK repeat stack from human ankyrinR. *The EMBO journal*, *21*(23), 6387-6396.
- Paulsen, C. E., Armache, J. P., Gao, Y., Cheng, Y., & Julius, D. (2015). Structure of the TRPA1 ion channel suggests regulatory mechanisms. *Nature*, *520*(7548), 511-517. doi:10.1038/nature14367
- Vedadi, M., Niesen, F. H., Allali-Hassani, A., Fedorov, O. Y., Finerty, P. J., Jr., Wasney, G. A., Yeung, R., Arrowsmith, C., Ball, L. J., Berglund, H., Hui, R., Marsden, B. D., Nordlund, P., Sundstrom, M., Weigelt, J., & Edwards, A. M. (2006). Chemical screening methods to identify ligands that promote protein stability, protein crystallization, and structure determination. *Proc Natl Acad Sci U S A*, *103*(43), 15835-15840. doi:10.1073/pnas.0605224103

Wang, C., Wei, Z., Chen, K., Ye, F., Yu, C., Bennett, V., & Zhang, M. (2014). Structural basis of diverse membrane target recognitions by ankyrins. *eLife*, 3.

doi:10.7554/eLife.04353

Conclusion

TRPV1 and TRPA1's frontline role in sensing painful stimuli makes them gateways to pain and inflammation. Understanding the molecular mechanisms behind their activation by both chemical and thermal stimuli is key to targeted design of channel-modulating drugs and small molecules.

Our discovery of a unique minimal set of residues sufficient to confer vanilloid sensitivity to chicken TRPV1 contributes new candidates to the pool of known molecular determinants of vanilloid sensitivity. In addition to the established T550 and E570 residues, we present two more residues, A566 and A665, in the S4-S5 pocket that play a more modest, but still important role. In addition, the importance of pore residues in capsaicin sensitivity is a novel concept and closer study of the region may provide new insights into the mechanisms that link ligand binding and channel gating. With the entrance of TRP channels into the structural era, we may soon be able to leverage biochemical data, like those presented here, to rationally design vanilloid-like molecules that specifically target other channels both within and outside the TRPV family. Given the potential similarities in the transmembrane domain architecture of TRP channels, modulation of channel function by ligands in the S4-S5 pocket could be a feature of many TRP superfamily rather than just TRPV channels. Similar dissection of other ligand-binding pockets, like the antagonist binding site in TRPA1, may lead to us understanding the workings of another site of TRP channel modulation.

The mechanisms behind temperature sensing are still quite mysterious; however the insect TRPA1 isoforms provide a simple system to probe how temperature sensitivity is modulated. Through electrophysiological measurements of progressively truncated channels, we have preliminary evidence for a structural feature important for promoting high temperature sensitivity, a potential electrostatic interaction between a short helix and “extra” ankyrin repeat. Understanding how the temperature sensitivity is altered may lead to new hypothesis as to temperature sensitivity is conferred.

Studies of TRPA1 ankyrin repeat domain fragments have the potential to provide empirical evidence for thermodynamically-proposed contributions to temperature sensitivity. We have been able to produce pure fragments of the TRPA1 ankyrin repeat domain that have been implicated in channel temperature sensitivity. Working with small fragments of the channel that are known to be important for temperature sensing could allow easier measurement of thermodynamic properties, like change in heat capacity. Since many thermodynamic properties are additive, studying key fragments of the channel may be sufficient to start describing the workings of the overall channel. This may shed light on the mechanisms behind temperature sensing by both ion channels and proteins in general.